Final Report

DOE Award Number: DE-FG36-08GO18053/A000
Recipient: Rensselaer Polytechnic Institute (RPI), Center for Automation Technologies and Systems (CATS)
Project Title: Adaptive Process Controls and Ultrasonics for High Temperature PEM MEA Manufacture
Project Principal Investigator: Daniel Walczyk (previously Raymond Puffer)
Consortium/Teaming Members: Arizona State University (ASU), Progressive Machine and Design (PMD), LLC; BASF Fuel Cell, GmbH; UltraCell, LLC.

Executive Summary:

The overall goal of this DOE-sponsored project was to enable cost effective, high volume manufacture of high temperature Proton Exchange Membrane (PEM) Membrane Electrode Assemblies (MEAs) by: (1) greatly reducing MEA pressing cycle time through the development of novel, robust ultrasonic bonding processes and application of adaptive process control to thermal bonding processes for high temperature (160-180°C) PEM MEAs; (2) achieving greater uniformity and performance of high-temperature MEAs by applying advanced testing, diagnostics and control methods to the entire MEA bonding process; and (3) optimizing all aspects of the bonding process for improved product quality, throughput, yield, cost savings, and energy conservation.

The research provides a deeper understanding of fuel cell manufacturing, particularly related to these types of fuel cells, in four crucial areas: the invention of a new ultrasonic bonding method for high- and low-temperature MEAs and demonstration of process scale-up; full characterization of ultrasonic and thermal bonding of MEAs; using the derivative of the complex AC impedance (1 kHz) for in-situ quality measurement and process control of thermal pressing of MEAs; and using cyclic voltammetry (CV) scans for process and quality control of thermally and ultrasonically pressed MEAs.

The technical effectiveness and economic feasibility of ultrasonic bonding and thermal bonding (with process control), respectively, over conventional thermal pressing for high-temperature PEM MEA manufacturing is clearly demonstrated with greater than 80% and 70% cost reductions, 95% and 85% reductions in electricity usage, and greater than 95% cycle time reductions for both. Furthermore, tooling designs, process control techniques, and single MEA and stack testing have been proven with hundreds of samples tested for thousands of hours combined.

The general benefit to the U.S. public is lower-cost and more robust fuel cells for use in a variety of industries including transportation, stationary power, telecommunications, homeland security, and military.

Actual Accomplishments vs. Project Goals/Objectives:

The high level objective of the project was to enable cost effective, high volume manufacture of high temperature Proton Exchange Membrane (PEM) Membrane Electrode Assemblies (MEAs) by: (1) greatly reducing MEA pressing cycle time through the development of novel, robust ultrasonic bonding processes for high temperature (160-180°C) PEM MEAs; (2) achieving greater uniformity and performance of high-temperature MEAs by applying advanced testing and diagnostics to the entire MEA bonding process; and (3) optimizing all aspects of the bonding process for improved product quality, throughput, yield, cost savings, and energy conservation. To achieve this objective, the project was broken down into 17 different tasks (with some sub-tasks) and organized into three different phases, as shown in Figure 1. Discussion of the specific tasks and sub-tasks along with a comparison of what was actually accomplished are provided below.

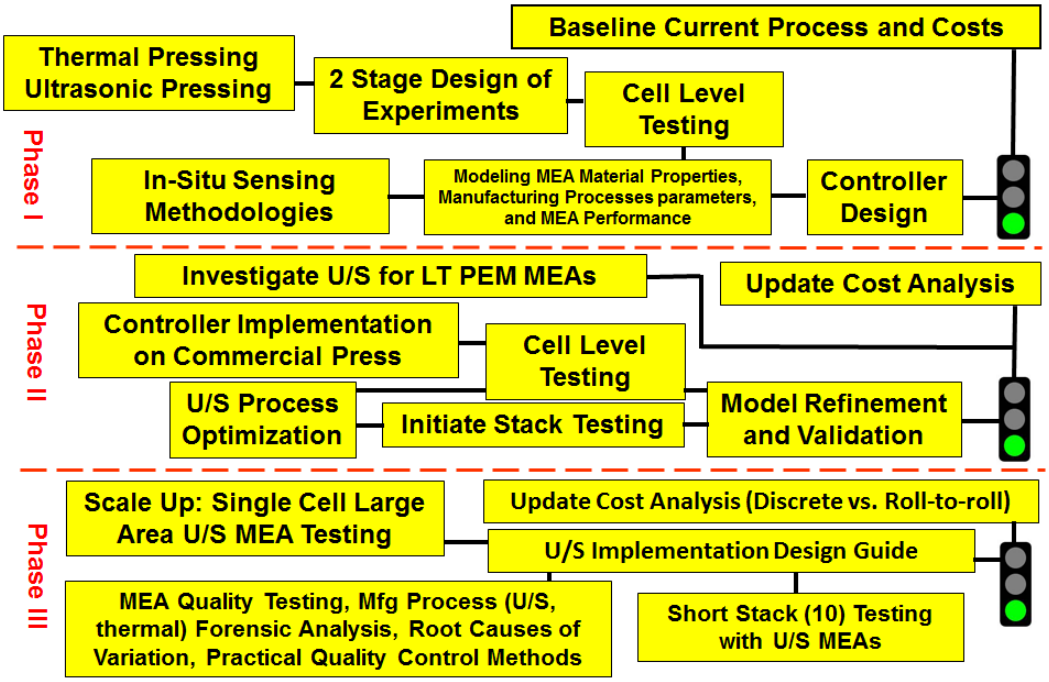

Figure 1 – Project organization into three different phases and 17 different tasks.

Task 1.0 – Baseline and Analysis of Current Process. CATS researchers will conduct an analysis of the current HT MEA manufacturing processes, from incoming component materials to completed MEA, to assembly into a stack and functional testing. CATS researchers will identify all process steps, methods, times, costs, and the effects of MEA architecture. The focus will be on 4- and 5-layer MEA architectures. A baseline cost analysis will be performed to identify the current manufacturing costs associated with hot pressing of high temperature MEAs, and estimates of the manufacturing costs associated with the improved pressing techniques. The analysis will be conducted based on production rates needed to satisfy the DOE projected high volume manufacturing case of 500,000 stacks/year for the automotive application.

> *The current recipe-based MEA manufacturing processes and equipment used by BASF Fuel Cell (Frankfurt, Germany and Somerset, New Jersey, USA) was fully characterized (i.e. 'baselined') including individual process steps, current challenges and manufacturing system cost modeling. Existing CATS equipment was arranged or modified, and equipment and tooling were designed (if necessary) and procured to allow for the production of 50 cm^2 MEAs in both 4- and 5-layer architectures.*

Task 2.0 – Comparison of Current and Proposed MEA Pressing Processes. CATS researchers will conduct a comparison of current manufacturing processes with the proposed adaptive control techniques used on thermal and ultrasonic presses. The focus will be on identifying the cost, capacity, and quality issues for the different methods of MEA pressing.

> *As a result of the cost analysis, the CATS researchers estimate MEA sealing operation cost savings of 57% and 82% using optimized thermal (without application of APC, which is addressed in Phase II cost analysis) and ultrasonics, respectively.*

Task 3.0 – Baseline Process Testing. CATS researchers will conduct baseline performance testing of current MEA pressing processes using commercial thermal and ultrasonic presses in 50 cm^2 and 18 cm^2 format MEAs. Design of Experiments techniques will be used to identify the relationships among incoming materials properties (electrode thickness, catalyst loading, membrane thickness, membrane acid content and concentration), pressing process parameters (time, temperature, pressure for thermal pressing, and time, pressure, and power for ultrasonic pressing), the resulting MEA physical and electrochemical

properties (thickness, acid content, concentration, electrode porosity) and the MEA performance in a single cell test fixture. These tests will be conducted in the CATS laboratory facilities and also on the BASF Fuel Cell (BFC) pilot MEA manufacturing line in Frankfurt Germany using electrode and membrane materials from the same production lots.

Following a significant effort by CATS researchers to establish high-temperature MEA manufacturing and testing capabilities, baseline testing of thermally and ultrasonically sealed 50cm^2 MEAs demonstrated that both processes produced cells that performed as well, if not better than production cells from BASF and process parameter effects and sensitivities were established. However, ultrasonics reduces cycle time for the sealing and welding processes by nearly two orders of magnitude.

Testing with an 18 cm^2 MEA format was abandoned due to resource and time constraints.

Task 4.0 – Model Development. CATS researchers will develop physics-based analytical and empirical model(s) to describe the relationships among: incoming component materials properties; manufacturing process parameters; resulting MEA physical and electrochemical properties; and the MEA performance in a stack.

Thermal response of thermal and ultrasonic MEA pressing was measured using embedded thermocouples. The thermal pressing model correlates well with experimental data, whereas the 6 DOF vibrational model of ultrasonic bonding to predict internal heat generation was too complex and would not converge to a solution. Future work would require model simplification. Finally, MEA weight loss is a function of compression, although not a linear model as proposed.

Task 5.0 – Development of In-situ Sensing Techniques. CATS researchers will develop in-situ sensing techniques and conduct experimentation using the experimental thermal and ultrasonic presses. EIS-based and other sensing techniques will be developed jointly by researchers at ASU (primary) and RPI. These techniques will be implemented on experimental press equipment at the CATS. The preferred approach for in-situ sensing will be Electrochemical Impedance Spectroscopy (EIS) without reactant gasses, although in-situ sensing of DC resistance, porosity, and MEA compressibility (spring constant) will also be investigated. The primary metric that will be used to select the preferred sensing technique(s) will be the ability to correlate sensed properties to the performance of MEAs in either a single cell test fixture or a short (5 cell) stack.

With regards to in-situ sensing of MEAs during thermal pressing in single test cells, ESI takes too long and direct DC resistance measurement does not correlate to MEA performance; but phase angle of a single frequency AC response appears to.

Task 6.0 – Controller Development. CATS researchers will lead the design of feedback controllers, and computer simulations to assess the performance of these controllers. Initial implementation of the controls will focus on the experimental thermal press, and later on the ultrasonic press.

In-situ measurement of a MEA's AC impedance phase angle (1 kHz signal in this case) during thermal pressing was successfully used to improve uniformity of MEA performance and decrease pressing time by >50%.

Task 7.0 – Phase I program review. The focus of this Phase I review will be on the ability of the Design of Experiments testing to identify the critical relationships among materials properties, manufacturing process parameters, the resulting MEA properties and the performance of the MEAs in the single cell test fixtures. In-situ sensing techniques that can be correlated to the performance of MEAs in the test fixtures must be demonstrated. The results of the baseline cost analysis (Task 1.0) must demonstrate that the proposed Adaptive Process Controls and Ultrasonic Pressing techniques provide the potential for significant manufacturing cost reductions over current pressing methods in order to proceed into Phase II. A quantitative Go/No Go decision point based on MEA costs will be determined at the end of Task 1.0.

Completion of Phase I was approved by DOE in December 2009.

Task 8.0 – APC Implementation. Implementation and evaluation of in-situ sensing and adaptive process control techniques will be performed on the commercial thermal press. This includes the design, analysis and construction of custom press tooling for the thermal press, and the necessary modifications and programming of the press controller. MEAs will be produced using APC and their performance will be compared to the baseline MEAs produced without APC.

APC was implemented for a fully automated thermal press using an updated control metric (compared to Task 6 method), i.e. when the derivative of the 1 kHz complex AC impedance goes to zero. Fully functioning cells can be produced in less than 5 seconds with; no degradation in performance as measured by single cell polarization curves, and no change in electrode pore structure or platinum crystallite size based on SEM imaging (both) and XRD testing (platinum size only).

Cyclic voltammetry (CV), which provides a means to measure electrochemically active catalyst area, can be applied as a quality control metric for single cells prior to stack assembly.

Task 8.1 – APC for Ultrasonics. CATS researchers will investigate the feasibility of in-situ sensing of MEA properties for APC during the ultrasonic sealing process. Because of the very short process cycle time associated with ultrasonics, the possible sensing methods are quite limited. Vibration analysis using either accelerometers or acoustic sensors is the most promising approach. The commercial ultrasonic welding tooling will be modified to include the selected sensor(s). CATS researchers will then conduct a designed experiment to determine if we can identify a relationship between sensed signal and MEA performance in a single cell test fixture.

APC for ultrasonic sealing of MEAs is not possible using an accelerometer mounted directly on the horn due to its adverse effect on the horn's resonance frequency. Mounting this sensor to the anvil instead is possible, but vibration attenuation through the MEA may confound closed-loop control.

Results of power vs. frequency data from an FFT of an acoustic signal from the ultrasonic sealing process were inconclusive.

The previously demonstrated repeatability of the ultrasonic sealing process combined with short cycle time reduce the need to implement closed loop control.

Task 9.0 – Evaluation of MEA performance. The MEAs produced using APC will be tested in single cell test fixtures and the performance of the MEAs will be compared to those tested during the Phase I experimentation. MEAs will also be tested in short stacks to determine cell to cell performance variations. Uniformity of MEAs produced via APC will be compared to those produced without APC.

New stack hardware and MEA geometry were designed, fabricated and successfully demonstrated to test up to ten 50 cm^2 cells in different short stack configurations. Temperature and performance variation within the stack were then quantified to inform design improvements and testing protocols for Task 13.

Task 9.1 – Evaluation of Larger Scale Ultrasonically Sealed MEAs. The feasibility of the ultrasonic sealing process will be evaluated for larger size MEAs, typical of the size anticipated for automotive stacks. CATS researchers will design and build or procure the necessary ultrasonic horn as well as the single cell test fixture(s) necessary to test the resulting large MEAs.

A larger scale MEA format (140 cm^2, dubbed 'A1' size) was chosen as representative of a size consistent with automotive FC stacks, although relatively small due to equipment limitations. Manufacturing and test hardware was successfully designed, fabricated/procured, debugged (e.g., updated flowfield design) and demonstrated in preparation for Task 13 testing.

Task 9.2 – Ultrasonic Sealing Process Optimization. CATS researchers will conduct a designed set of experiments of the ultrasonic sealing process in order to develop optimum ultrasonic sealing processes for MEAs. The suitability of process parameters will be based on the ability to meet specifications for MEA thickness, acid content and performance. Initially, this optimization study will be performed for the standard 50cm^2 MEAs. Later in Phase III, a similar study will be performed for large size MEAs.

An investigation into ultrasonic sealing of high-temperature PEM MEAs with 50 cm^2 active area indicates that optimal performance is achieved by mild compliance in the anvil support material, high sealing pressure (but not enough to crush electrode) and low energy flux.

Task 9.3 – Annealing Process Optimization. CATS researchers will conduct a designed set of experiments to determine the optimal annealing process parameters for both thermally and ultrasonically sealed high temperature PEM MEAs. Annealing process parameters that will be varied include temperature and time. Weight and thickness of all MEAs will be measured both before and after annealing. A mix of component thicknesses will be tested. MEAs will then be tested for performance using standard protocols.

Based on a designed set of experiments and statistical analysis, higher temperature and longer times lead to greater loss of water (boiling off) and greater reduction in membrane thickness. Furthermore, higher temperature leads to the best MEA performance (~20% improvement). Lower soak time is best at the higher temperature; specifically, time can be cut by as much as 50% without adversely affecting MEA performance.

Task 9.4 – Evaluate Feasibility of Ultrasonic Sealing and APC for Low Temperature (Nafion) MEAs. CATS researchers will conduct experiments to determine the feasibility and benefits of using ultrasonics and APC for sealing of low temperature (Nafion) MEAs. A designed set of experiments will be conducted to determine optimum process parameters for LT MEA pressing, and comparisons will be made to LT MEAs pressed using traditional thermal pressing. If the APC experiments described in Task 8.1 are successful in reducing MEA variability and/or improving performance for HT MEAs, we will also attempt to use it for LT MEAs.

It is possible to ultrasonically bond low temperature Nafion fuel cells, although it requires higher energy flux and sealing pressure than high temperature fuel cells. Electrode composition plays an important role in performance for ultrasonically sealed low temperature cells suggesting that starting materials (e.g., gas diffusion electrode) may need to be customized for this process. Finally, ultrasonic bonding to dry Nafion may lead to better performance and quicker manufacturing.

Task 9.5 – Durability Testing of Ultrasonically Sealed MEAs. CATS researchers will conduct durability testing on MEAs produced using ultrasonic sealing. In order to perform an accelerated stress screening test, we will conduct start/stop cycling of MEAs in accordance with test protocols employed by BASF Fuel Cell. A comparison will be made of voltage degradation over time for ultrasonically sealed MEAs with that of thermally sealed MEAs. This task will be conducted on a time available basis depending on availability of test stands.

Ultrasonically sealed MEAs exhibited excellent stability under extreme start/stop operating conditions during 190 hour durability tests per our industrial collaborators test protocol. There was no cell voltage degradation observed during the entire test and the cell internal resistance change was minimal. No change in catalyst utilization was observed as well during the test duration.

Task 10.0 – Updated Cost Analysis. An updated MEA manufacturing cost analysis will be presented, similar to the one performed in Task 1.0. This analysis will be used to validate the Phase I cost savings estimates, and will be a critical decision metric for entry into Phase III (Task 11.0). A cost analysis of potential savings from ultrasonic welding will also be performed.

Based on new cycle times from Phase II experimentation, updated cost reductions are 76% for thermal pressing with APC and still 82% for ultrasonic sealing (with similar results for ultrasonic welding expected). Additional benefits of APC may be downstream in stack assembly, because more consistent MEAs are produced and faulty ones can be identified and removed.

Task 11.0 – Phase II program review. The focus of this review will be on the degree of success to which APC and ultrasonic sealing techniques improve the performance and uniformity of the resulting MEAs, and the degree to which ultrasonic welding and sealing improves process capacity and yield. The target goal capacity increase resulting from the use of ultrasonics for sealing of MEAs is tenfold.

Completion of Phase II was approved by DOE in October 2011.

Task 12.0 – Short Stack Testing. CATS researchers will test ultrasonically and thermally bonded high temperature MEAs, the latter with and without adaptive process control applied, in 5- and 10-cell short stacks. Thermal gradients and performance (polarization curves) in the stacks will be measured as a function of load, operating conditions, and the number of cells to better understand the causes of cell-to-cell performance variation. Performance will also be measured for 5-cell stacks consisting of ultrasonically and thermally bonded MEAs for steady-state durability and subjected to variable stack compression. Poorly manufactured MEAs will also be purposely included in the stack to show how this affects stack performance.

After an initial hardware debugging period, insulated FC stacks consisting of ten 50 cm^2 MEAs and a mid-stack cooling plate were successfully demonstrated as consistent and able to efficiently identify faulty cells. MEAs bonded thermally with APC and ultrasonically, which were tested in 10-cell stack, exhibited consistent temperature across the stack length and essentially identical performance to single cell tests. Stack testing also allows for efficient testing of individual cells.

Task 13.0– Testing of High Temperature MEAs with Larger Active Area. Ultrasonically and thermally bonded MEAs with larger active area (140 cm^2) will be tested to obtain statistically significant performance data for comparison with the 'standard' MEA size (50 cm^2). The areal temperature distribution of several single cells will be measured followed by standard performance testing to help explain performance differences between MEAs with different active areas and made using different bonding methods. Additional MEA characterization will include steady-state durability and accelerated start/stop testing of single cells. Finally, APC will be implemented for thermal pressing of 140 cm^2 MEAs followed by MEA testing to determine if the basic control approach is scalable.

High temperature PEM MEAs with larger active area (140 cm^2) made by ultrasonic and thermal bonding exhibited essentially identical performance, although issues with single cell test hardware degraded performance below that of the standard size (50 cm^2). However, testing performed by project collaborator BASF on an even larger ultrasonically bonded MEA (605 cm^2) made by RPI demonstrated better performance to ones made by thermal pressing and equivalent to BASF specifications.

Task 14.0– Quality Testing of Thermally and Ultrasonically Bonded High Temperature MEAs. CATS researchers will investigate the causes of excessive variation in ultrasonically and thermally bonded high temperature MEAs using more diagnostics applied during the entire fabrication and cell build process. The primary diagnostic, cyclic voltammetry or CV (change in capacitance), measures Platinum surface area along with in-situ and post impedance measurement (seal quality characterization) using a full frequency scan. XRF will also be used to measure Pt loading before testing. In addition, the team will purposely make poor quality MEAs to test the effectiveness of capacitance CV and impedance measurements for quality control.

CV scans (within a defined range of scan rates) of high temperature MEAs before and after heat treatment can be used to detect faulty MEAs for process and quality control purposes by providing resistance and capacitance values for individual cells both outside and within a stack.

Task 15.0– Expanded Cost Analysis. CATS researchers will perform a cost analysis that compares roll-to-roll manufacturing and discrete manufacturing (current) approaches for high temperature MEAs.

Continuous roll-to-roll ultrasonic sealing was deemed impossible due to the high-temperature membrane's visco-elastic properties, so discrete roll-to-roll manufacturing via a pin-on-belt transfer system (BASF proof-of-concept prototype) and a walking beam transfer system (current BASF production method) were considered. Although station-to-station cycle time in both cases could be reduced below the current value (10 sec), no additional experimental work was performed to confirm this. Furthermore, there are no clear cost advantages expected because of differences in capital and consumable costs between the two transfer approaches. Hence, the cost analysis from Task 10.0 is still considered valid.

Task 16.0– Ultrasonic Bonding Implementation Design Guidelines. CATS researchers will develop guidelines and analytical models that allow manufacturing engineers to design/specify tooling (horn, anvil, registration fixture) and determine optimal process parameters for bonding high temperature PEM MEAs using ultrasonics. The step-by-step design procedure will be explained in Quarterly reports and a journal article.

The current state of knowledge related to ultrasonic bonding of PEM membrane electrode assemblies was captured in a design guide and distributed to BASF and other fuel cell companies interested in using this technology (subject to licensing agreements). This design guide is provided in Appendix A for reference.

Task 17.0- Phase III program review. This review will focus on lessons learned during the program, and on an analysis of the benefits of applying ultrasonics to pressing high temperature PEM MEAs. Target values for reductions in manufacturing cost, cycle time, and energy savings (electrical) for only the MEA sealing operation are 70-75%, 75-85%, and 90%, respectively. These reductions are based on the following assumptions: manufacturing in high volume (i.e. yearly production of 500,000 automotive fuel cell stacks x 400 high temperature PEM MEAs per stack); output of 0.25 kW/MEA; and MEA baseline thermal bonding metrics of manufacturing cost at $1.50/MEA, cycle time of 100 seconds/MEA (sealing operation only), and energy savings of 0.69 kW·hrs/MEA = 2.78 kW·hrs (electrical)/kW (stack power). Each of the metrics will be achieved without adversely affecting MEA performance.

Completion of Phase III was approved by DOE in December 2013.

Project Activity Summary

Task 1.0 – Baseline and Analysis of Current Process.

CATS researchers completed development of a process flow chart that describes the current MEA manufacturing process, along with an MS Excel spreadsheet that will be used to record the detailed process information including process steps, methods, times, costs and the effect of alternative MEA architectures. The basic MEA assembly process for a 5-layer MEA (Anode, Cathode, Membrane, two sub-gaskets) is as follows:

- Laser cut inner window (ID) in sub-gasket
- Weld electrodes to sub-gaskets
- Seal membrane between electrodes (thermal sealing process shown in Figure 1)
- Laminate two sub-gaskets
- Laser cut outer perimeter (OD)
- Anneal MEA
- Inspect and package.

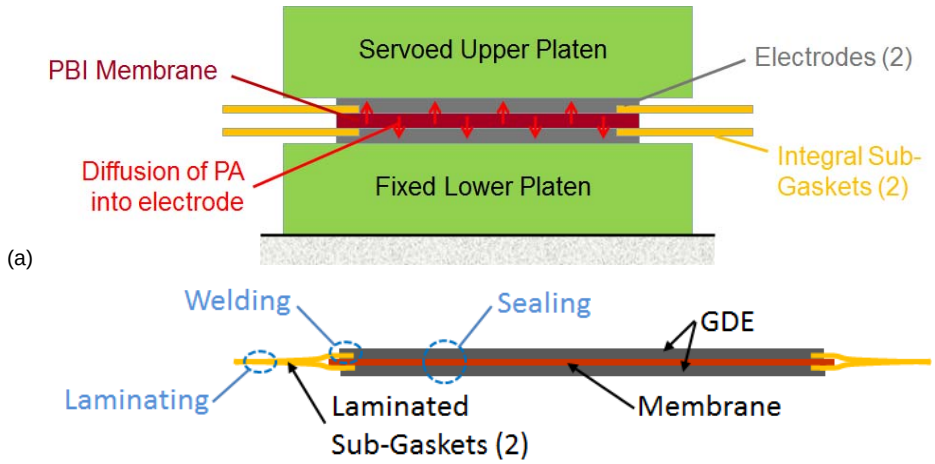

Figure 1: Schematics of (a) thermal sealing process for high-temperature MEAs and (b) assembled 5-layer MEA architecture.

An assembled 50 cm^2 MEA, standard size used for this research, is shown in Figure 1b (schematically) and Figure 2 (in fixture before OD laser trim). Following travel to the BASF facility in Somerset, New Jersey to observe the new Enhanced Pilot Line (EPL) that was commissioned during 2Q2009, researchers (including three industrial engineers) completed development of the aforementioned interactive Excel tool, which describes the entire MEA assembly process, and was used for our manufacturing cost analysis of the MEA thermal pressing process (i.e. baseline process). Assumptions used in the cost model include:

- Baseline cost analysis based on processes used at the Somerset, NJ plant
- Production facility will be located in the U.S.
- Current costs for utilities, services, and equipment.
- Only the sealing process is included.
- Production quantity of 500,000 automotive stacks per year.
- Each stack contains 400 cells and produces 80KW.
- Production facility operates two 8 hour shifts per day, 5 days per week, 50 weeks per year (2/5/50)
- Based on current data at the time, the MEA thermal sealing cycle time used Phase I cost analysis was 90 seconds for sealing plus 10 seconds for station-to-station transfer.

The actual MEA component material costs were not included in the analysis, since the researchers felt that they did not know now, nor could predict future costs of MEA materials for the target production volume.

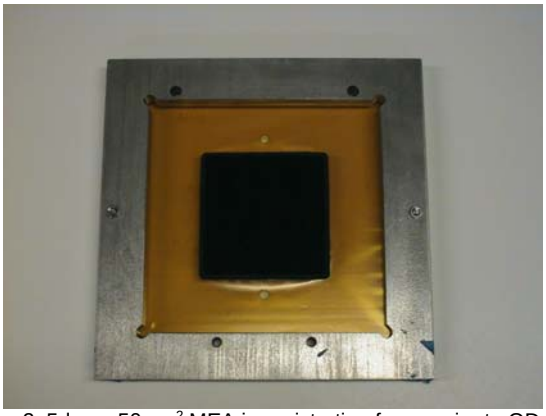

MEA ID#: A_____

Electrodes

Property	Anode	Cathode
Lot #		
ID #	A	C
Catalyst Loading (g/m^2)		
Thickness (μm) – 5X		
Average Thickness (μm)		
Compressive Stiffness (N/mm)		
Air Permeability		

Membrane (Celtec-P 1000)

Lot #		
Thickness (μm) – 5X		Avg.
PA Concentration (g/l)		
Ionic Conductivity (S/cm)		

Subgasket-to-Electrode Ultrasonic Welding

Operator		Date		Actual Value
Kapton Thickness (μm)				
Energy Flux (J/mm^2)				
Pressure (N/mm^2)				
Amplitude Booster	0.6X	1.5X	2.5X	
Anode Weld Thickness (μm) – 4X				
Cathode Weld Thickness (μm) – 4X				

MEA Sealing (Area = 5000 mm^2)

ULTRASONIC

Operator		Date		Actual Value
Energy Flux (J/mm^2)				
Sealing Pressure (N/mm^2)				
Amplitude Booster	0.6X	1.5X	2.5X	
Backer Support Hardness – Durometer (Type D)				

OR

THERMAL PRESSING

Operator		Date		Actual Value
Temperature (°C)				
Sealing Pressure (N/mm^2)				
Sealing Time (sec)				

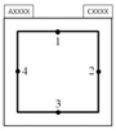

POST PROCESSING

Operator		Date				
Thickness (μm) – 5X						Avg.
Weight (g)						
Was MEA Annealed @ 160°C for 30 min. - Yes or No						
Thickness (μm) – 5X						Avg.
Weight (g)						

TESTS: Fuel Cell Testing Compression Testing Titration BASF Baseline Testing

Figure 2: 5-layer 50 cm^2 MEA in registration frame prior to OD laser cut (left) and traveller documenting all MEA manufacturing procedures (right)

The results of the first-order cost analysis performed concurrently with Task 3 are shown in Table 1. Categories included the 'Current Thermal' process used by BASF, the 'Optimized Thermal' process which reflects the 30 second thermal sealing time plus 10 second station-to-station transfer time used to effectively make MEAs (without APC), and the 'Ultrasonic' which reflects the 3 second bonding time plus 10 second station-to-station transfer time. The potential manufacturing cost savings for the sealing operation alone is 57% using optimized thermal without APC and 82% using ultrasonics. The use of ultrasonics for sealing of MEAs holds the potential for major reductions in MEA manufacturing costs by greatly reducing the sealing (electrodes to membrane) costs and providing similar reductions in welding (electrode to sub-gasket) costs.

Table 1: Phase I Manufacturing Cost Estimates

	Current Thermal	Optimized Thermal	Ultrasonic
Cost Category			
Capital Depreciation	$0.0896	$0.0319	$0.0071
Tooling	$0.0521	$0.0463	$0.0416
Labor	$0.0386	$0.0137	$0.0080
Electricity	$0.0579	$0.0206	$0.0002
Chilled Water	$0.0293	$0.0104	$0.0000
HVAC (CapEx & Operations)	$0.0009	$0.0007	$0.0000
Maintenance	$0.0121	$0.0043	$0.0010
Materials			
Space	$0.0041	$0.0015	$0.0004
Disposal Costs	$0.0896	$0.0319	$0.0086
GRAND TOTAL per MEA	$0.3741	$0.1612	$0.0668
GRAND TOTAL per KW	$1.4965	$0.6446	$0.2672

TOTAL MANUFACTURING COST REDUCTION	n/a	-56.93%	-82.14%

Task 2.0 – Comparison of Current and Proposed MEA Pressing Processes.

This task was performed concurrently with Task 1.0, and the results of the cost comparison are also shown in Table 1. Clearly, the potential for MEA manufacturing cost savings by the use of ultrasonics is much greater than for the implementation of APC. APC will primarily benefit the down-stream stack assembly process.

Task 3.0 – Baseline Process Testing.

This task, one of the most important for the entire project and time-consuming for Phase I (i.e. Tasks 1-7), sought to establish baseline performance testing of 50 and 18 cm^2 MEA formats thermally and ultrasonically sealed using thermal pressing and ultrasonics. This required characterizing incoming material from the same lots, sealing MEAs using these two processes in a designed set of experiments to establish the downstream effects and sensitivities of process parameters, and to experimentally characterize these effects measuring physical and electrochemical properties of the resulting MEAs and also their performance via single cell testing.

50 cm^2 MEA Testing Only: Although testing of both 50cm^2 and 18cm^2 size MEAs was proposed, the smaller size was eliminated for a number of reasons:

- The proposed budget did not support the purchase of several sets of 18cm^2 size test hardware in addition to the 50cm^2 size hardware, since their costs were significantly more than what was estimated
- After consulting with BASF Fuel Cell (BFC) scientists, we decided to perform a minimum of 24 hours of testing on each MEA rather than the 10 hours (original plan) to provide a better measure of the true performance of the MEAs. However, this limited the number of tests we could perform in the available time.
- We decided to include one additional process variable in our initial design of experiments. This also increased the amount of testing that will be required, but this increase was limited by the availability of test stands (2).

Incoming Material: The experimental work that was defined required a significant amount of material. All MEA component materials required for the Phase I research were provided by BASF Fuel Cell, including PBI membrane, anode, cathode, sub-gasket, tooling barrier materials; and cell gasketing. Nafion used in early MEA testing was available in-house.

Manufacturing and Test Equipment: Tasks 3 (along with 5 and 6) required procurement and installation of various pieces of equipment and custom-designed hardware. Basic performance testing of MEAs required the following pieces of equipment.

- A fuel cell test stand identical to the CATS existing existing test stand and a pair of test cells were purchased from Fuel Cell Technologies to handle 50 cm^2 cells and short stacks. Both test stands were upgraded to the same hardware and software configurations to accommodate zero volt loading capabilities for single cells and stacks producing up to 60 VDC at 800 W maximum power, and software was developed to allow several automated test protocols to ensure testing consistency throughout the DOE project.
- A PARSTAT 2273 state-of-the-art potentiostat was purchased for electrochemical impedance spectroscopy and cyclic voltammetry measurements.
- An Agilent 4338B milliohmmeter was acquired to measure membrane protonic resistance and contact resistances at a constant 1 kHz frequency.
- One piece of equipment that was specially designed and fabricated for this project was a precision thickness gauge, consisting of a high-precision LVDT and digital readout, for measuring all incoming material and pressed MEAs with micron accuracy.

The experimental work required customization of existing unit process equipment and the design/fabrication of special tools and fixtures. Specific modifications made to MEA sealing equipment are described below.

- The ultrasonic welder was retrofitted for both higher pressing loads and compression control including: (1) a large bore and short stroke air cylinder was mounted to press MEAs up from underneath the ultrasonic horn at a higher load than the stock machine and (2) the addition of physical hard stops to allow for variable compression percentages similar to the current manufacturing process.
- The thermal press was retrofitted for accurate compression control by designing, fabricating and mounting a set of four rigid hard stops (vertical posts) that provide gap height control between the heated pressing tools with 10-15 μm resolution.

Specialized tooling for cutting and sealing MEAs was also specified and procured including:

- 1.5 and 2.5X ultrasonic boosters along with 25, 63 and 127 cm^2 square horns with different surface roughnesses ranging from polished to medium and fine female knurled.
- Steel rule dies to enable cutting of sub-gasket ID and OD, and electrodes.

All aspects of MEA component manufacturing and pressing required the design and fabrication of custom tools and fixtures including the following.

- Ten pairs of matching stainless steel frames (see Fig. 1) were designed to precisely align anode and cathode gasket/electrodes during MEA pressing and the MEA assemblies to all manufacturing stations (seal and laser cut).
- An alignment fixture was designed to fit around the stainless steel MEA hot press tooling donated by BASF Fuel Cell to align MEA frame sets to the tooling. A similar fixture was also designed and fabricated from 316 stainless steel for ultrasonic sealing.
- A laser cutting fixture was designed and fabricated with a stainless steel honeycomb MEA support surrounded by a stainless steel frame to precisely align the MEA frame sets during laser cutting of the gasket opening and final outer dimensions of the completed MEAs.

Manufacturing and Experimental Operating Procedures: Prior to running any major experimental investigations, operating procedures were developed for all incoming material qualification, manufacturing operations, and MEA performance evaluation based on acceptable industrial practice. These procedures are described in more detail below.

- All incoming materials used in the manufacture of the MEAs were measured for thickness. These measurements were made in five locations (four corners and center of square) on both the membrane and the anode and cathode electrodes, averaged, and monitored for consistency.
- A MEA traveler, shown in Figure 2, was developed to capture incoming material condition, and identify operator information and lot number of incoming components.
- A detailed procedure for sealing MEAs in the thermal press using hard stops to control compression instead of pressure control was developed and documented.
- A repeatable documented procedure for ultrasonic MEA sealing was developed to cover the proper techniques and methods to change the ultrasonic horn and tooling, align the horn and anvil, interact with the machine controller, seal MEAs, and shutdown the machine.
- A custom program was developed to ensure consistent laser cutting of MEA components required by the DOE program tests.
- MEA performance is inferred from a polarization curve (current density vs. voltage measurement) obtained from the FC test stand. Current density at 0.6 V and 0.4 V were identified as output variables, and ANOVA analysis was performed on data from design experiments (discussed later) to identify statistically significant input parameters.

Significant effort in Phase 3 was spent designing experiments, preparing MEA components and sealing MEAs under different manufacturing conditions, assessing the resulting performance, and drawing useful conclusions. Each set of experiments is described in detail below.

Sealing of Low-Temperature MEAs – Early in Phase I and with DOE support, the project team thermally and ultrasonically sealed a small number (8) of low-temperature MEAs with a 10cm^2 active area using BASF electrode and Nafion 117 membrane. After a 1 hour burn-in, polarization curves were obtained for the MEAs at 30°C and 80°C. The main conclusions from his study include:

- Thermal sealing results generally match those in the literature with the exception of pressing time > 1 min. (no improvement)
- For ultrasonic sealing, higher pressure improved performance at 30°C, but not at high 80°C.
- Ultrasonically sealed MEAs performed better than thermally sealed ones at low operating temperature while the reverse was true at high operating temperature.
- Ultrasonically sealed MEA performance is expected to improve by performing simple process optimization (e.g., DOE).
- Cycle time for hot pressing is ~1 min., whereas it's ~1 sec. for ultrasonic sealing.

Thermally vs. Ultrasonically Sealed MEAs - The objective of both sealing methods is to laminate the PBI membrane between two layers of GDE. The ultrasonic sealing procedure was in the order of 100's of milliseconds while thermal sealing required 1-2 minutes to achieve the required % compression. Annealing at 160°C for 30 minutes was required for all the ultrasonic MEAs to reach the specification curve performance, as shown in Figure 3. Without annealing, excess acid is available in the GDEs, thereby causing high resistive losses and poor gas transport in the MEA.

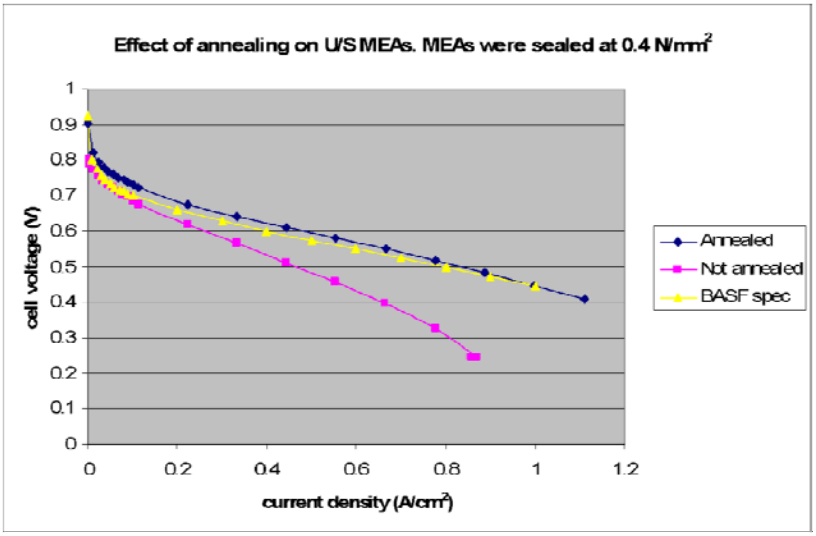

Figure 3: Effect of annealing on ultrasonically sealed, high-temperature MEAs (Note: BASF spec refers to the companies production MEA that is sealed thermally)

Sealing of High-Temperature MEAs – A full-factorial set of 'screening' experiments was planned and executed for both thermal and ultrasonic sealing of high-temperature MEAs followed by statistical analysis of the results. A baseline set of experiments were run to determine working range of parameters for thermal sealing. These experiments made it clear that hard stops rather than pressure control are required for repeatable MEA manufacturing. Effective values for temperature, compression and time were established. Baseline ultrasonic sealing of MEAs was conducted in parallel to determine parameters for the minimum sealing pressure and energy flux settings necessary to result in an MEA that was physically sealed and would work.

Full-factorial, two-level designed set of experiments with two replicates were conducted for thermal and ultrasonic sealing using the process parameter ranges previously established. For thermal pressing, sealing time (15 and 30 sec), sealing temperature (140 and 160°C), % compression (15 and 25% of total thickness), and annealing condition (160°C for 30 min. in air or not) were varied randomly based on a 2^4 experimental matrix. In general, performance of thermally sealed MEAs was comparable to BASF MEA specifications (also thermally sealed) as shown in Figure 4. For ultrasonic sealing, energy flux (0.4 and 0.6 J/mm^2), sealing pressure (0.4 and 0.8 N/mm^2), amplitude booster (1.5 and 2.5X), and support material stiffness (90A durometer and steel) were varied randomly based on another 2^4 experimental matrix. All ultrasonically sealed MEAs were annealed, because excess acid is available in the GDEs causing high resistive losses and poor gas transport in the MEA. All MEAs were clamped in cells to 20% compression with PFA gaskets, incubated at 0.2 A/cm^2 with H_2/Air for 18 hours, and polarization curve measured (0-5A

with 0.5A intervals and 5-50A with 5A intervals with 2 min. delay at each current level) after 18 hours. Performance metrics include current densities at 0.4V and 0.6V, and cell resistance (mohms-cm^2). In general, performance of ultrasonically sealed MEAs (annealed) was equal to or better than BASF MEA specifications (thermally sealed), as shown in Figure 5.

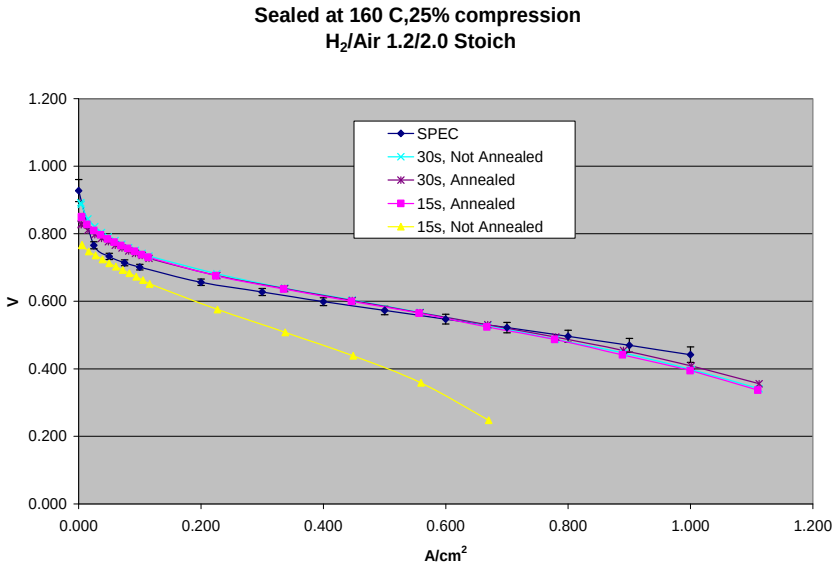

Figure 4: Polarization curves showing performance of pre- and post-annealed thermally sealed MEAs compared to BASF specifications.

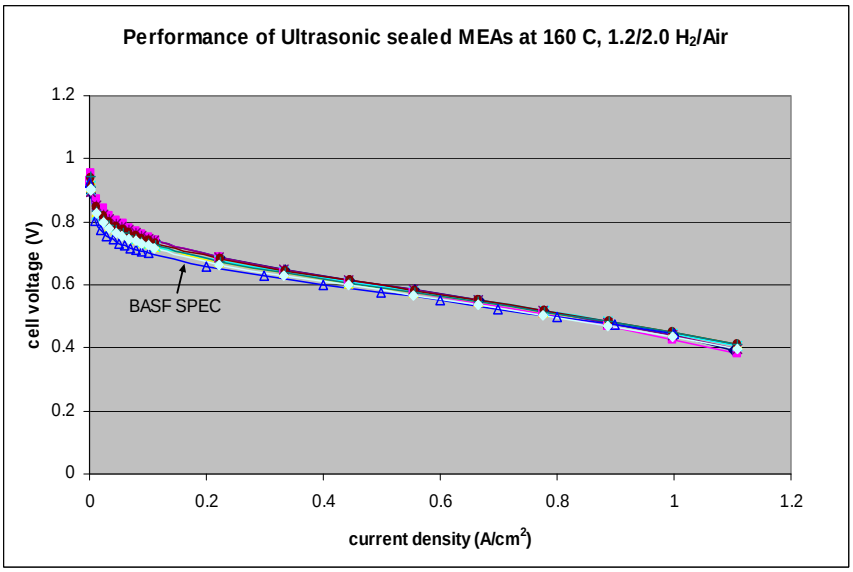

Figure 5: Polarization curves showing performance of post-annealed ultrasonically sealed MEAs compared to BASF specifications for thermally sealed production MEAs.

Analysis of Variance (ANOVA) was conducted on the experimental results. For thermal sealing, annealing was clearly the statistically significant process parameter affecting MEA performance, i.e. annealing is required. For ultrasonic sealing, sealing pressure (lower is better) was the statistically significant parameter based on polarization curves and support material stiffness (lower is also better) to some degree. It is believed that higher sealing pressure can result in destruction of GDE pores, thereby inhibiting gas and acid transport. With regards to cell resistance, amplitude booster (more amplitude is

better) was the only statistically significant parameter. A higher booster means more displacement resulting in better MEA contact and low cell resistance.

Feedback from Industrial Collaborator – In July 2009, RPI researchers gave a presentation on preliminary results of our screening experiments to Thomas Schmidt, Director of Research for BASF Fuel Cell. Performance curves for both thermal and ultrasonically pressed MEA were evaluated. Also, materials from the same production lots used in our experiments were provided to BASF personnel, and they produced MEAs for comparison with those we had produced. As a result, several conclusions were reached by Dr. Schmidt, including:

- The membrane being used in our experiments was too thin and had an adverse impact on our test results.
- The anodes used in our experiments showed low performance under reformate/air. Further investigation revealed that this material had not passed BASF internal QC standards.

Although these issues did not invalidate the major conclusions reached in our tests because the relative differences from process parameter variation remain, BASF promised to provide new materials that had passed QC for future rounds of experiments.

Additional Thermal Sealing Experiments – In addition to the designed experiments previously mentioned, other thermal sealing experiments (i.e. press MEA and test) were performed to verify different hypotheses posed by members of the project team. Each set of experiments and the general findings are described below.

- MEAs were sealed by cold pressing (i.e. compressing anode-gasket/membrane/cathode-gasket to a particular percent compression with room-tempeature tools) to examine the effect of heat in the sealing process. The MEAs made using this method performed surprisingly well, although the polarization curves were slightly worse than those made with the heated tools. The long-term performance of cold-pressed MEAs will have to be tested.
- Through-thickness temperature measurements vs. time were performed by placing small thermocouples at the different material interfaces of a MEA (between the barrier material and both electrodes, and between the membrane and the electrodes) and measuring the temperatures over time as the MEA was sealed in the heated press. The results of these tests showed a rapid increase in the temperature of all of the interfaces up to the surface temperature of the tool, which took approximately 10 sec., then a gradual increase in temperature over the next 20 seconds to the final temp of either 140°C or 160°C.
- Experiments to determine MEA weight loss during pressing were performed to determine the relationship between MEA compression and weight loss during sealing. MEA components were weighed and thickness was measured prior to and after pressing to determine the weight loss and compression levels. This resulted in a relationship were the higher the compression level, the more weight is lost by the MEA. Results were used to begin validating a compression model for thermal pressing.

Additional Ultrasonic Sealing Experiments – Additional ultrasonic sealing experiments were also performed based on hypotheses posed by team members. These experiments and their results are described below.

- Similar to thermal sealing, through-thickness temperature measurements vs. time were performed at the membrane/electrode interfaces on the upper and lower side of the MEA during the few seconds of the ultrasonic sealing process.
- Preliminary testing was conducted to successfully demonstrate that ultrasonic MEA sealing with metal plates placed between the electrodes and the horn and anvil was possible. This was a precursor to the APC testing that will allow for monitoring the in situ changes in the resistance of the MEA during the ultrasonic sealing process.
- Tests are being conducted on laminating of subgasket material together.
- A few MEAs were assembled and then ultrasonically annealed by multiple applications of pressure and energy with an absorbent material placed on the outsides of the MEA to wick away the expelled water. The desired physical thickness loss and weight loss percentages were achievable, but the polarization curves of the initial samples were substandard. Further work was proposed for Phase II.

- The pull strength of 128 ultrasonically welded electrode/gasket specimens (two each in the machine and transverse directions for 32 samples) was compared to thermally welded specimens using similar test parameters. The general finding was that ultrasonically welded samples meet or exceed the strength of thermally welded samples.

Task 4.0 – Model Development.

Significant progress was been made on modeling of the relationships among material properties and sealing process parameters. Empirical models, specifically linear regression models are available from the analysis of variance performed as part of Task 3, are readily available, but these are only useful for process optimization within a limited range of process parameters and offer little insight into the process physics. Instead, the focus of this task was primarily on developing multi-physics transient and structural thermal models of thermal and ultrasonic sealing.

Material Properties: Thermal and structural modeling properties were measured for both membrane and electrode materials. A combination of Thermo Gravimetric Analysis (TGA) and Differential Scanning Calorimeter (DSC) testing was conducted on membrane and electrode samples to determine the Specific Heat (C_p) values for these materials. Thermal conductivities (k) were experimentally measured for multiple electrode and membrane samples also. Membrane and electrode test samples were tested in a Dynamic Measuring Analysis (DMA) machine to estimate the storage (E') and loss (E'') moduli of the materials, which was used to predict internal heating in the ultrasonic sealing model.

Modeling of MEA Thermal Sealing: A transient FEA model of sealing with a thermal press, where heating is due to external conduction at electrode outside surface, was developed using COMSOL and verified with in-situ temperature measurements. Transient temperatures at each material interface were measured with small thermocouples connected to a datalogger, as shown in Figure 6a and 6b, respectively. A typical FEA thermal plot is seen in Figure 6c. Although there is rapid rise in temperature initially, the final $\Delta T=15°C$ requires >1/2 minute as the thermal mass of the platen equilibriates. Figure 6d shows the good agreement between model and experimental results.

(a)

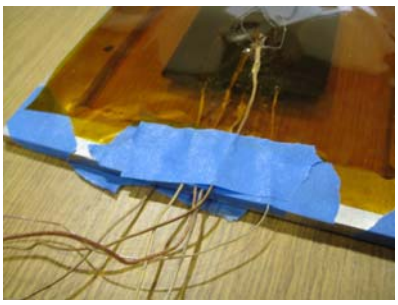

(b)

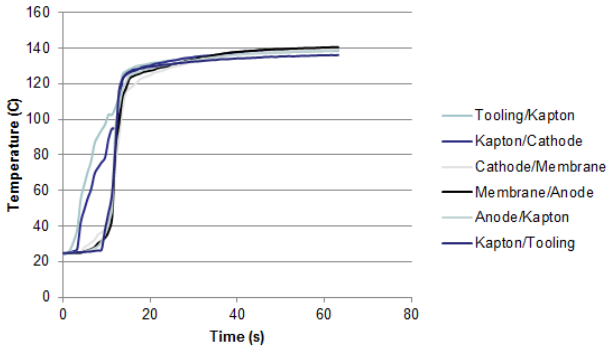

(c)

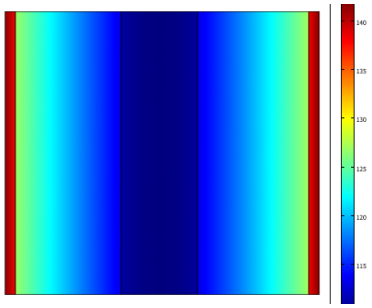

(d)

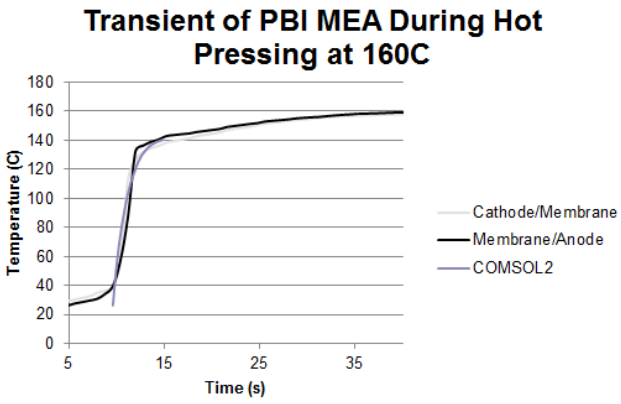

Figure 6: (a) Thermocouples located at each material interface prior to thermal sealing, (b) plot of transient temperatures due to 140°C thermal press platens, (c) typical FEA thermal response 2-D plot of MEA cross-section and (d) temperature response of model compared to experimental data.

Modeling of MEA Ultrasonic MEA Sealing: The MEA ultrasonic sealing process, where there is internal heat generation at membrane/electrode interfaces, was modeled using a combination of vibration and FEA theory. The vibrational model – masses coupled in series with a spring and spring/damper in parallel for each of the three layers (GDE, membrane, GDE), as shown in Figure 7a – had 6 degrees of freedom, *x1→x6*. Model input is a high frequency (20 kHz) and low amplitude (20 μm) vibrational signal along with a constant preload (pressing pressure) from the ultrasonic horn. Because of the extreme ratio of the model spring stiffness to the model mass, the natural frequencies are very high. This necessitates the use of a stiff computational solver. Heat dissipated by the dampers in real time is used in a COMSOL FEA transient thermal analysis with internal heat generation at each of the MEA material interfaces (GDE/membrane × 2).

Temperatures at each of the material interfaces during ultrasonic sealing of a MEA were measured using miniature thermocouples at the outside of the top and bottom electrodes and at the interfaces of the membrane and electrodes. The temperature plots in Figure 7b show rapid rises at the GDE/membrane interfaces.

Although several symbolic solvers and a numeric solver were used to model the ultrasonic bonding process, none have been successful. This shows the complexity of solving the model. It is theorized that the wide disparity in order of magnitude between the parameters, as well as the number of degrees of freedom, is simply too complex to solve at this time; hence, further development was abandoned due to time and resource constraints.

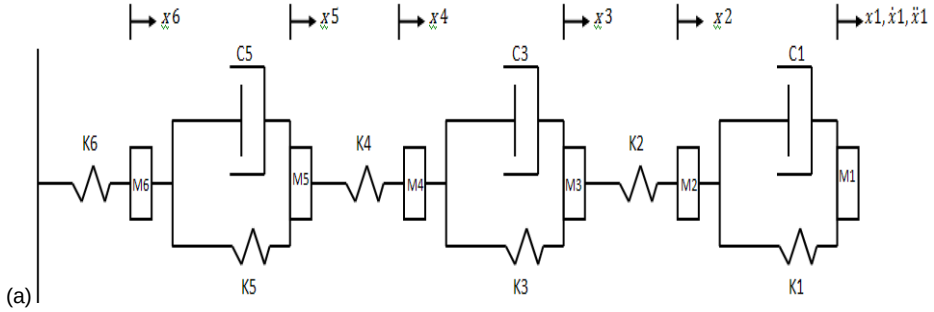

(a)

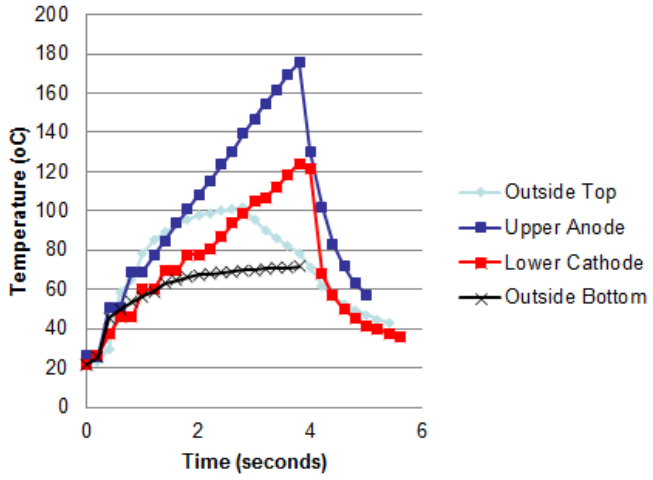

(b)

Figure 7: (a) Three-layer (GDE, membrane, GDE) vibrational model of heat dissipation from ultrasonic sealing of MEA and (b) temperature response

Modeling of MEA Mass Loss as Function of Compression: A simple conservation of volume model was proposed for describing the behavior of water/acid excreted from the membrane into the electrode

during compression by thermal or ultrasonic sealing. Since the difference in stiffnesses between electrode and the softer sol-gel membrane is at least an order of magnitude, it is believed that the water- and acid-entrained in the PBI matrix (i.e. membrane composition) essentially permeates the porous electrode due to high compression. MEAs were pressed at 160°C and the weight lost during pressing was measured. The experimentally determined relationship between percent compression and weight loss during pressing is shown in Figure 8. Preliminary compression tests have shown that MEA weight loss beyond a certain threshold (i.e. beyond holding capacity of electrode) is a function of % compression, although other physical effects may have to be captured in the model is developed (e.g., loss of water due to boiling, addition of water due to membrane hydrolyzation with humid air).

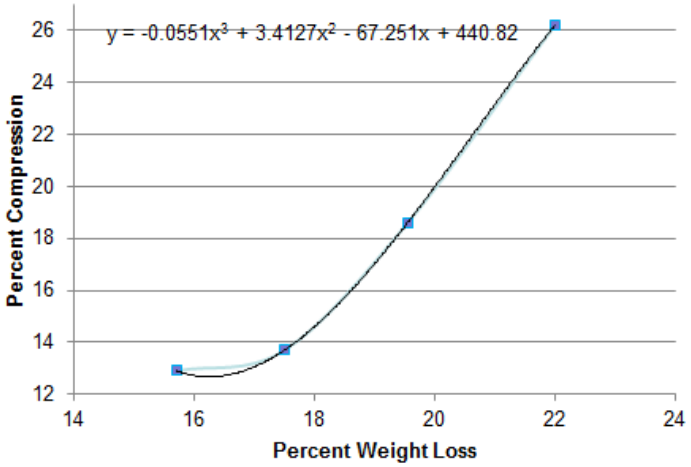

Figure 8: MEA weight loss as a function of % compression for MEAs thermally pressed at 160°C.

Task 5.0 – Development of In-situ Sensing Techniques.

Team collaborator Arizona State University (ASU) attempting to apply Electrochemical Impedance Spectroscopy (EIS) without reactant gasses as an in-situ measurement technique for real time adaptive process control (APC). EIS is used to characterize the area and integrity of the contact between electrode and membrane. The ASU team experimented to determine if the EIS measurement taken without reactants is a valid measure of MEA performance in a stack. However, this approach was deemed a long shot as the time constant for a full frequency sweep may be too long for use as a control method.

CATS researchers then investigated the use of simple DC resistance measurement, combined with high precision position (thickness) measurement as an indication of MEA cell performance. Unfortunately, MEA performance did not correlate with DC resistance. It can, however, serve as a simple GO/NO GO screening method to identify MEAs that should be rejected due to shorting, both as a final inspection after MEA assembly, and prior to the assembly of stacks.

As an alternative to ESI and DC resistance, CATS researchers successfully used single frequency, (1 KHz) AC impedance in-situ measurement as a predictor of MEA performance. Figures 9 shows plots of impedance and the associated phase angle for measurements taken in our commercial press. We find that the phase angle (ratio of impedance to capacitance) has the closest correlation to MEA performance. Experiments were conducted on the implementation of this technique as a method of feedback control for the pressing process using our precision commercial press. Initially, the adaptive process control technique was demonstrated with a “man-in-the-loop” technique.

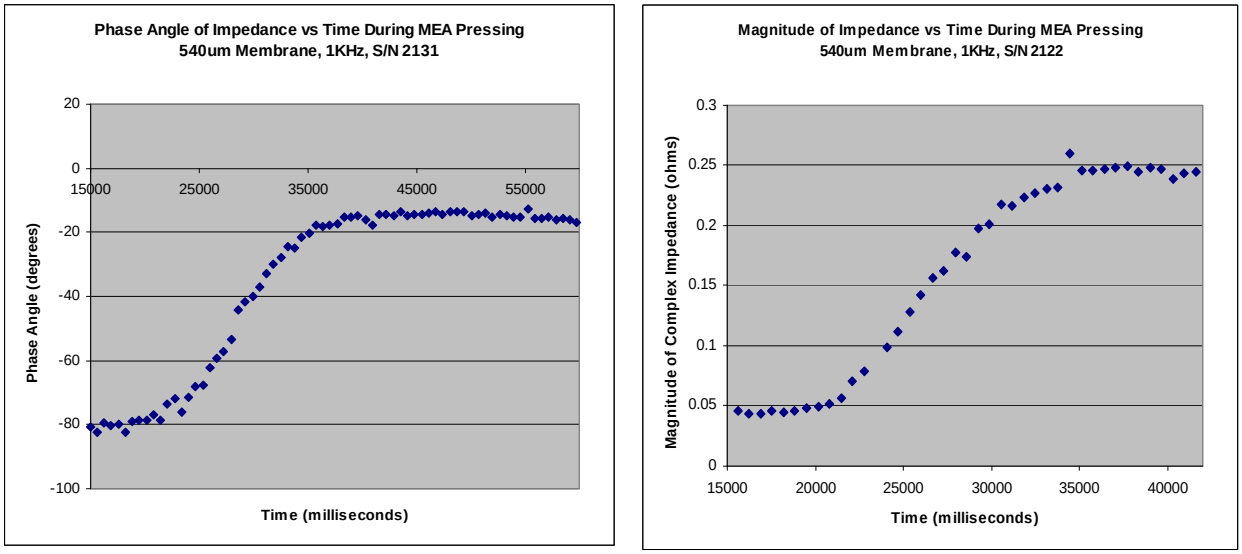

Figure 9: Plots of phase angle (left) and associated impedance magnitude (right) at 1 kHz frequency AC impedance measurement.

Task 6.0 – Controller Development.

As mentioned in the Task 5, a component of in-situ measurement of AC impedance, i.e. phase angle, correlates with MEA performance and may provide a means to apply real time APC for thermal pressing. For the envisioned closed-loop APC system shown in Figure 10, a milliohmmeter reads the complex impedance of the MEA at 1KHz. This Information from is fed to the press controller to control the pressing time; specifically, to determine when to stop pressing the MEA. The goal of APC is to produce uniformly performing MEAs. In addition to its usefulness in APC of MEA manufacturing, in-situ AC impedance measurements promise to be a valuable tool for screening and matching MEAs before assembling them into a stack.

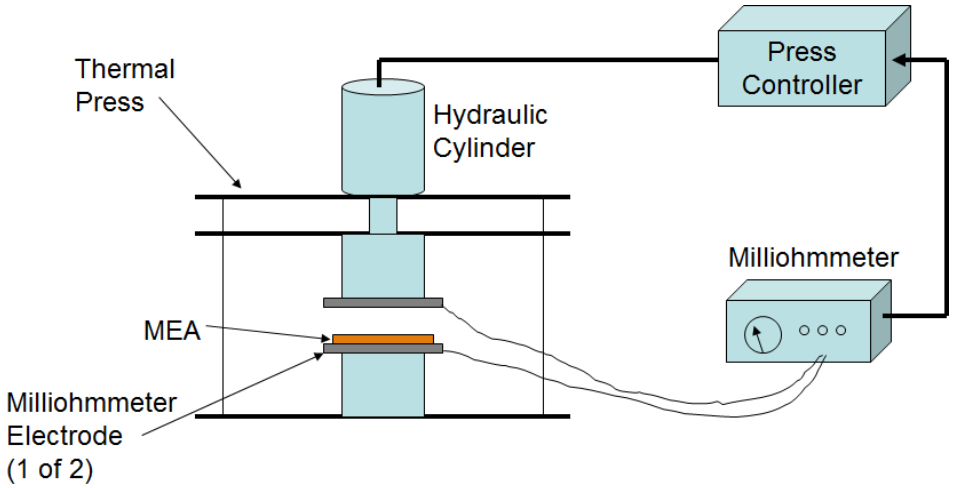

Figure 10: Schematic of physical instrumentation and feedback control for in-situ impedance measurement

CATS researchers conducted initial performance tests of twelve thermally pressed MEAs using APC with the measured phase angle of a 1KHz impedance signal. Automation of this approach was demonstrated by the “man-in-the-loop” method. Figure 11 shows an apparent tight cluster of performance of resulting MEAs when using a phase angle of -18° (based on Figure 9) as a trigger point for stopping the pressing process. When this method was used, researchers were able to achieve a 60% reduction in process cycle time compared to the standard thermal process.

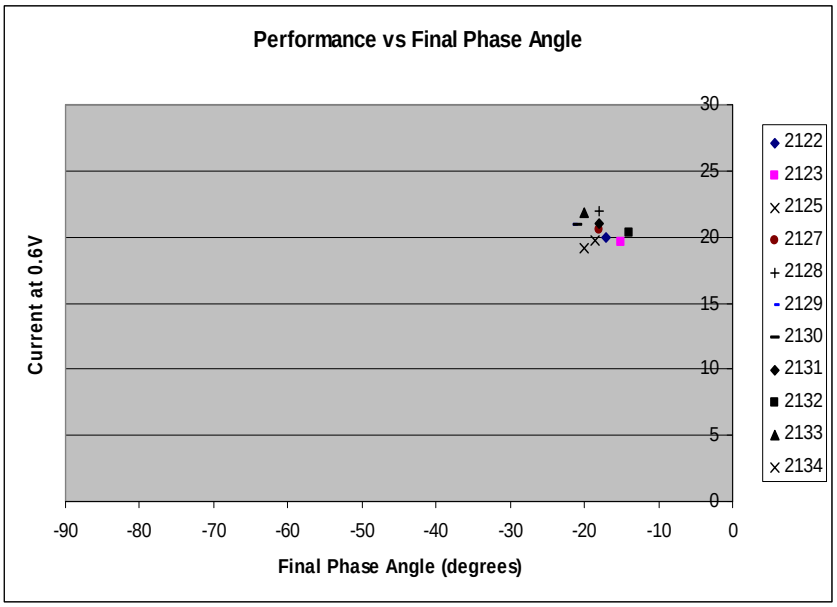

Figure 11: Plot showing uniformity of MEAs (i.e. current at 0.6V) pressed using APC

Task 7.0 – Phase I program review.

The Phase I program review was conducted on November 12, 2009, and RPI CATS was instructed that entry into Phase II had been approved by DOE on December 2, 2009.

Task 8.0 – APC Implementation.

Implementation of APC methods were studied in this task as a means to reduce process variability and cycle time for the thermal bonding of membrane electrode assemblies (MEAs) by halting the operation at an optimal cycle time. During the bonding process, anode and cathode electrodes are bonded to a phosphoric acid/PBI membrane forming the core components of the fuel cell. The thermal bonding cycle ends when a measured process control parameter reaches an optimal value. Furthermore, a novel quality control metric is being studied in which the electrochemical capacitance is quantified in a few seconds. This quality control process can be used to access MEA performance prior to cell assembly.

APC Implementation with Updated Control Metric: Controls engineers at PMD, builder of the precision thermal press used for this research, were consulted concerning the controls software and hardware architectures of the press. Consequently, software modifications to the press needed to access necessary data from press instrumentation including an LVDT for press position, load cell for calculating applied pressure, and the multi-zone temperature controller were completed. This information, in addition to complex AC impedance measurement, was used in our experiments on the application of APC to MEA sealing. Furthermore, modifications needed to electrically isolate the press tooling from the press structure, and to collect complex AC impedance measurements were made.

The first set of experiments using the new hardware and software configuration on the commercial press focused on documenting the AC impedance response for MEAs were sealed at 160°C, 25% compression and a range of pressing times: 30, 10 and 5 seconds. A second set of MEAs were pressed at room temperature with 25% compression for 30 seconds to observe the complex impedance behavior as a function of sealing temperature. The experimental setup involved placing stainless steel shim stock on each side of the MEA components to be sealed, to serve as electrodes, as shown in Figure 12. An Agilent 4338B milliohmmeter was then connected to these electrodes and was used to measuring the complex AC impedance of the MEA at 1 kHz during pressing. Electrical isolation of the MEA from the sealing tool was provided by placing Kapton™ film on either side of the stainless steel shim stock.

Figure 12: PMD precision thermal press modified for APC.

Fuel cell performance evaluation of all the MEAs was conducted after burn in at 160°C and 200 mA/cm^2 for 18 hours, followed by polarization curve measurements. The average of fuel cell measurements at various sealing times and the cold pressing is shown for a full range of current density in Figure 13a, and a close up of the activation overpotential region in Figure 13b. All the MEAs pressed at times <30 seconds exhibited a lower activation overpotential region which indicates higher acid content at the interface for these MEAs and will be confirmed by titration studies. The significant finding is that reducing the sealing time to 5 seconds produces MEAs that perform the same as the baseline MEAs that are sealed for 30 seconds.

(a)

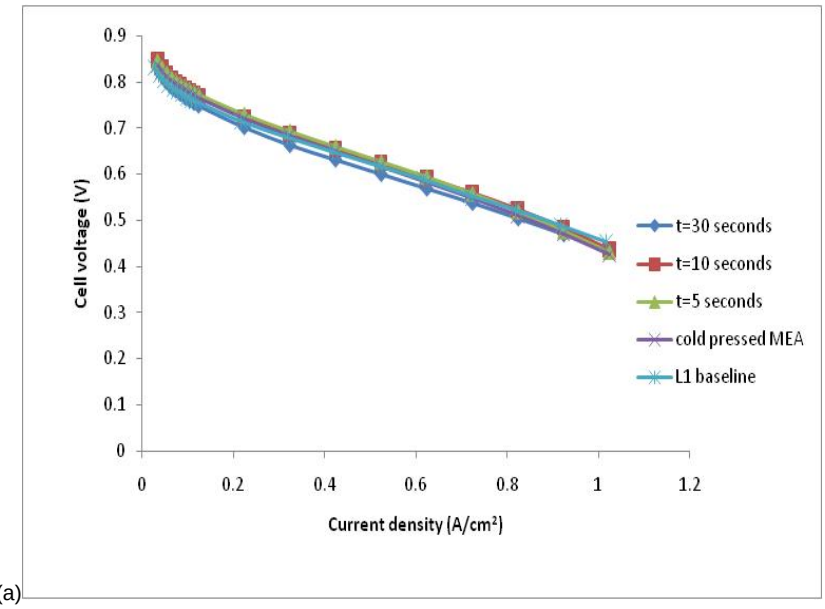

(b)

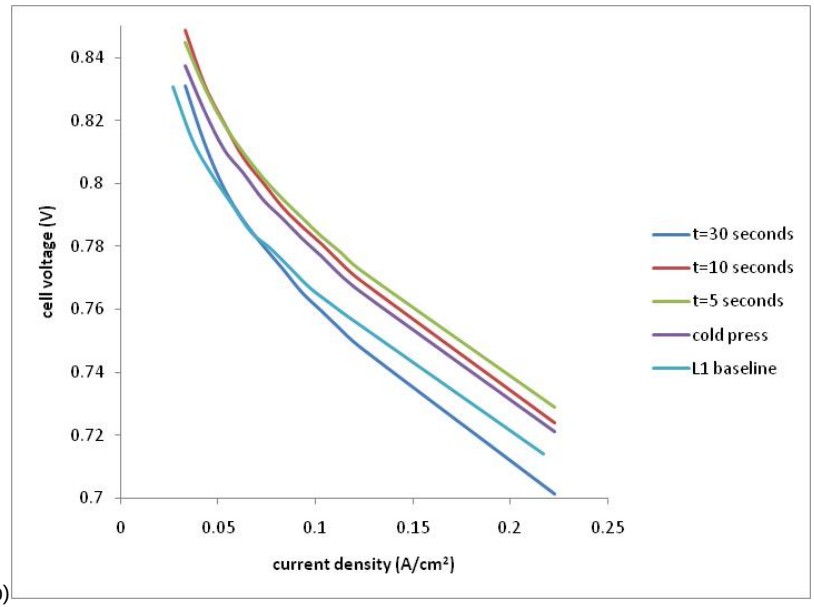

Figure 13: Polarization curves for MEAs thermally pressed for three different cycle times and two different temperatures. Baseline (L1 = 50 cm^2 size) data also included.

The electrochemical impedance at a frequency of 1000 Hz was selected as the process control parameter for the thermal press. The 1000 Hz impedance provides an indication of cell performance in a time period that is orders of magnitude less than the 5 second time it takes for the control criterion to be satisfied. The process control parameter must be acquired faster than the cycle time to allow the thermal bonding process to be controlled by the measurement.

As a result the aforementioned experiments, we identified a characteristic in the impedance plot which is believed to identify the conditions at which formation of the electrochemical cell is accomplished. This indicates when MEA is "done", and to stop the pressing operation. From these experiments, it appears that pressing longer than necessary actually degrades performance. Past experience with in-situ impedance measurements (Task 6) pointed to the phase angle of the complex impedance as the important MEA quality metric. However, during the aforementioned round of tests, we looked beyond the phase angle to a 2-dimensional impedance plotted graphically during pressing. This data visualization showed us that the impedance starts out large and quickly converges to a small nominal value after which it changes very slowly. Our experiments have shown that this convergence signifies the formation of the electrochemical cell. Before the impedance reaches the nominal value, the components have not yet been effectively sealed. This nominal value of complex impedance is not necessarily the same for every cell, and its magnitude may indicate some quantitative information about the performance of the cell. The method, at that point, could qualitatively show that the cell will operate.

At this point, the APC for thermal pressing had been proven out using the new hardware control system. Figure 14 shows the polarization curves for two representative MEAs produced using our new hardware and software controls, compared to the BASF average specification curve. Adaptive process controls were used to stop the pressing cycle once the derivative of the complex impedance went to zero. In both cases shown below the actual pressing cycle time was less than five seconds, an order of magnitude less than the current thermal press cycle time.

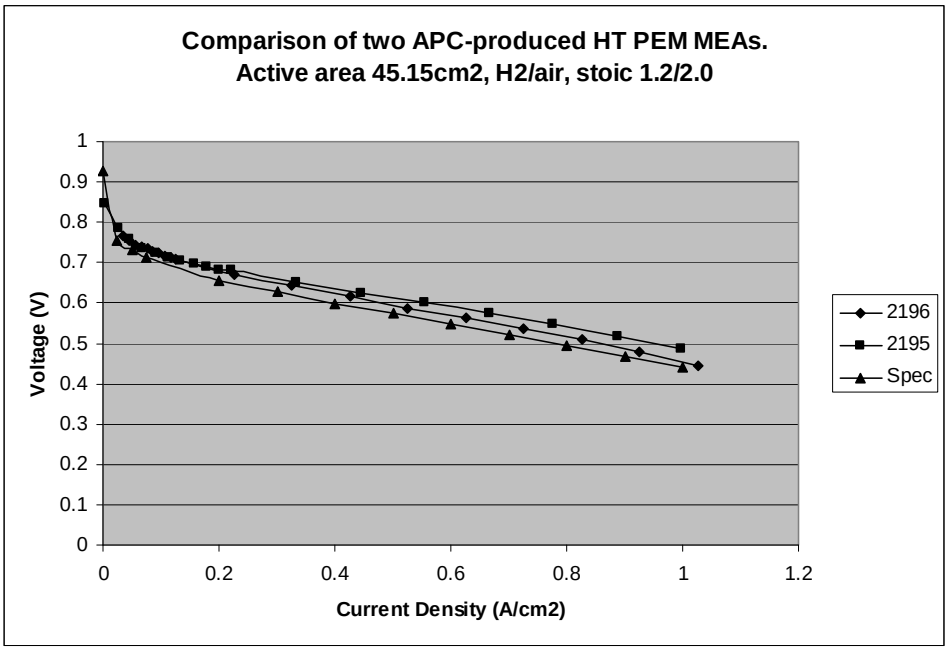

Figure 14: Comparison of two MEAs thermally pressed with APC to BASF specification

The electrochemical impedance at 1 kHz decays as the thermal press compresses the MEA. The impedance change during the thermal bonding process with APC implemented is plotted in Figure 15. It can be seen that the impedance drops to a minimum within 5 seconds of contact between the press and the MEA. The resistance slowly climbs following the decline of impedance to a minimum. When the derivative of impedance as a function of time hits zero the press disengages and the cycle is over.

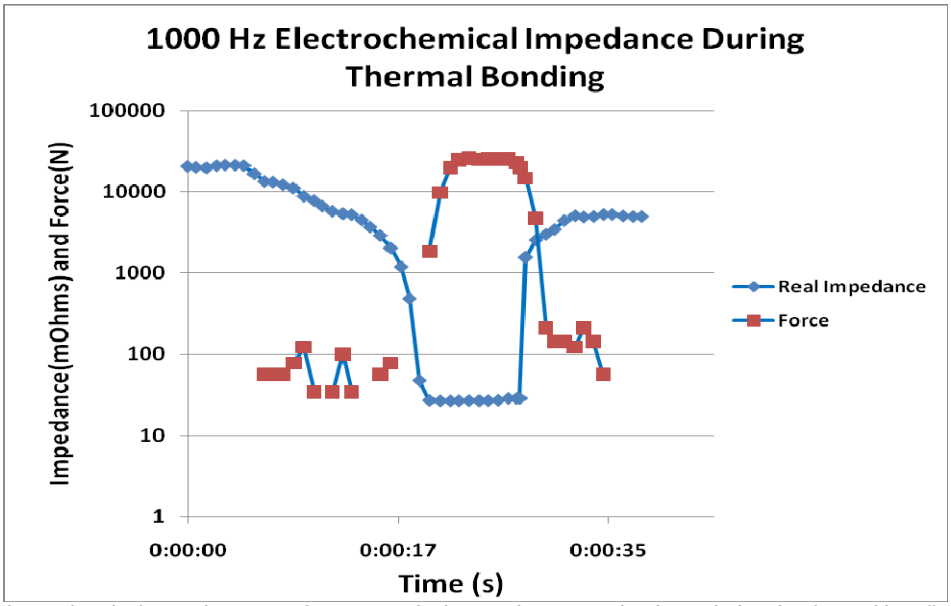

Figure 15: Electrochemical Impedance at a frequency of 1 kHz and compressive force during the thermal bonding cycle with 160˚C bonding temperature used.

Using Cyclic Voltammetry for Quality Control After Cell Assembly: A Cyclic Voltammetry (CV) protocol was developed to measure the electrochemical capacitance during or just after the thermal bonding of the MEA. The electrochemical capacitance is proportional to the electrode surface area wetted with electrolyte, which is an important metric for cell performance. The electrode surface area wetted with

electrolyte increases during the hot pressing operation as electrolyte is driven from the membrane into the electrode.

CV testing was conducted to measure the electrochemical capacitance which is proportional to electrochemically active catalyst area. The active portion of the catalyst area is wetted with electrolyte during thermal bonding of the MEA as phosphoric acid is squeezed from the membrane into the electrode. Catalyst that is not in contact with phosphoric acid is not active. Measurement of electrochemical capacitance provides a means of indicating a significant factor that affects the performance of the fuel cell.

The electrochemical capacitance measurements were conducted at room temperature with air exposed to both electrodes. Under such conditions, it is possible to apply the technique as a quality control metric prior to cell assembly. The MEA was polarized from -100 mV to 100 mV. The scan rate was varied between 50 and 1000 mV per second. A CV plot of the current as a function of potential is shown in Figure 16.

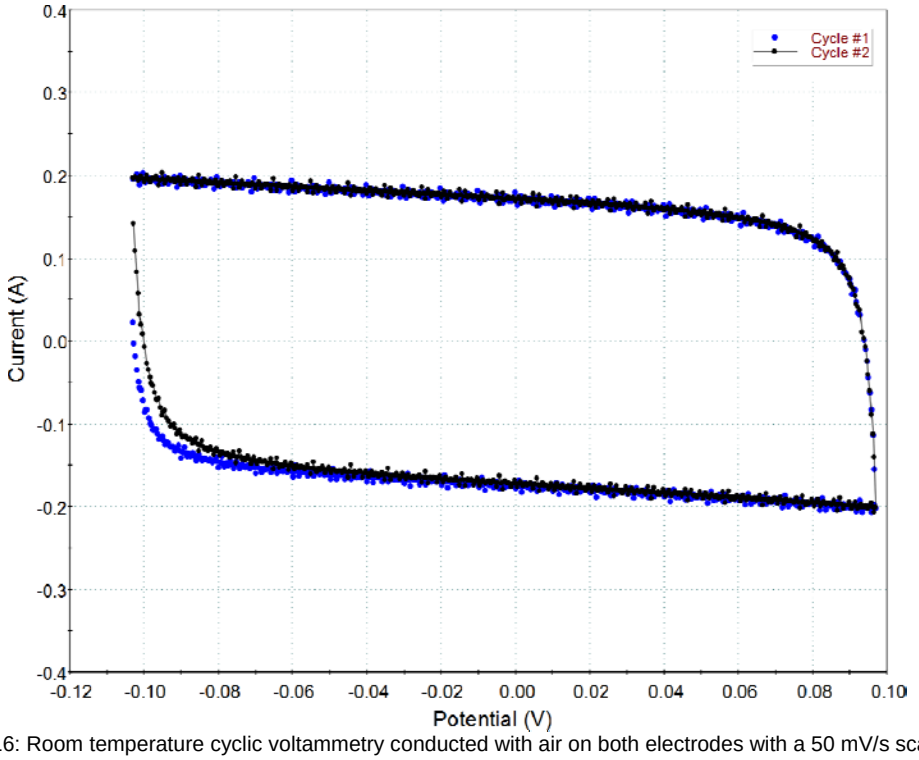

Figure 16: Room temperature cyclic voltammetry conducted with air on both electrodes with a 50 mV/s scan rate.

Figure 16 provides an indication of electrochemical capacitance, which is proportional the measured current and inversely proportional to scan rate. The current is positive while the potential between the anode and cathode electrodes is increasing and negative while the potential decreases. The measure current equals half of the total difference in current between the positive and negative scan directions. The higher the current at any given scan rate, the greater the electrochemical capacitance and the greater the catalyst area exposed to the phosphoric acid electrolyte.

There is an optimal amount of phosphoric acid penetration into the electrodes. Although electrochemical active catalyst area rises with phosphoric acid penetration into the electrode, the reactant diffus3ion resistance increases. As a result, an optimal electrochemical capacitance exists at which point the electrochemically active catalyst area is adequate without excessively impeding reactant diffusion. Low levels of phosphoric acid penetration increase the ion conduction loss in the catalyst layer due to the need for phosphoric acid in the electrode to conduct protons from the membrane to the catalyst sites.

The slope of the current as a function of voltage in Figure 16 provides an indication of an electronic short across the PBI-phosphoric acid membrane. Ideally, a cell has a high resistance or low slope which indicates a lack of shorting between the electrodes. This resistance to electron conduction across the

membrane is not related to the ion conduction resistance, which is measured by the electrochemical impedance technique at a frequency of 1 kHz.

Additional Testing to Show Effect of APC and Ultrasonic Bonding: APC Thermal and Ultrasonic bonding to seal MEAs does not reduce cell performance. In fact, these processes may actually increase cell performance and reduce variability. Additional testing was conducted to support these assertions:

- Ultrasonic bonding did not visually damage the pore structure of the electrodes based on scanning electron microscopy (SEM) imaging, as shown in Figure 17.
- An increase in Platinum crystallite size was not observed during MEA bonding as indicated by no increase in peak width of the platinum (111) acquired using X-ray Diffraction (XRD) peak width broadening, as shown in Figure 18.

No crystallite size increase should be confirmed with other techniques such as gas adsorption and TEM. The factors causing variance in cell voltage should be defined to enhanced ability to detect differences caused by independent variables such as MEA bonding method and provide quality control prior to cell build.

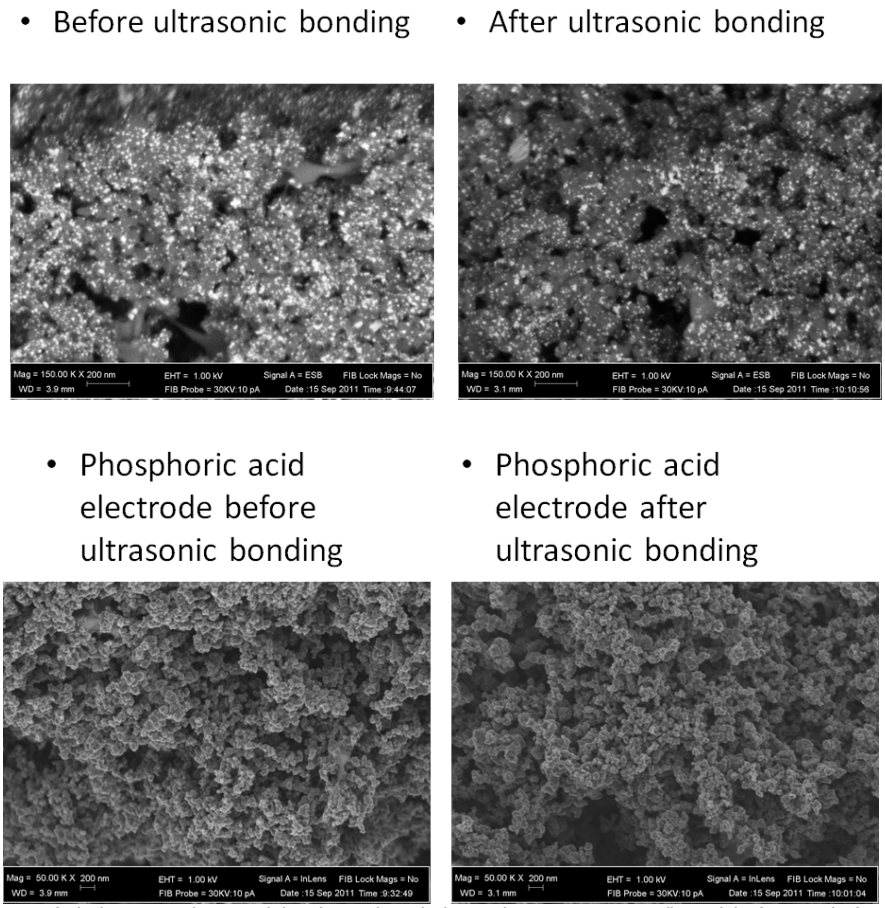

Figure 17: Comparison of platinum catalyst particles (upper) and electrode pore structure (lower) before and after ultrasonic bonding using SEM imaging

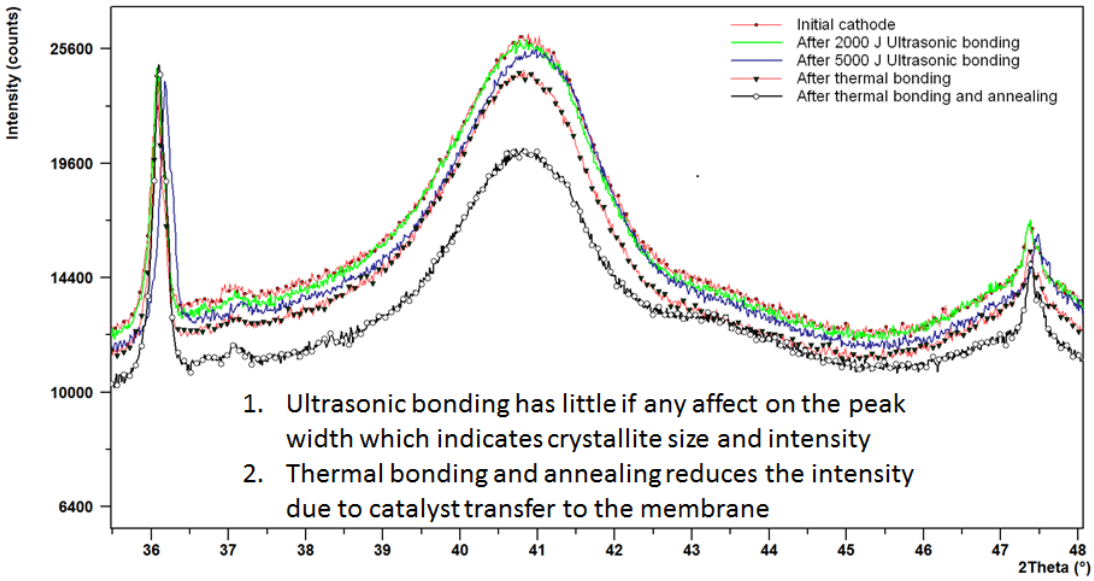

Figure 18: Effect of MEA Bonding Method on the Platinum 111 Peak

Task 8.1 – APC for Ultrasonics.

Ultrasonic welding is characterized by short cycle times (1/2 sec weld, 2 sec seal), so application of APC is inherently more difficult to do than with thermal welding. Applying the APC method for thermal pressing, which involves direct electrode contact, would require additional material layers, and this would affect the ultrasonic welding process. In addition, 6Hz sampling (+ integration time) is too slow for meaningful control of the process. If horn vibration were to be measured directly with an accelerometer, the acceleration level for any reasonably priced accelerometers would be exceeded and the directly mounted sensor would affect the tool's resonance frequency.

A non-contact sensing method, involving measurement of the acoustic signal during ultrasonic welding using a condenser microphone located near the welder, was investigated. Specifically the signal power versus frequency was determined by performing off-line Fast Fourier Transforms (FFT) of the raw signal, as shown in Figure 19. The FFT of two situations – (1) welding with loose tooling and (2) welding with anvil and horn misaligned – is shown in Figure 20. Preliminary results are inconclusive, so further work is warranted. One possibility is to mount an accelerometer onto the anvil instead. However, the consistency of the ultrasonic welding process, as compared to thermal welding, may not warrant the use of APC.

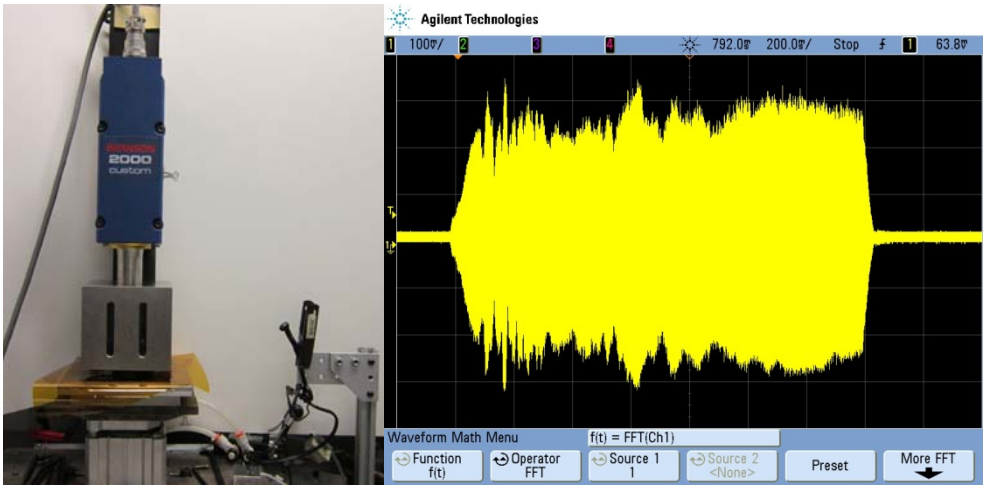

Figure 19: Condenser microphone mounted near MEA ultrasonic sealing station (left) to measure acoustic signal using an oscilloscope (right).

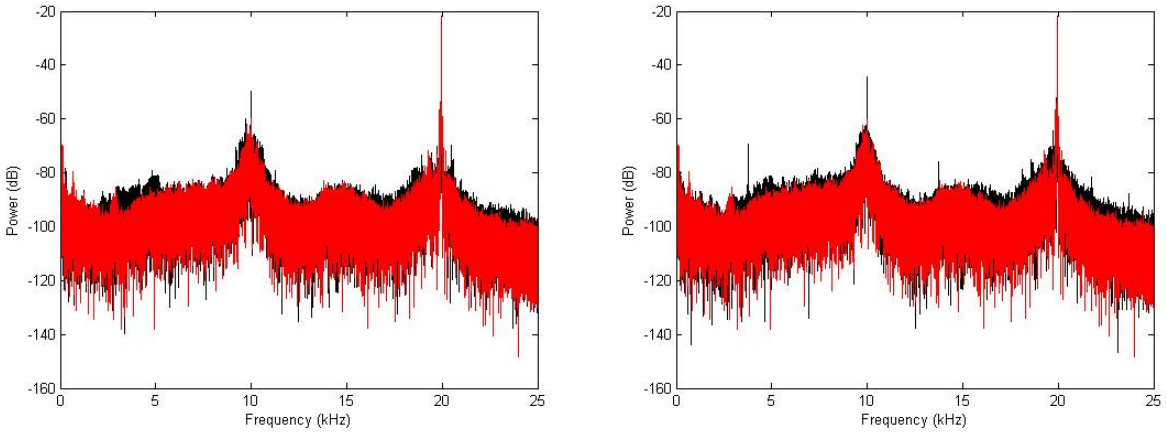

Figure 20: Left – comparison of good MEA weld (red) vs. welding with loose anvil bolts (black); Right – comparision of good MEA weld (red) vs. welding with misaligned Anvil (black).

Task 9.0 – Evaluation of MEA performance..

A short stack was designed (exploded and colored CAD images shown in Figure 21) and with the following engineering specifications:

- Accommodates testing of 50 cm^2 MEAs
- Maximum current draw of 50A.
- 5000 SCCM of hydrogen and 18000 SCCM for air requirements
- Customizable cooling configuration
- End plate has flat surfaces to mate with press during compression testing including counter sunk and counter bored bolt holes, and pocket for heater membrane with heater cover that is flush with surface
- Has features for collecting data on temperature and voltage at each cell
- Internal reactant manifold - each component designed with through holes for gas flow
- Teflon insulator and collector plated designed with O-ring groove to seal reactant gasses between end plates and mono-polar plates and
- Same flow field patterns as current single cell test hardware.

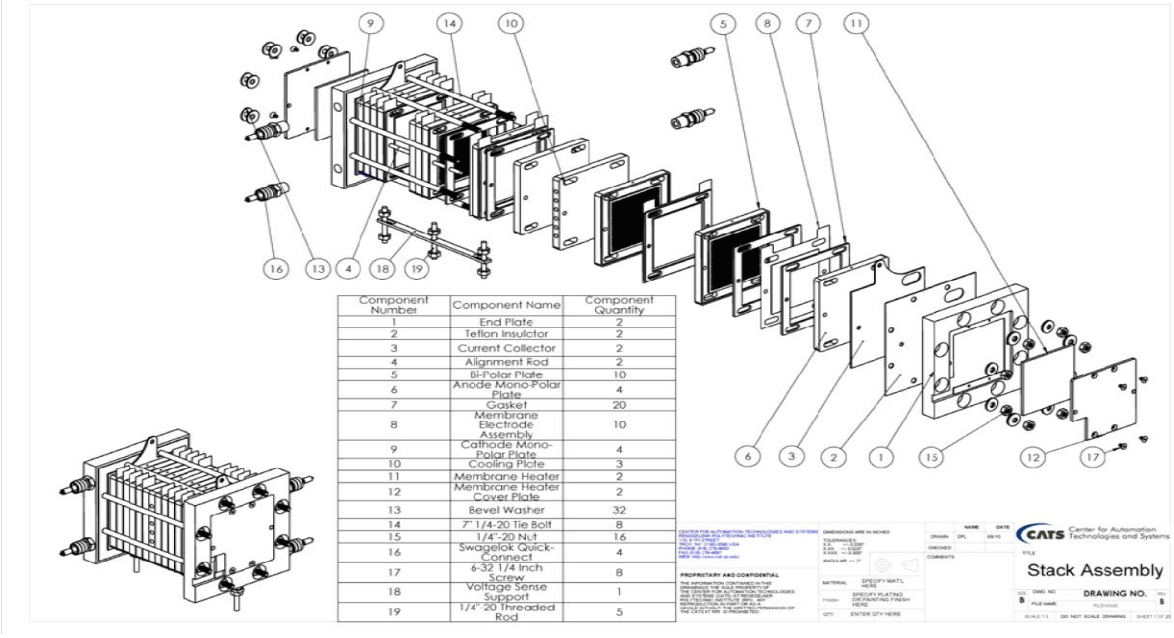

Component Number	Component Name	Component Quantity
1	End Plate	2
2	Teflon Insulator	2
3	Current Collector	2
4	Alignment Rod	2
5	Bi-Polar Plate	10
6	Anode Mono-Polar Plate	4
7	Gasket	20
8	Membrane Electrode Assembly	10
9	Cathode Mono-Polar Plate	4
10	Cooling Plate	3
11	Membrane Heater	2
12	Membrane Heater Cover Plate	2
13	Bevel Washer	32
14	7" 1/4-20 Tie Bolt	8
15	1/4"-20 Nut	16
16	Swagelok Quick-Connect	4
17	6-32 1/4 Inch Screw	8
18	Voltage Sense Support	1
19	1/4"-20 Threaded Rod	5

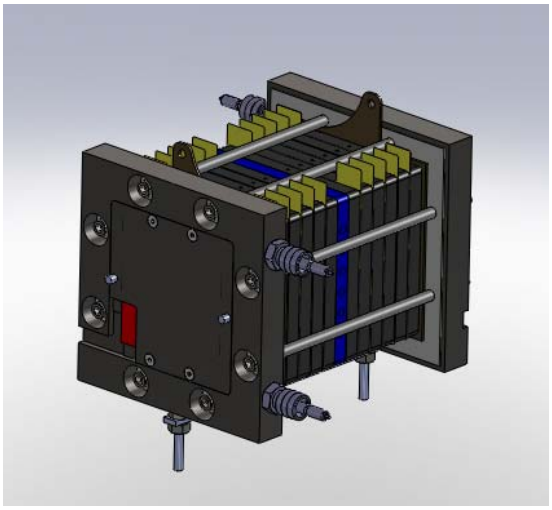

Figure 21: CAD images of short stack with 10 standard size cells.

Components were manufactured and/or procured and the stack was assembled. The stack in a 10-cell configuration with a single cooling plate is shown in Figure 22a. Monopolar and bipolar plates were made from POCO graphite. MEAs with reactant gas and inlet and exhaust manifold holds is shown in Figure 22b.

(a)  (b) 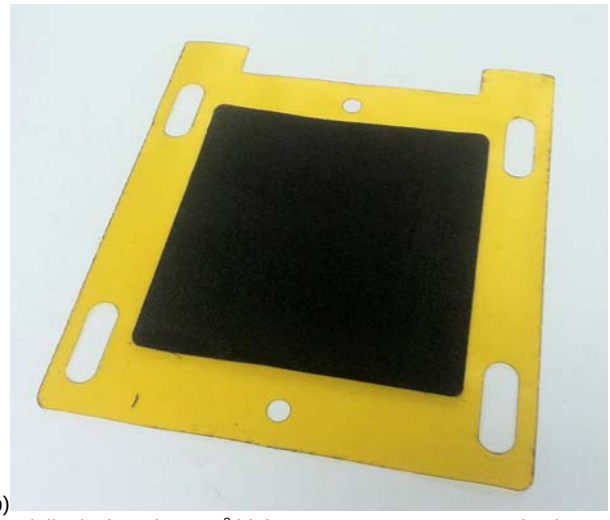

Figure 22: Pictures of (a) 10-cell short stack and (b) specially designed 50 cm^2 high-temperature MEA to test in short stack

Initial tests were run using a 5-cell stack with no cooling plates, shown in Figure 23, to prove out the data collection for voltage and temperature at across each cell. Figure 25 is the polarization curve for each cell in the 5-cell stack. Upon inspection of this particular test, it was discovered that there was a gas leak at cell 4 which caused it to have poor performance. With the initial testing, it was also shown that we can track the temperature gradient across the stack. A graph of the temperature at each cell during burn-in is shown in Figure 25.

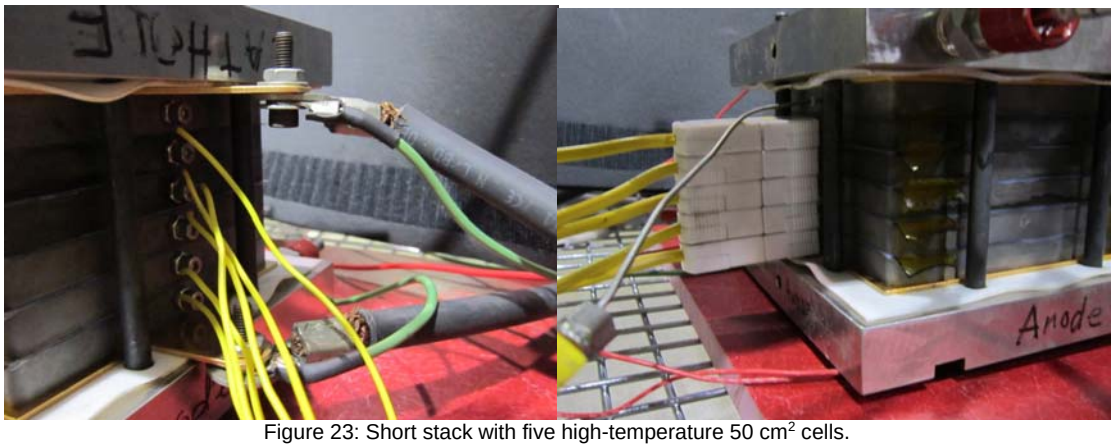

Figure 23: Short stack with five high-temperature 50 cm^2 cells.

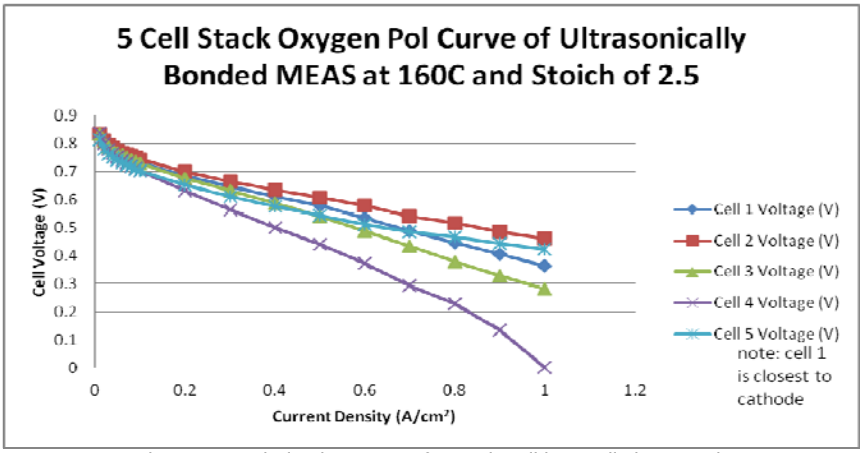

Figure 24: Polarization curves for each cell in 5-cell short stack

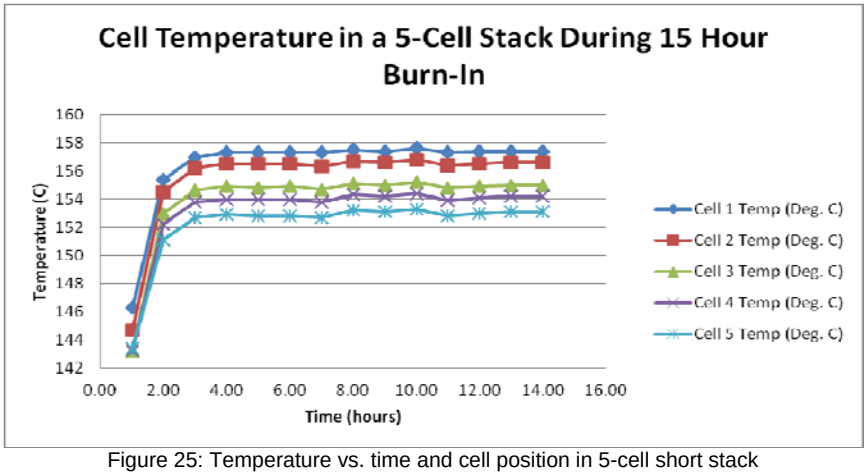

Figure 25: Temperature vs. time and cell position in 5-cell short stack

Figure 25 clearly shows variation in temperature across the stack in this first experimental test. The 4°C temperature difference between Cell 1 and 5 is attributable to a non-optimized heating configuration and no exterior insulation used. To quantify the difference in performance of cells within a stack that are operating at different temperatures, we investigated the effect of temperature on cell voltage – initial experimentation (Figure 26) shows approximately 1 mV/°C sensitivity between 145-170°C for three different current levels. Future experimental work (Task 13) would focus on obtaining a more uniform temperature through balanced heating, addition of 1-2 cooling plates, and insulating the entire stack.

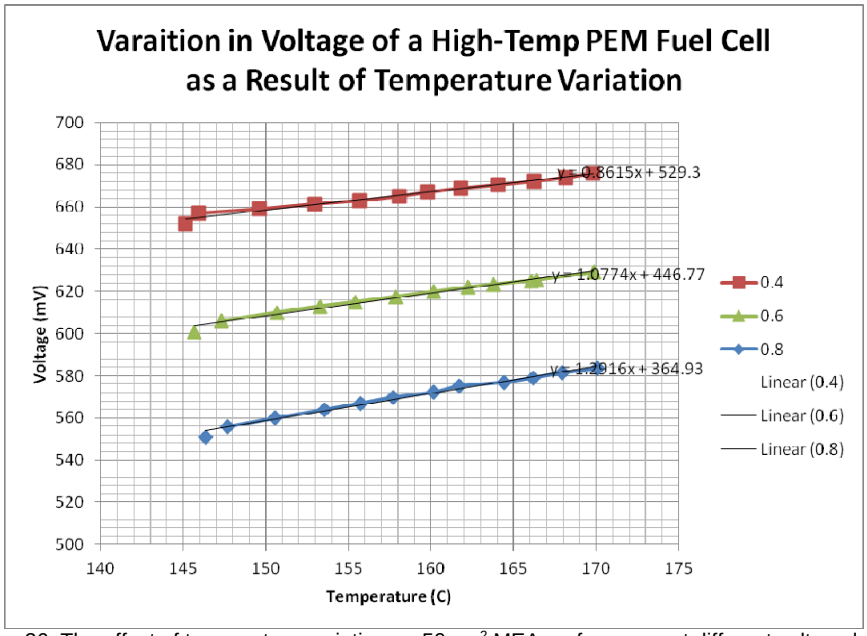

Figure 26: The effect of temperature variation on 50 cm^2 MEA performance at different voltage levels

Initial tests with a 5-cell stack provided an opportunity to prove out the stack hardware and debug the fuel cell test stand. At the point, use of ultrasonically bonded MEAs represented the first known attempt to test multiple cells of this type in a stack. Differences between stack and individual cell performance may be attributable to differences in operating temperature (thermal jacketing and cooling plates required), reactant gas leakage, and cell compression.

Task 9.1 – Evaluation of Larger Scale Ultrasonically Sealed MEAs.

An investigation of larger scale ultrasonic MEA sealing began with a series of technical meetings with engineers at Branson Ultrasonics in Danbury, CT to discuss the challenges associated with the design and construction of ultrasonic horns for our application including: material choices and limitations; available acid resistant coatings; size limitations for our 20 kHz machine; horn surface treatment (knurling); booster options; and required modifications needed to handle the higher press loads. A maximum horn size of 8" x 8" was compatible with our 20 kHz ultrasonic welder, which would theoretically allow us to produce an MEA size of 400cm^2, representative of the largest size required for an automotive application. However, due to the pressure that would be required for our investigations in high temperature PEM MEA pressing, which far exceeded the capability of our 20 kHz machine structure, we decided to choose an MEA size at the lower end of that required for automotive fuel cells, i.e. 140 cm^2 (called an A1 size).

Fabrication of the larger A1 cells required a redesigned ultrasonic press combined with a 15 kHz system. The original C-frame-style press from Branson used for all previous research visually flexed when placed under loads required for 45cm^2 cells. An H-Frame press, required for any larger MEAs, was brought on-line. As shown in Figure 27, the press was designed to maintain parallelism of the ultrasonic horn (top) and anvil (bottom) during loading. Tooling alignment is obtained through the use of matching spherical dome and seat supporting the bottom tooling, as shown in Figure 28. The large surface area of the geometry distributes high loads without damaging the structure.

Two small pneumatic guide cylinders (50 mm bore) are used to move the lower tooling into place, followed by a large load cylinder below (8 inch bore) to supply lamination force/pressure. The combined loads of the main and guide cylinders are capable of generating up to 5,600 lb$_f$ at 100 psi, or 10,000 lb$_f$ at 200 psi cylinder pressures. Lamination loads (at the MEA) range from 45 – 100 psi, thus requiring up to 9,400 lb$_f$ to laminate a 605 cm^2 MEA, which is the maximum size envisioned for this press.

Figure 27: 15kHz ultrasonic lamination press. Bottom tooling is adjustable to obtain precision alignment after tooling assembly. H-Frame layout maintains tooling alignment.

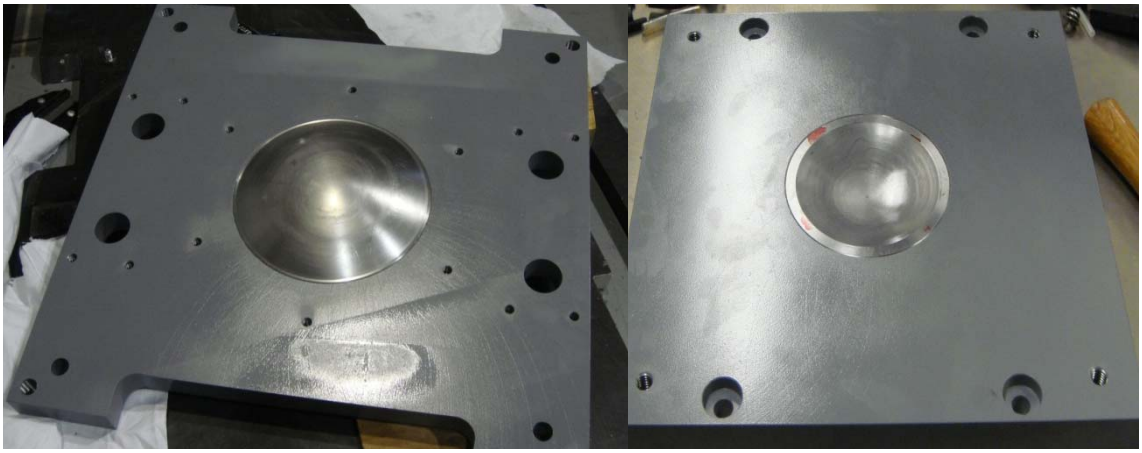

Figure 28: Matching spherical dome and seat are used to support the lower tooling. The geometry allows for a gimbal style alignment adjustment, but also supports high loads required during lamination.

In additional to the modified ultrasonic press, thermal press tooling, MEA registration frame for all manufacturing operations, the corresponding fixturing tools at each operation to hold MEA components in proper registration, and a single cell test fixture were designed and then procured/fabricated. Prior to ordering a large ultrasonic horn for the large MEAs, we conducted tests which indicated that it is feasible to apply a fine knurl pattern to the anvil rather than the horn, and achieve the same MEA performance. This design change significantly reduce tooling costs, as the anvil is a much less costly component than the horn, and it would also allow several re-facings of the horn at a lower cost. Various components are shown in Figures 29-32. Note the new ultrasonic welder anvil design in Figure 30a, where compression load is applied by a large pneumatic cylinder from below.

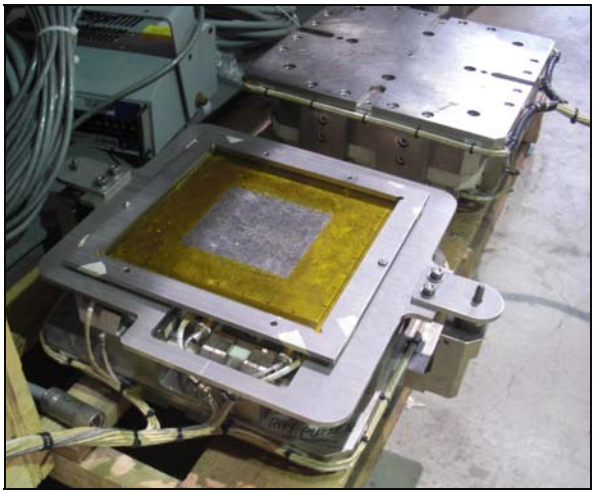

Figure 29: A1 thermal press tooling showing adapter and frame

(a) 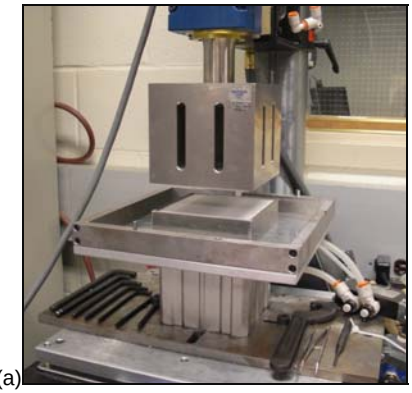 (b) 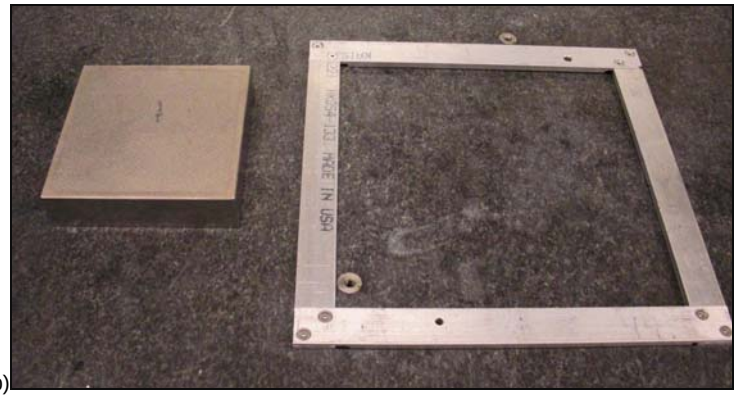

Figure 30: (a) Ultrasonic welder with welding anvil installed and (b) A1 sealing anvil and welding spacer

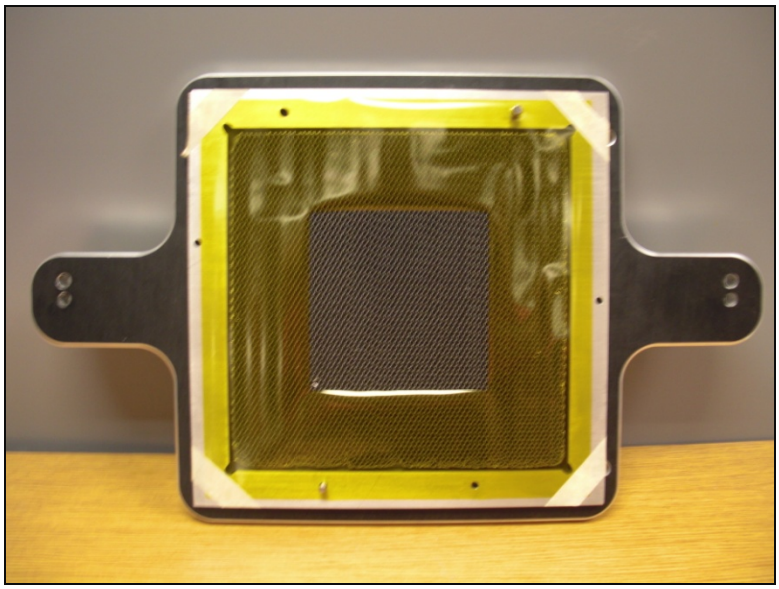

Figure 31: Laser fixture to hold A1 MEAs for cutting

(a) 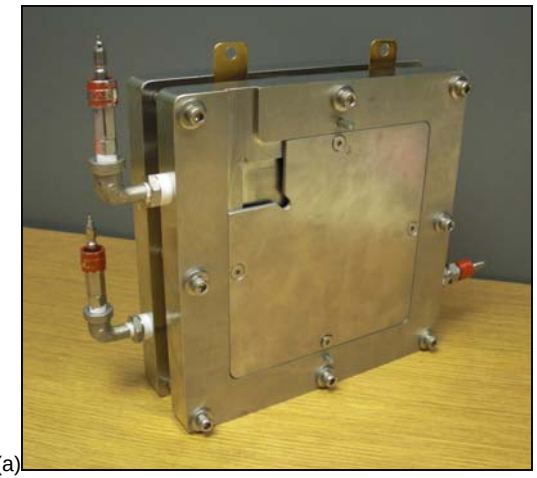 (b) 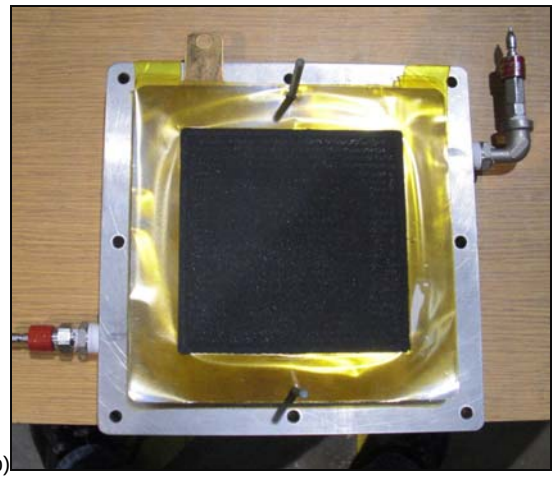

Figure 32: (a) A1 MEA test cell (heaters not shown) and (b) The A1 MEA shown installed in the test cell

Several A1 MEAs were made using the ultrasonic and thermal sealing tools, although testing this size presented some difficulties. Because of the relatively large size compared to the standard 50 cm^2 MEAs, the required mass flow rate to produce a polarization curve was essentially tripled. Accordingly, one of the fuel cell test stands was updated with higher capacity mass flowrate controllers and load bank.

The performance was not been shown to be comparable to that of the 50 cm^2 MEAs, although this was attributable to poor flowfield design. Our reasoning was that the performance of several A1 MEAs made with thermal press tooling was consistent with that of the ultrasonically sealed A1 MEAs, although not at the level of the L1 MEAs. It was believed that the large channels may have been preventing compression of the active area, and the larger lands might be starving the cell. Therefore, a new flow field was designed for the test cell and used to test the A1 cells. Because of the larger flow channel cross sectional area, the flow enters through a manifold built into the back of the plate; thus ensuring that the flow will not be limited by the geometry. The flow channel and land widths were as close as possible to those of the L1 plates. The new A1 plates have 11 parallel channels.

With the A1 MEA manufacturing process and testing set, further testing of MEAs was reserved for Task 13.

Task 9.2 – Ultrasonic Sealing Process Optimization.

A set of experiments was designed and conducted to develop optimum ultrasonic sealing conditions for MEAs (standard 50 cm^2 size used for study). A series of baseline MEAs were made with 320 µm thick PBI membranes and ultrasonically sealed at 0.44 N/mm^2 pressure, 0.4 J/mm^2 energy and with a 90A durometer urethane anvil support backer. All MEAs were sealed with 2.5X booster and MEAs heat treated at 160°C for 30 minutes prior to single cell build and testing. The optimization tests involved two additional energy levels, a lower level of sealing pressure, and a polycarbonate material anvil support backer, as listed in Table 2. The ultrasonic tooling test setup is shown in Figure 33.

After the heat treatment, MEAs were built in the single cell hardware with 20% compression using rigid PFA gaskets. The burn in period involved heating the cell to 160°C at 0.2 A/cm^2 for 18 hours followed by polarization curve measurements with air and oxygen. The H_2/Air polarization curves were recorded with 1.2/2.0 stoich and the H_2/O_2 curves with 1.2/9.5 stoich.

Table 2: Input Process Parameters for Optimization Tests

MEA	Anvil Support Backer	Sealing Pressure (N/mm^2)	Energy (J/mm^2)
Baseline	90A	0.44	0.4
Backer Test	Polycarbonate	0.44	0.4
Pressure Test	90A	0.66	0.4
Energy Test	90A	0.44	0.2

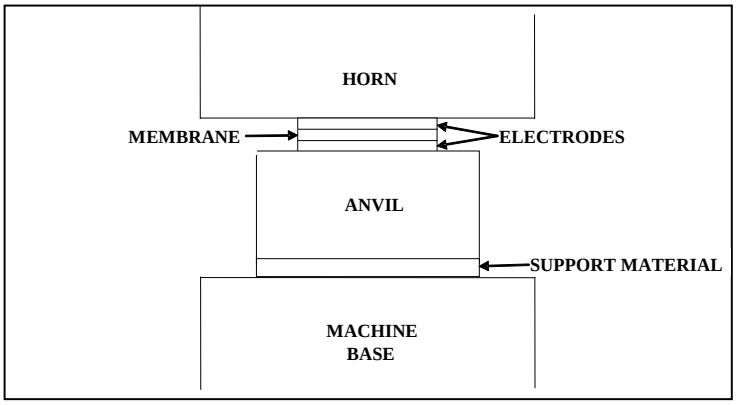

Figure 33: Diagram of Ultrasonic Tooling with MEA Components and Support Material Location

Anvil Support Backer Effect: The fuel cell performance with the 90A durometer and polycarbonate anvil support backers is shown in Figure 34. During the sealing process, the MEA components were placed upon an anvil during the application of the load and ultrasonic energy for sealing. The anvil was a flat, polished, stainless steel block that could either be bolted directly to the solid mounting plate or with a layer of constant-thickness urethane of a known durometer placed between the anvil and solid mounting plate to provide some compliance in the anvil during the ultrasonic sealing cycle.

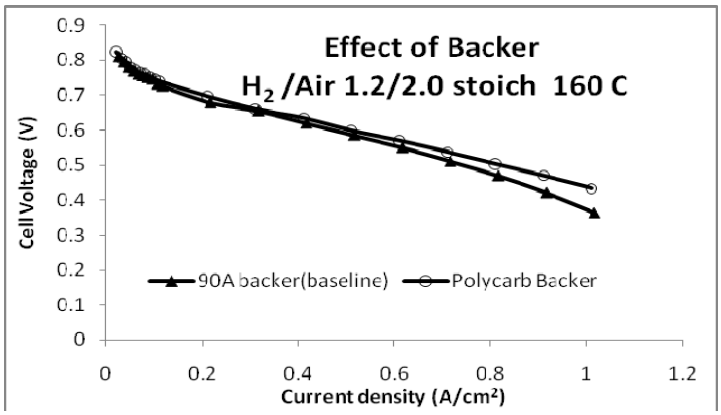

Figure 34: Effect of Backer Support on Fuel Cell Performance

Our Phase 1 results suggested that placing a compliant backer, e.g. a 90 A durometer urethane, between the stainless steel anvil and the leveling base evenly distributed the applied load and adjusted for any inconsistencies in the MEA components and equipment setup during ultrasonic sealing. Although the urethane anvil support backer was previously shown to improve performance over no backer (steel on steel), the urethane material absorbed energy during the ultrasonic process and increased in temperature. Polycarbonate was introduced as another variable in the optimization schedule, but this time on the opposite spectrum from the urethane as the Makrolon® polycarbonate has a compressive modulus an order of magnitude greater than that of stainless steel. The polycarbonate backer resulted in better performance in the fuel cell especially toward higher current densities. To clearly identify the effect of the backer variables, main effect plots for current density at 0.6 V and 0.4 V are shown in Figure 33 with steel backer results from Phase I included for comparison purposes.

From Figure 35, the stiffer polycarbonate is clearly the optimal backer material that exceeds baseline performance at both intermediate and high current densities. It also resulted in better control over the finished MEA thickness.

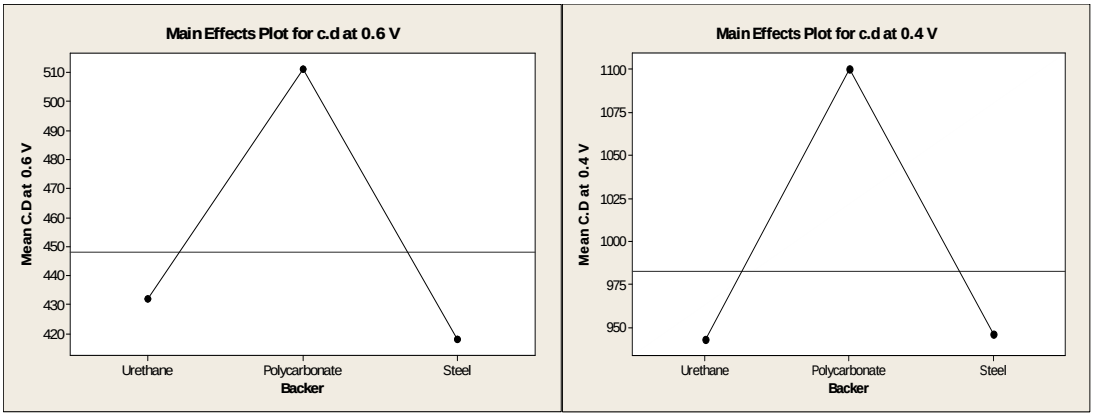

Figure 35: Main Effects Plots for Current Density at 0.6V and 0.4V for Tested Backer Materials

Sealing Pressure Effect: Sealing pressure is the force applied during ultrasonic welding through the MEA components placed on the anvil divided by the contact area of the components. For a 50 cm^2 MEA, applying a load of approximately 2.2 kN results in 0.44 MPa. Phase 1 involved a low and high variable namely 0.44 and 0.88 MPa respectively, and it was concluded that the higher sealing pressure resulted in destruction of pores in the gas diffusion layer resulting in electrode flooding with phosphoric acid. This optimization study involved an additional pressure variable of 0.66 MPa. The fuel cell performance and main effects plot with 0.44 and 0.66 MPa pressure levels is shown in the Figures 36 and 37, respectively. Our phase 1 results with 0.88 MPa pressure level is also shown for comparison purposes in the main effect plot. Based on the optimization tests, the 0.66 MPa sealing pressure provided better performance at both intermediate and higher current densities.

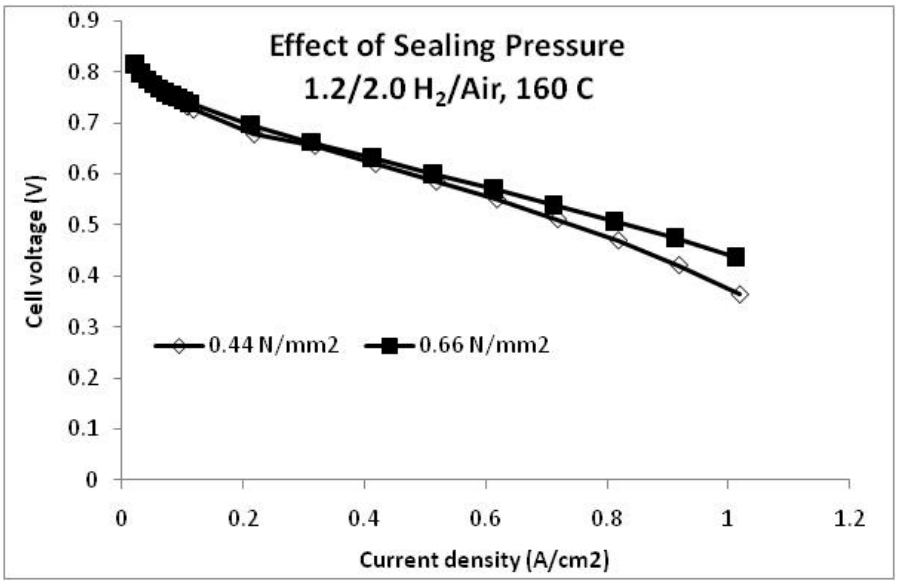

Figure 36: Effect of Sealing Pressure on Fuel Cell Performance

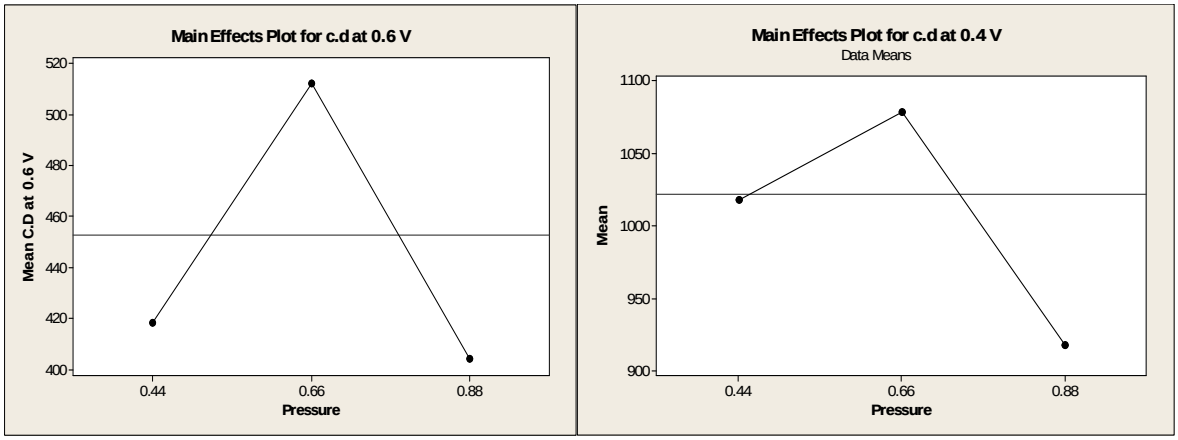

Figure 37: Main Effect Plots for Current Densities at 0.6V and 0.4V for tested Sealing Pressures

Energy Flux Effect: Energy Flux is the energy imparted in Joules into the MEA components per unit contact area. The energy level determines the amount of time that the ultrasonic energy is applied to the MEA. The energy level needs to be sufficient enough to seal the electrodes to the PBI membrane but high energy levels can agglomerate Teflon particles in the gas diffusion layer or damage the electrode structure by separating the carbon fibers. Too high energy levels can thus damage the structural integrity of the electrode thus compromising the critical membrane-electrode interface. Phase 1 results suggested that energy level was not a statistically significant input process variable over the tested range; however the higher energy level resulted in a lower performance of the two selected energy levels (0.4 and 0.6 J/mm^2 respectively). This optimization DoE involved an even lower energy level of 0.2 J/mm^2 and the fuel cell performance of the energy flux effect is shown in Figures 38 and 39. Based on these results, the lowest energy level maintained the structural integrity of the MEA while resulting in better MEA performance.

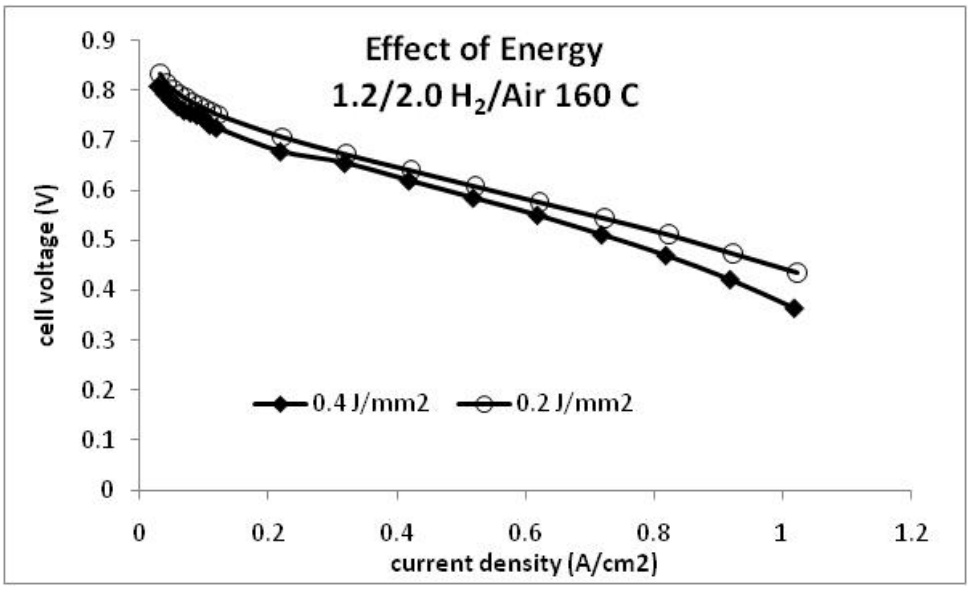

Figure 38: Energy Flux Effect on Fuel Cell Performance

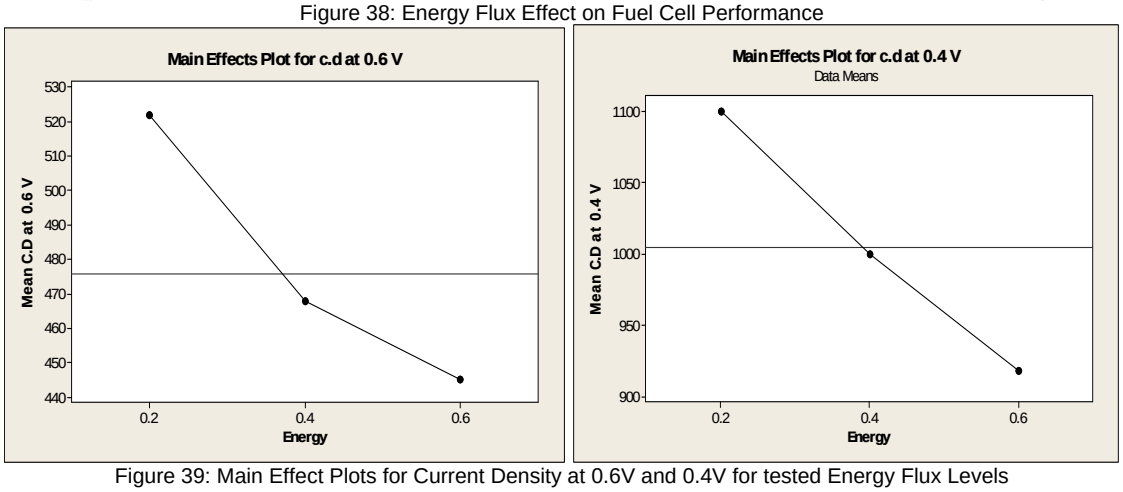

Figure 39: Main Effect Plots for Current Density at 0.6V and 0.4V for tested Energy Flux Levels

Summary: The optimization DoE was designed to further investigate ultrasonic sealing process variables, namely backer material, sealing pressure and energy flux and their effect on performance. The results suggest that a polycarbonate backer with an intermediate sealing pressure level (0.66) and a lower energy level (0.2) exceeded baseline performance providing further insight into the ultrasonic sealing process. Further testing is to be conducted with the goal of investigating variable ranges where the values of the ultrasonic sealing energy flux and pressure in the manufacturing of the MEAs have a performance level that is within a plateaued range for the purpose of allowing process parameters to be set with an acceptable tolerance range during production while maintaining the overall superior performance of the fuel cell.

Task 9.3 – Annealing Process Optimization.

The objective of this study was to identify statistical significance of heat treatment process parameters i.e., temperature of the heat treatment and its duration in an effort to reduce cycle times. A 2-factor, 3-level, 2-replicate DOE was designed with temperature levels of 120, 140 and 160°C, and soak times of 15, 30 and 45 minutes. Single cell evaluation of heat treated MEAs was performed after 18 hour burn-in period at 200 mA/cm^2 followed by polarization curve measurements at 160°C. Examples of the polarization curves for all factor combinations are shown in Figure 40.

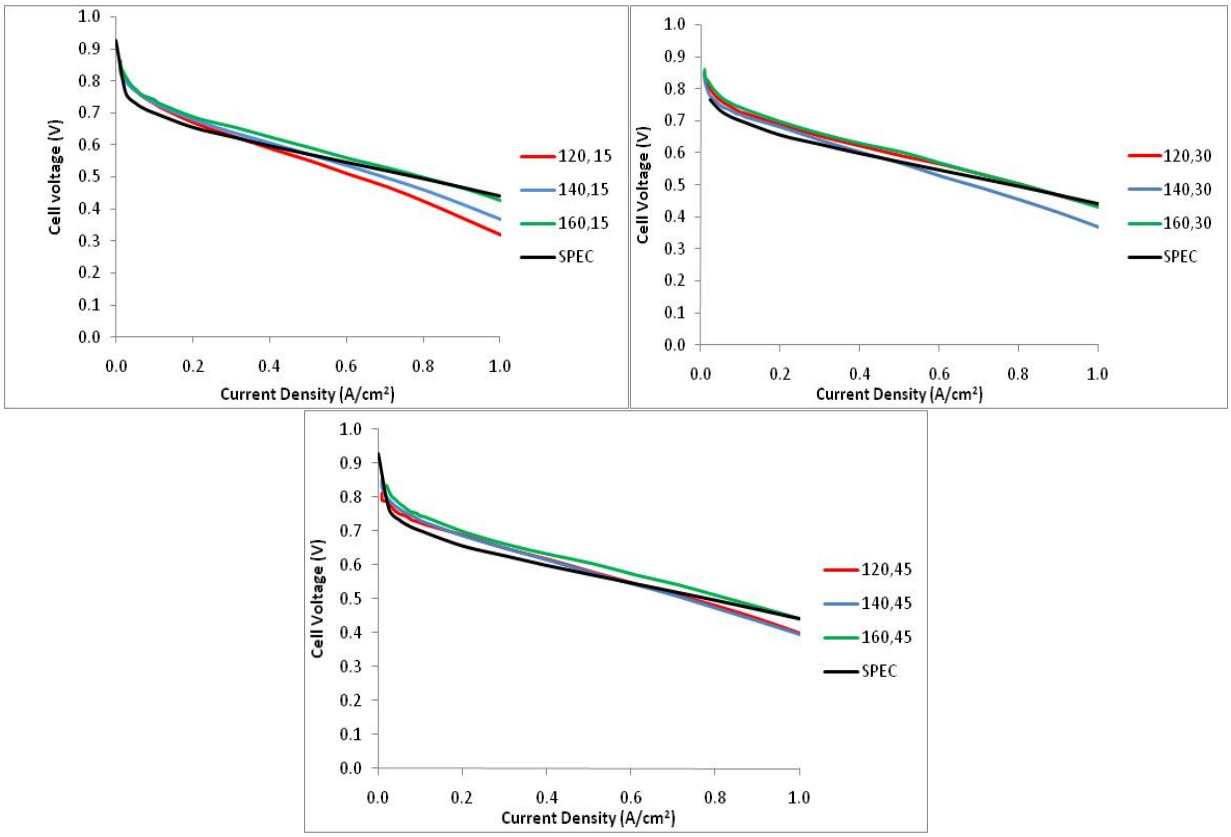

Figure 40: Single Cell Performance of ultrasonically sealed MEAs at 160°C and 1.2 H_2/2.0 air stoich. The MEAs were heat treated at various temperatures and times prior to cell build.

Analysis of Variance (ANOVA) was performed to determine the p-value which describes the effect of temperature and time on output parameters namely (1) weight change of MEAs before and after heat treatment (b) thickness change of MEAs before and after heat treatment (c) current density obtained at 0.6 V and (d) current density obtained at 0.4 V. The analysis was done with 95% confidence and a p-value of <0.05 signifies a statistically significant input parameter. A table of p-values for all the output parameters is shown in Table 3.

Table 3: ANOVA p-values for various input and output parameters

Input parameter	Weight change	Thickness change	Current density at 0.6 V	Current density at 0.4 V
Temperature	0.005	0.012	0.007	0.143
Time	0.009	0.047	0.1	0.76
Interaction	0.743	0.082	0.001	0.000

The thickness change and weight change of MEAs before and after the heat treatment were statistically significant for both temperature and time. Higher temperatures and longer duration resulted in increased weight loss and thickness loss, as shown in Figure 41. The thicknesses of the MEAs were in the range of 865-890 microns depending on the heat treatment conditions. Typically two weight loss regions are observed for phosphoric acid PBI membranes during heat treatment. First is the loss of free water occurring at temperatures between 60-100°C and the second weight loss occurs at temperatures >130°C due to loss of water produced by acid dimerization. Increasing temperatures will result in continued water loss as the dimerization reaction proceeds. As shown in Table 3 and Figure 42, ANOVA of the fuel cell data revealed temperature as a statistically significant factor for current density at 0.6 V with higher heat treatment temperature resulting in better performance. This can be correlated to the increasing water loss due to acid dimerization thereby increasing phosphoric acid concentration in the

MEA resulting in better performance. This effect is however not observed at higher current densities. Further analysis of the fuel cell data reveals that the duration of heat treatment is not a statistically significant parameter and the MEAs heat treated at 160°C and 15 minutes matched the SPEC performance. Heat treatment of the MEAs longer than 30 minutes actually resulted in a negative effect on performance. This is a significant finding as this could enable the cycle time of the heat treatment process to be reduced by as much as 50%.

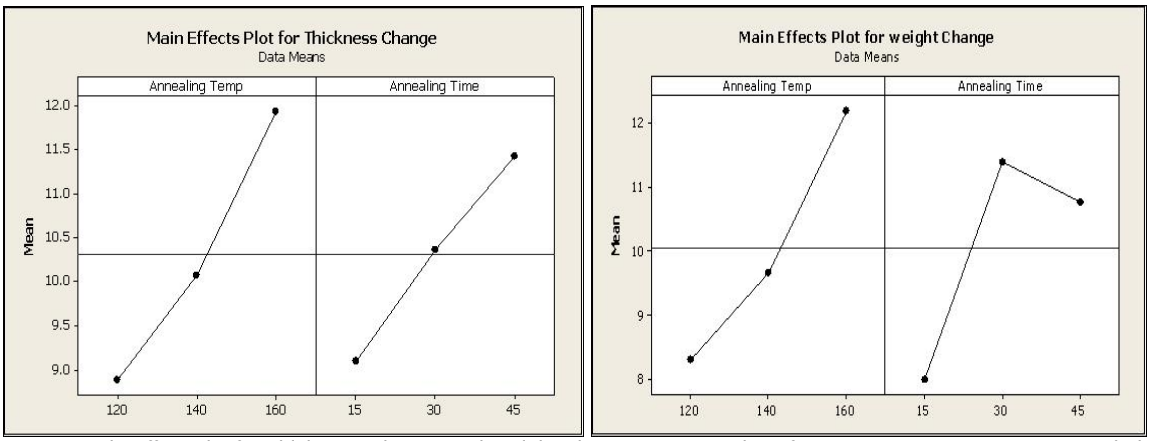

Figure 41: Main Effect Plot for Thickness Change and Weight Change as a Function of Heat Treatment Temperature and Time

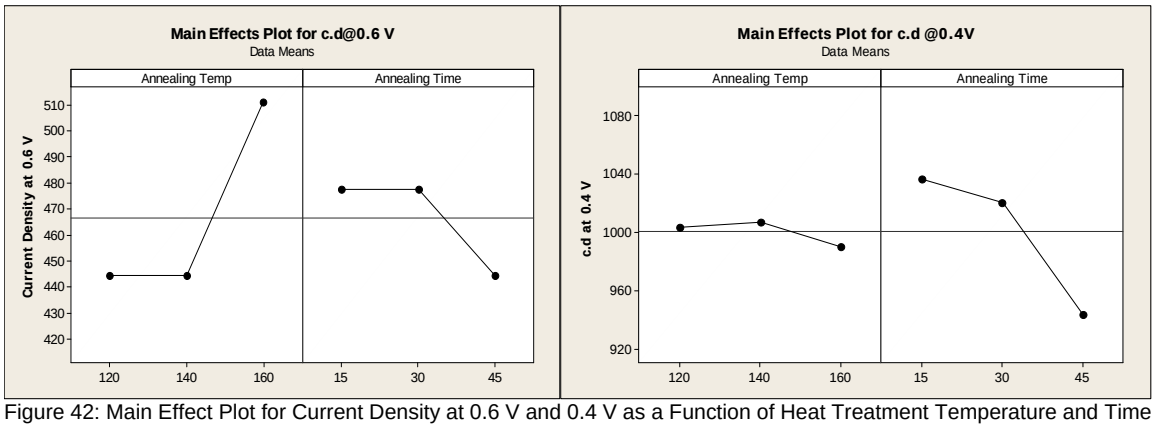

Figure 42: Main Effect Plot for Current Density at 0.6 V and 0.4 V as a Function of Heat Treatment Temperature and Time

Task 9.4 – Evaluate Feasibility of Ultrasonic Sealing and APC for Low Temperature (Nafion)

Low temperature Proton Exchange Membrane (PEM) fuel cells currently dominate the fuel cell market, yet there are materials-, cost-, reliability-, and manufacturing-related challenges that hinder widespread commercial success of this promising technology. With regards to manufacturing, one of the main process bottlenecks is thermal bonding of electrode and membrane components into a unitized membrane electrode assembly (MEA). Work performed for this this task has shown that ultrasonic bonding can serve as a direct replacement for thermal bonding for low-temperature PEM fuel cells with dramatic reductions in cycle time and energy consumption but no significant degradation in performance. This task focused on the possible use of ultrasonic bonding for low-temperature PEM MEAs operated at 65°C.

Polarization curves and 1 kHz impedance were measured for MEAs with a five-layer architecture comprised of Nafion 115 membrane (10 cm^2 active area) and carbon paper-based gas diffusion electrodes (GDE) that were thermally bonded and ultrasonically bonded using commercial equipment in the configurations shown in Figure 43. A schematic and the geometry of an example MEA are shown in Figure 44. The effect of membrane condition (conditioned and dry), electrode type (commercially available, custom-made with lower platinum loadings), and process conditions were investigated.

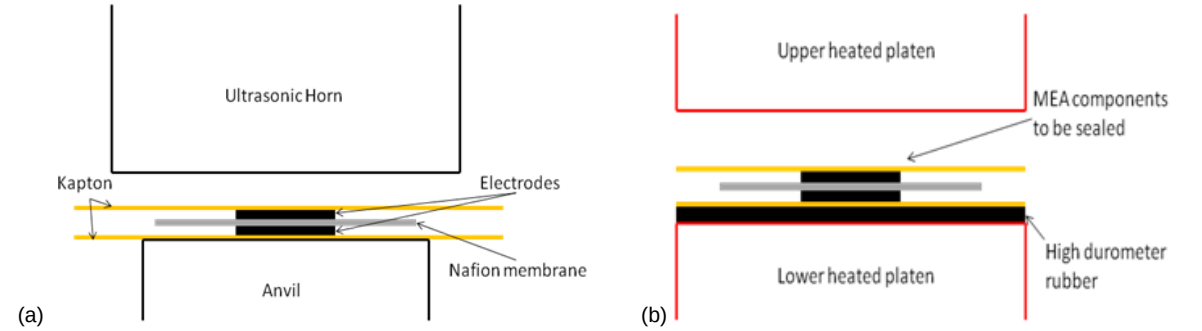

(a) (b)

Figure 43: Schematics of (a) labeled MEA made by hand in ultrasonic setup prior to bonding and (b) MEA in press prior to thermal sealing.

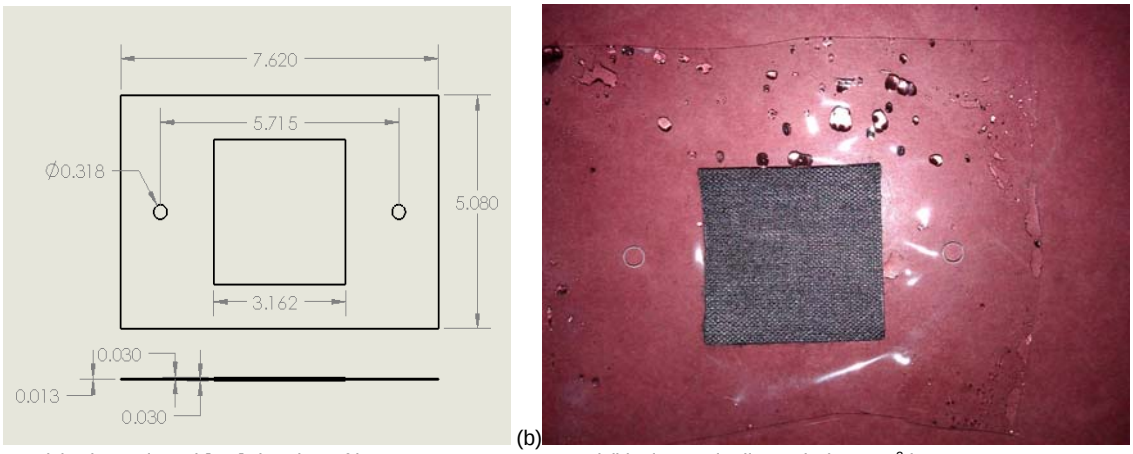

(a) (b)

Figure 44: (a) Dimensioned [cm] drawing of low temperature MEA and (b) ultrasonically sealed 10 cm^2 low-temperature MEA with alignment holes

Experimental results demonstrate clear trends. Both custom-made GDEs with lower platinum loading performed best suggesting that electrode architecture and composition can be optimized for ultrasonic bonding. There was little difference in performance between dry and conditioned membrane, which helps explain current industrial practice of using dry membrane in assembly. Statistical analysis of an experimental design where ultrasonic bonding energy and pressure were varied suggests that neither parameter significantly affects MEA performance and that the process is robust. Similar analysis of thermal bonding with temperature and pressure varied suggests that temperature has a significant effect on MEA performance. However, the most important results of all experimentation are that process cycle time and energy consumption are reduced by 94% and 98%, respectively, using ultrasonic bonding.

A follow-up study compared performance between ultrasonically and thermally bonded low temperature MEAs and characterized the performance losses from the new bonding process. A randomized, full factorial experiment was designed and conducted to examine performance of MEAs with 10 cm^2 active area while varying three factors; bonding method (ultrasonically and thermally pressed using previously optimized bonding parameters), membrane condition (dry and conditioned Nafion® 115), and electrode catalyst loading (0.16 and 0.33 mg Pt/cm^2). Ultrasonic MEAs performed as well as their thermal MEAs across all tested current densities with pure oxygen supplied to the cathode. However, thermal MEAs outperformed ultrasonic MEAs at current densities above 0.4 A/cm^2 with air supplied to the cathode.

Impedance spectroscopy, cyclic voltammetry, and flow sensitivity analysis were used to characterize the performance losses of the ultrasonic MEAs. The data suggests the presence of oxygen diffusion losses above 0.4 A/cm^2 when air was supplied to the cathode. Ultrasonic MEAs were three times more sensitive to changes in air flow rate on the cathode than the thermally MEAs. Increasing the platinum catalyst loading from 0.16 to 0.33 mg Pt/cm^2 resulted in a performance enhancement of approximately 20 mV and 65% greater electrochemical surface area. Understanding the effect of ultrasonic bonding on

various performance losses will help optimize the MEA bonding process. Analysis of specific losses present for ultrasonic MEAs may also provide insight into the design of MEA components for ultrasonic bonding.

Task 9.5 – Durability Testing of Ultrasonically Sealed MEAs.

Durability testing on two ultrasonically pressed MEAs was conducted employing start-stop cycling per industrial collaborator (BASF) test protocols. Each MEA was subjected to a 190 hour test cycle during which thermal and load cycling was conducted. A total of 20 start-stop cycles were performed. Figure 45 shows a typical test cycle. Figure 46 shows the voltage and current density during the initial ten hour test period and during the final ten hour test period. There was no measured degradation in performance over the duration of the tests. In order to evaluate electrochemical catalyst activity at beginning of life (BOL), and end of life (EOL), cyclic voltammetry was employed. This test, shown in Figure 47, confirms that there was no loss in electrochemical catalytic activity over the life of the test.

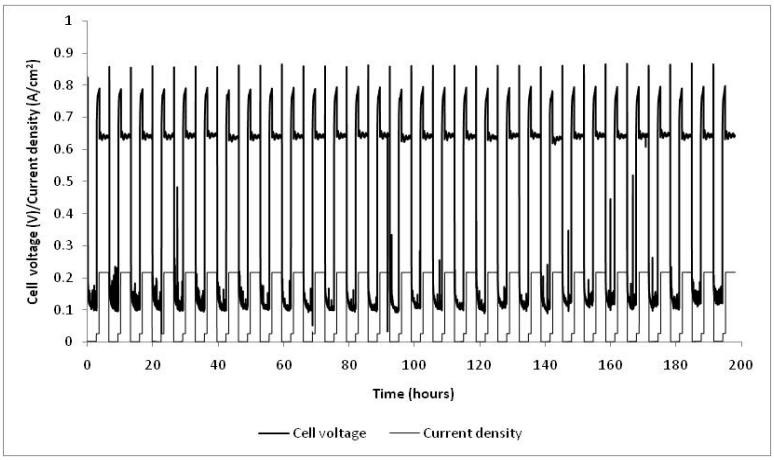

Figure 45: Typical test cycle for ultrasonically sealed 50 cm2 MEAs

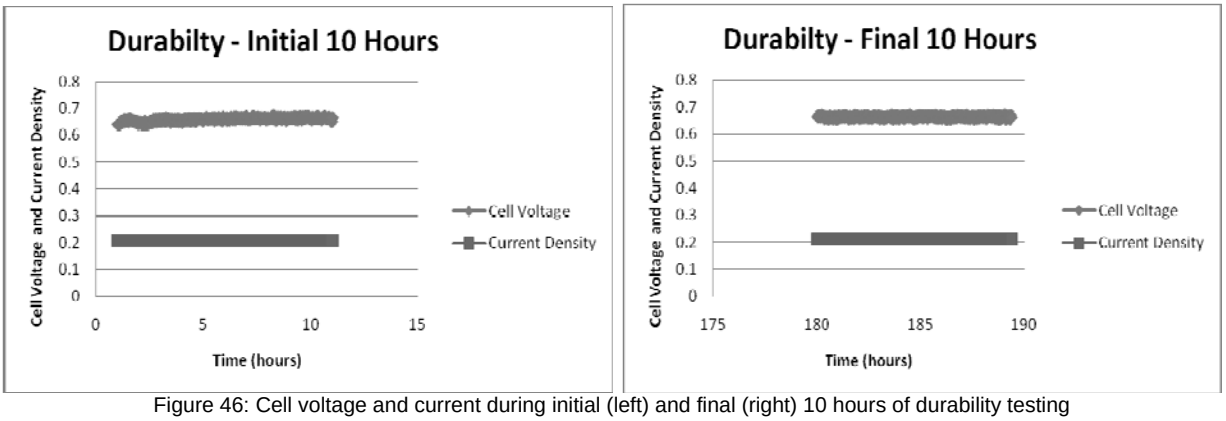

Figure 46: Cell voltage and current during initial (left) and final (right) 10 hours of durability testing

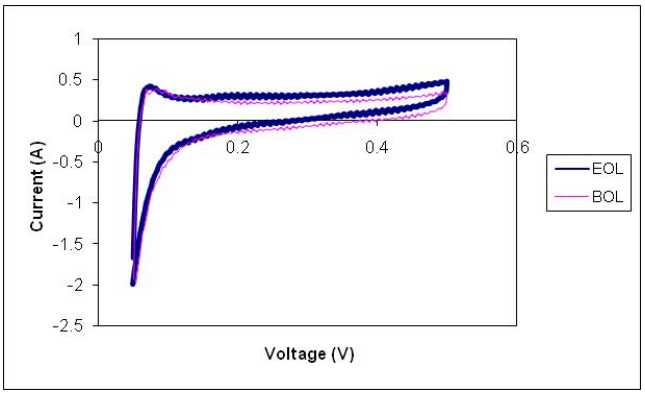

Figure 47: Cyclic voltammetry plots for beginning and end of life of MEA subject to 190 hour durability test

In summary, the ultrasonically sealed MEAs exhibited excellent stability under extreme start/stop operating conditions. There was no cell voltage degradation observed during the entire test and the cell internal resistance change was minimal. No change in catalyst utilization was observed as well during the test duration.

Task 10.0 – Updated Cost Analysis.

The Phase I cost analysis was updated based on the new process cycle time achieved using thermal sealing with APC, i.e. 5 second sealing time plus 10 seconds for station-to-station transfer time, as shown in table 4. The potential manufacturing cost savings for the sealing operation alone is 76% using thermal without APC and 82% using ultrasonics.

Table 4: Phase II Manufacturing Cost Analysis Summary (Seal Process only)

	Current Thermal	**Thermal w/APC**	**Ultrasonics**
Cost Category			
Capital Depreciation	$0.0896	$0.0120	$0.0071
Tooling	$0.0521	$0.0463	$0.0416
Labor	$0.0386	$0.0052	$0.0080
Electricity	$0.0579	$0.0077	$0.0002
Chilled Water	$0.0293	$0.0039	$0.0000
HVAC (CapEx & Operations)	$0.0009	$0.0007	$0.0000
Maintenance	$0.0121	$0.0016	$0.0010
Materials			
Space	$0.0041	$0.0005	$0.0004
Disposal Costs	$0.0896	$0.0120	$0.0086
GRAND TOTAL per MEA	$0.3741	$0.0899	$0.0668
GRAND TOTAL per KW	$1.4965	$0.3597	$0.2672
TOTAL MANUFACTURING COST REDUCTION	n/a	-75.97%	-82.14%

Task 11.0 – Phase II program review.

The program review was conducted on September 21, 2011 with Nancy Garland and Jesse Adams in attendance. RPI CATS was notified of a ‘Go’ decision for Phase III on October 5, 2011.

Task 12.0 – Short Stack Testing

5-Cell Stacks: Research activities for Task 12.0 continued the work from Task 9.0, where capabilities to test up to ten 50 cm^2 MEAs in a stack was developed and demonstrated. Five-cell stack tests were run with both thermally and ultrasonically bonded MEAs, and polarization curves with air were produced for two iterations of each sealing process. Figure 48 (left) is an example of the polarization curves that were obtained for thermally bonded MEAs (note: Cell 1 is located closest to the cathode end plate). The figure shows a tight grouping of performance for each MEA as well as good performance across the stack. In one of the replicate experiments, one of the MEAs was assembled backwards, i.e. with the cathode on the anode side, and produced poor performance in that cell. This was detected through examination of the polarization curve and then verified upon disassembly of the stack. The set of polarization curves with the poorly performing cell is shown in Figure 48 (right). These tests demonstrated that: stacks of high-temperature MEAs were able to run well; the dedicated test stand and software successfully collected all the desired measurements of temperature and voltage; the performance of the individual MEAs in the stack was comparable to single cell tests; and a faulty MEA is easily detected.

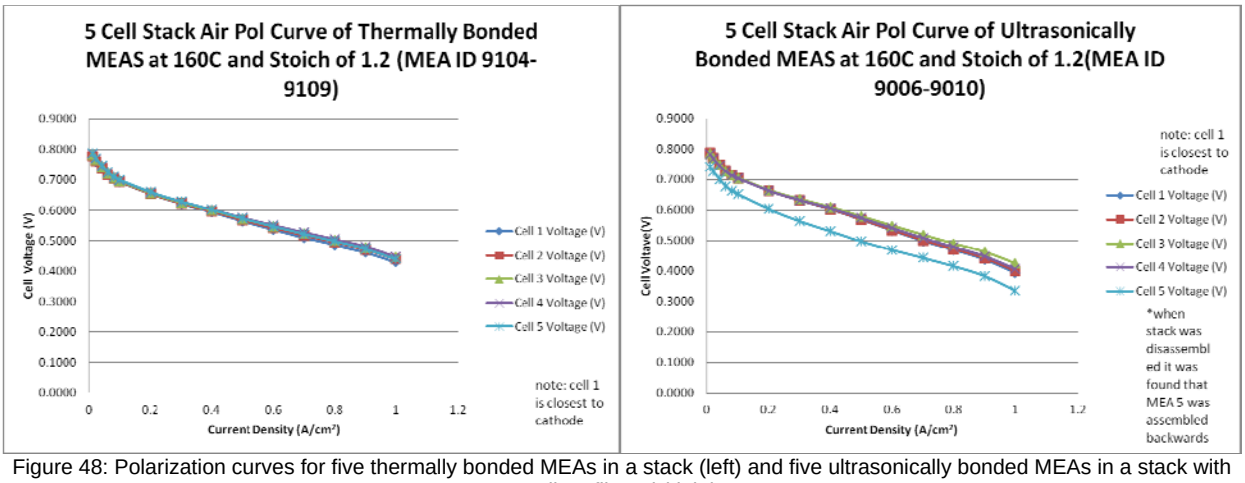

Figure 48: Polarization curves for five thermally bonded MEAs in a stack (left) and five ultrasonically bonded MEAs in a stack with cell #5 flipped (right)

10-Cell Stack Details: The stack hardware was configured for testing ten cells simultaneously. Features and improvements made to the stack, shown in Figure 49a, include:

- Materials
  - poco-graphite bipolar plates
  - stainless steel end hardware
  - gold plated copper current collectors
  - Teflon insulators
- O-ring seals at end-cells
- Flat gaskets at MEAs
- Tie rods with belleville washers and heat shrink tubing (to avoid shorting)
- Stainless steel cooling plate placed near stack center
  - compressed air for cooling (internal channels)
  - neighboring cells have same design as end “polar” cells
- Temperature and voltage are measured for each cell (see Figure 49b)
- Thermal insulation box (see Figure 49c).

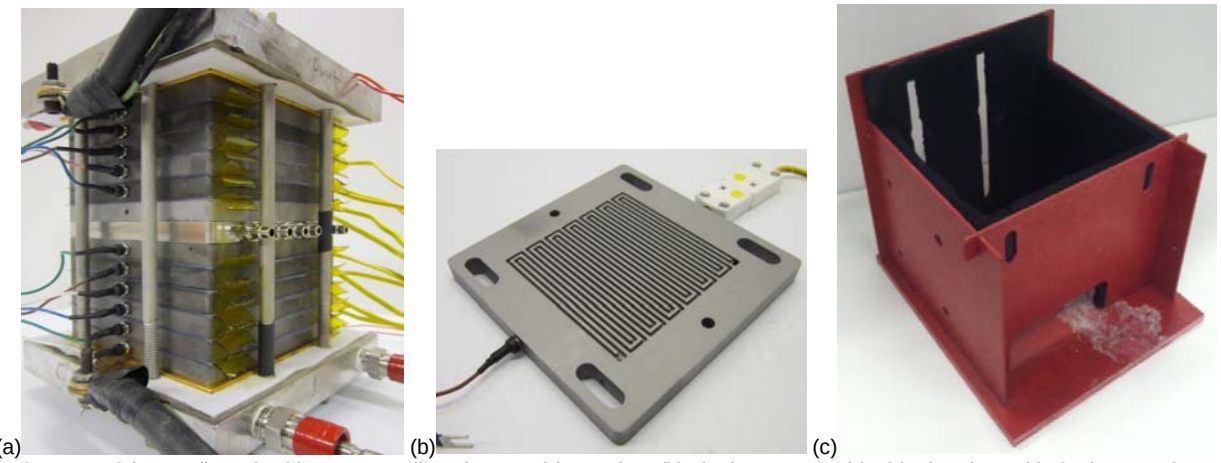

(a) (b) (c)

Figure 49: (a) 10-cell stack with center cooling plate read for testing, (b) single poco graphite bipolar plate with dual serpentine flowfield pattern along with temperature and voltage probes and (c) insulated box used to help regulate temperature during testing

10-Cell Stack with Thermally Bonded Cells: Two 10-cell stacks consisting of all thermally pressed MEAs were assembled and tested. Polarization curves were taken with oxygen and air on the cathode. Beginning of life polarization curves for the first thermally pressed stack are shown in Figure 50 (left) for oxygen and Figure 50 (right) for air. Note the consistency in performance among all the thermally bonded cells, and the slightly improved performance of cells with oxygen instead of air, as expected.

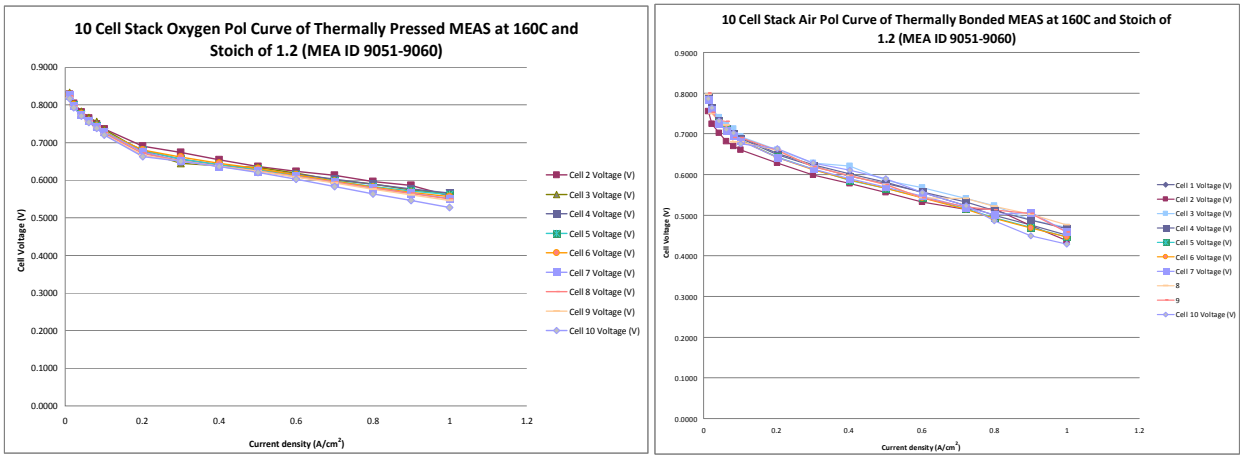

Figure 50: Polarization curves for 10-cell stack of thermally bonded 50 cm2 MEAs with cathode supplied with oxygen (left) and air (right)

10-Cell Stack with Ultrasonically Bonded Cells: The polarization curves in Figures 49 and 50 show stack performance for a ten-cell stack of ultrasonically bonded MEAs: air on cathode side at beginning of test (Figure 51 (left)); air on cathode side after 200 hours (Figure 51 (right)); oxygen on cathode side at beginning of test (Figure 52 (left)); and oxygen on cathode side after 200 hours (Figure 52 (right)). Except for cell 10 with air, all cell polarization curves are tightly grouped indicating uniformity in performance.

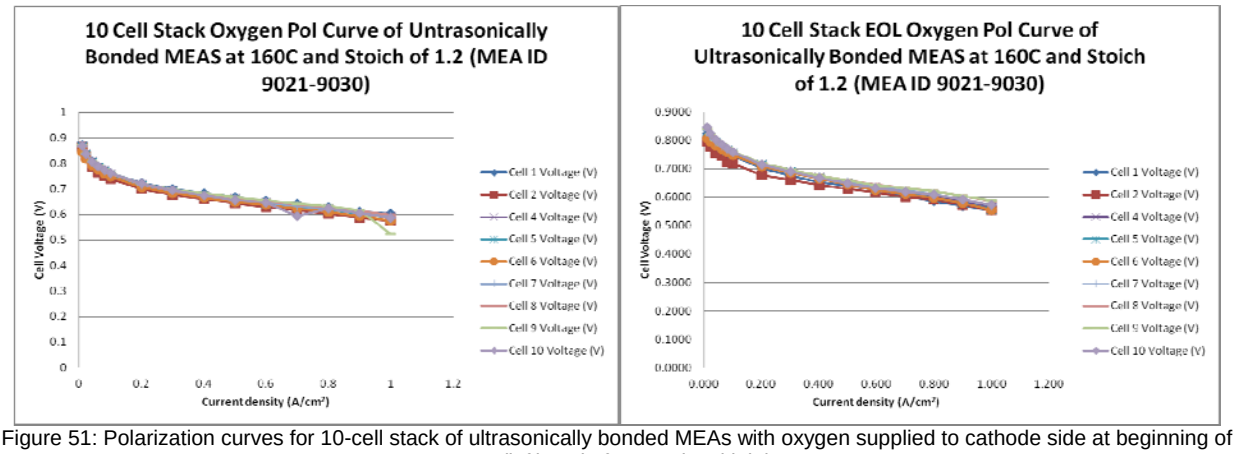

Figure 51: Polarization curves for 10-cell stack of ultrasonically bonded MEAs with oxygen supplied to cathode side at beginning of test (left) and after 200 hrs (right)

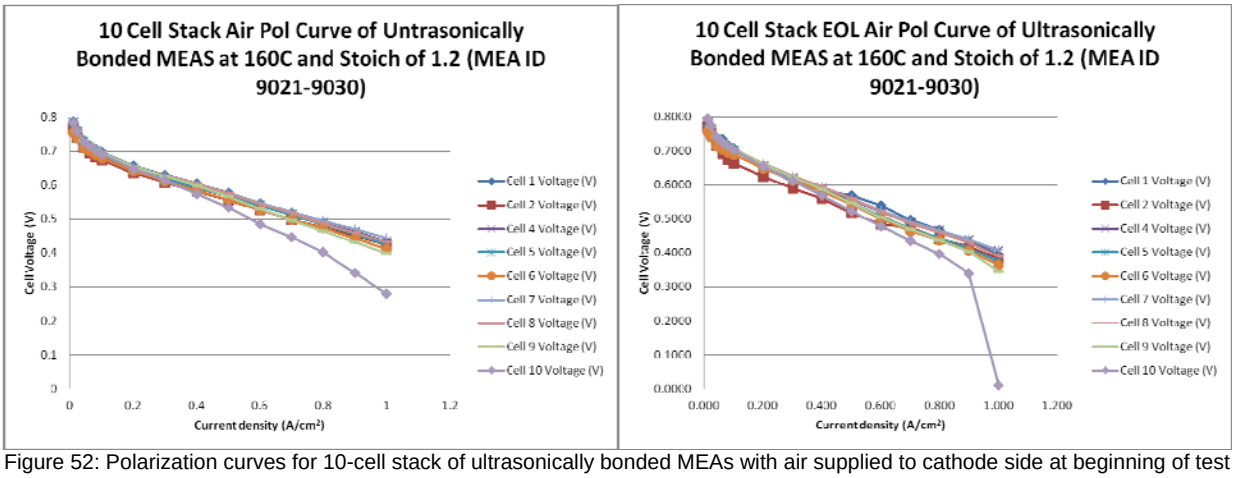

Figure 52: Polarization curves for 10-cell stack of ultrasonically bonded MEAs with air supplied to cathode side at beginning of test (left) and after 200 hrs (right)

Temperature Sensitivity: Variation in temperature and reactant gas flow distribution due to cell position was verified to have minimal effect on stack performance. In one particular case, steady-state temperature distribution was found to range between 157.3 and 162°C at 0.4 A/cm^2 (see Figure 53a) for a 10-cell stack with a 160°C setpoint. Temperature-voltage characterization at the single cell level indicates that this level of variation contributes to ~4 mV cell voltage variation at same current densities, as shown in Figure 53b.

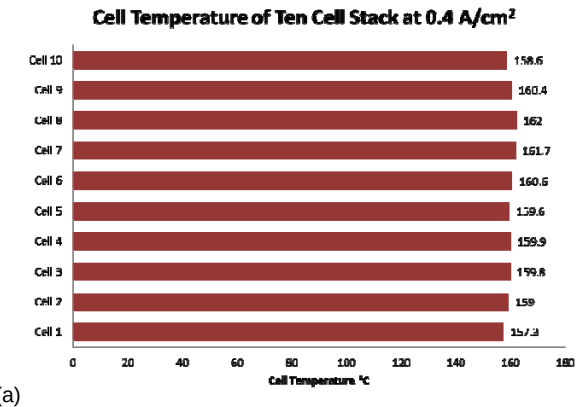

(a)

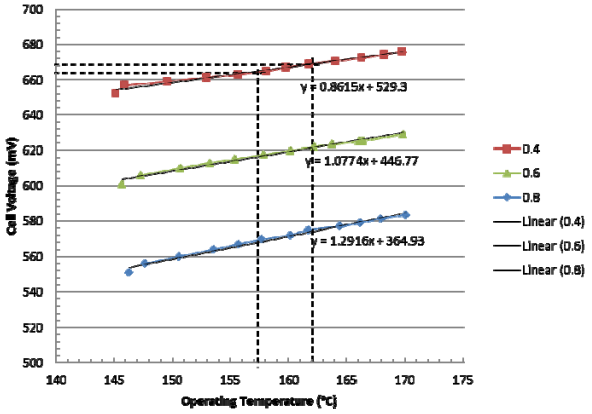

(b)

Figure 53: (a) Cell temperature distribution in 10-cell stack operating at 0.4 A/cm2 and (b) expected variation in cell voltage due to this temperature variation.

Comparison: Figure 54 summarizes a comparison of thermally and ultrasonically bonded MEAs operating in 10-cell stacks. Performance deviation between the two processes is negligible. The lower data series in Figure 52 illustrates the cell-to-cell variation in performance observed for thermally and ultrasonically bonded MEAs. With the exception of a single cell in the ultrasonically bonding stack, one standard deviation in cell-to-cell voltage performance at 1 A/cm^2 was less than 7% of the average cell potential. At typical operating current densities (0.6 A/cm^2), it remained below 4%. Cell-to-cell performance varies little throughout the stack architecture (for thermal or ultrasonic processing). We concluded that there is no detrimental impact of the ultrasonic bonding process on stack performance, and the stack architecture is a valid platform for simultaneous testing of cells.

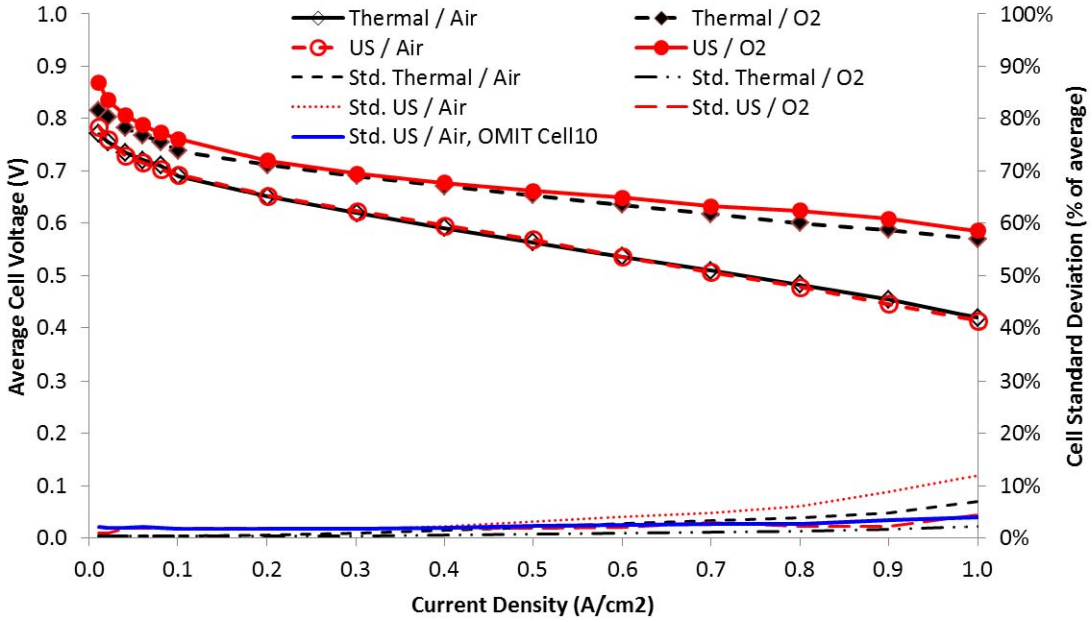

Figure 54: Average and standard deviation ("std") of performance for ultrasonically and thermally bonded MEAs in a 10-cell stack (1.2 stoich H_2 / 2 stoich O_2 and air).

10-Cell Stack with 5 Thermally Bonded Cells and 5 Ultrasonically Bonded Cells: A stack consisting of five thermally bonded and five ultrasonically bonded MEAs was fabricated and tested. The polarization curves for H_2/Air and H_2/O_2 are shown in Figure 55. The stacks were constructed with the MEAs alternating, i.e. the odd cells were thermally bonded and the even were ultrasonically bonded. By inspection of Figure 55 (left), there does not appear to be any significant difference in performance between cells when the stack was operated on H_2/O_2, but the H_2/Air (Figure 55 (right)) shows a very clear division between the odd and even numbered cells, which corresponds to a performance difference between the thermally bonded (slightly better) and ultrasonically bonded (slightly worse) MEAs.

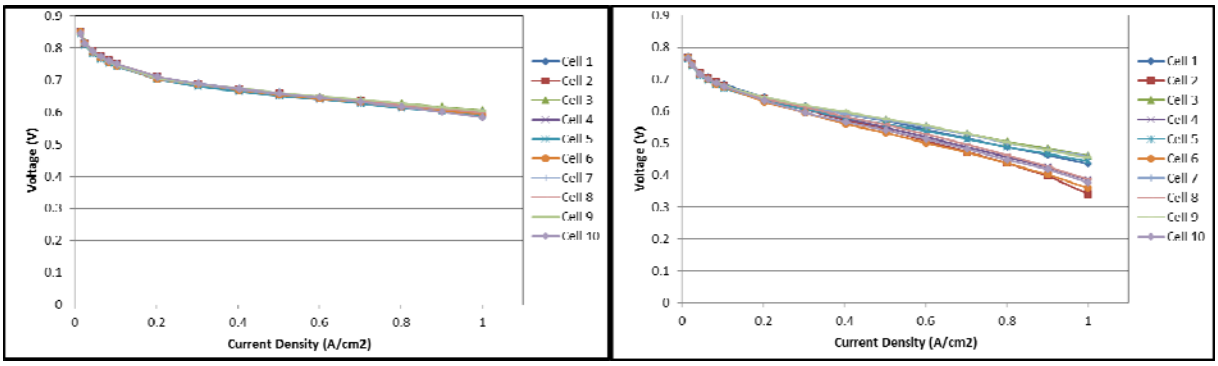

Figure 55: H_2/O_2 (left) and H_2/Air (right) polarization curves for 5 each of thermal and ultrasonic MEA stack

To gain further insight into the performance, the data from both tests was plotted as the average polarization curve performance for each manufacturing method and the standard deviation was plotted on the same graph. These plots can be seen in Figure 56. Note that in Figure 56 (left), the vertical axis for voltage had to be changed in order to detect the difference in average performance between the two different MEA types. From this test, it can be seen that both manufacturing processes have similar performances, but with thermally bonded slightly outperforming the ultrasonically bonded MEAs with air on the cathode.

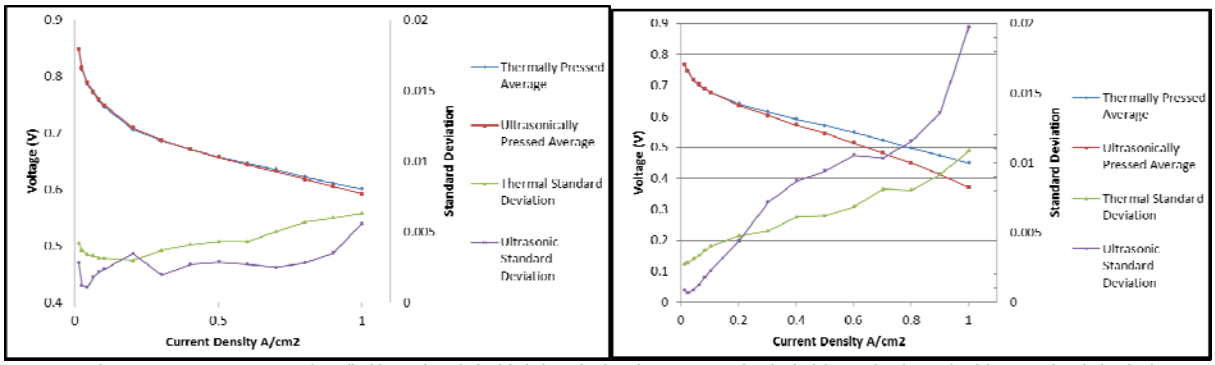

Figure 53 – Average H_2/O_2 (left) and H_2/Air (right) polarization curves for hybrid stack plotted with standard deviation

Stack Testing Summary: The stack can be used to quickly determine whether changes in processes or process parameters have any significant effect on performance. Using a single cell testing fixture, it would take ten times longer to gather enough data to be able to draw correlations between changes in MEA fabrication. With a testing cycle around 15 hours, that means the difference between one day of testing and ten days of testing. In addition, it streamlines the data collection process stack testing and provides more consistent results; since a stack delivers the same testing situation for all 10 cells being tested, while MEAs tested in single cells may experience different operating conditions. The capability to detect differences in cell performance has been shown by alternating ultrasonically and thermally bonded MEAs in the same stack, and the resulting polarizations show grouping in cell performance based on manufacturing method.

Task 13.0– Testing of High Temperature MEAs with Larger Active Area.

Scaling to 140cm^2 has been a challenge due to fuel cell test hardware failures, rather than the ultrasonic process itself. Following material and design improvements made to the test cell's flowfield plate along with debugging of the test hardware and equipment, the performance of thermally and ultrasonically 140cm^2 MEA was finally approaching the baseline 45cm^2 MEA, as shown in Figure 54. Thermally and ultrasonically bonded MEAs with 140cm^2 active area had previously been shown to have negligible deviation. Elevated ohmic losses are believed to be caused by insufficient current collector thickness and poor electrical interface between current collector and bipolar plate

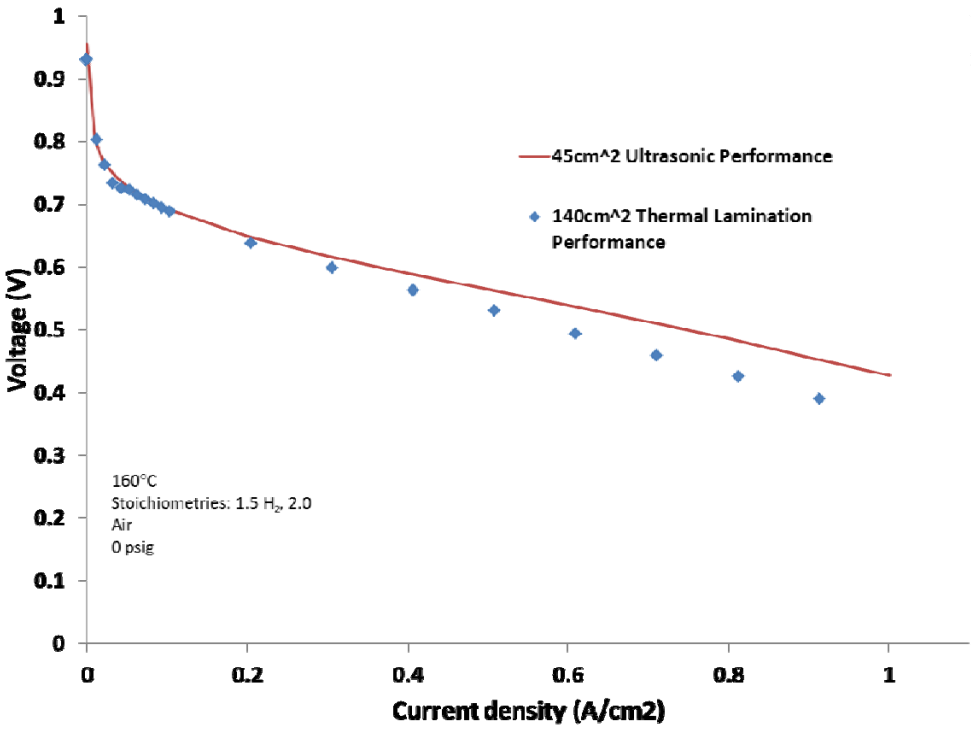

Figure 54: 140cm^2 thermally laminated MEA performance compared to a baseline 45cm^2 ultrasonic MEA.

As further proof that the 140 cm^2 test hardware was responsible for the lower performance shown in Figure 2, MEAs with 650 cm^2 active area, the largest to date, were recently bonded ultrasonically using the 15 KHz machine, tested by project collaborator BASF Fuel Cell using their own test hardware, and performance was compared to thermally pressed MEAs made by BASF. Details of the MEA are withheld due to proprietary concerns. The performance of the ultrasonically bonded MEAs (RPI 605 cm^2) running on H_2/O_2 at 160°C was actually better than the thermally bonded ones (BFC 605 cm^2), as shown in Figure 55.

The overall conclusion is that ultrasonic bonding provides at least equivalent performance to thermal bonding for a wide range of MEA sizes.

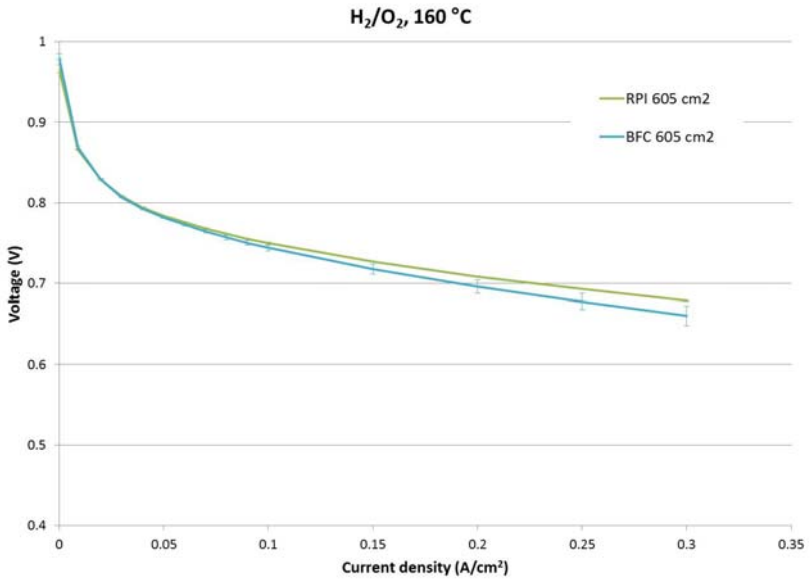

Figure 55: Comparison of 605 cm^2 ultrasonically bonded MEA to BASF Fuel Cell thermally bonded MEA.

Task 14.0– Quality Testing of Thermally and Ultrasonically Bonded High Temperature MEAs. .

This task focuses on the development of real time quality control related to functionality of MEAs. A functional test which provides some measure of electrochemical bond area and quality, as well as the detection of electrical shorts between anode and cathode electrodes has been developed. The test utilizes cyclic voltammetry, yet avoids the need for the typical controlled atmosphere which would be costly to implement in a manufacturing environment. The application of CV in an ambient and symmetric environment (same on both electrodes) results in a response very similar to that of an electrochemical capacitor. Thus, analysis of the data is well understood and borrows from knowledge related to super capacitors.

Ten polybenzimidazole (PBI) MEAs were prepared using ultrasonic lamination techniques, then run through the ambient CV scan, 8 of the 10 MEAs were then heat treated, all 10 MEAs were run through a second CV scan, and a 10 cell stack was then prepared and run through various operating points. Stack performance was then compared to the CV results for proof of concept of the proposed measurement method. Results indicate that the use of ambient condition CV may be useful in process and quality control related to the detection of electrical shorting, reduced active area (due to gross membrane misalignment), and the successful development a quality electrochemical interface during heat treating.

Approach: Cyclic Voltammetry (CV) is applied as is typical for the measurement of electrochemical capacitors. The detection of electrochemical active area and electrical shorts is feasible. In this study MEAs were clamped between two carbon plates, which are, in turn, clamped between two gold plated current collectors and connected to the leads of the potentiostat. For purposes of measurement technique development, five different voltage scan rates were run on each sample (30, 50, 75, 100, 150 mV s^{-1}). Scan rate influences the current response rate, following the familiar state equation of a capacitive circuit.

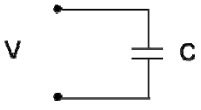

$$I = \frac{dV}{dt}C$$

In an ideal sense, the current response to cyclic voltage scans would produce a box-like characteristic relationship of current to voltage. A scan rate of 100 mV s^{-1} on a 0.3 F ideal capacitor would produce a response similar to that shown in Figure 56. More rapid scan rates result in larger currents. Larger capacitances also result in larger currents. In reality, devices are more complex.

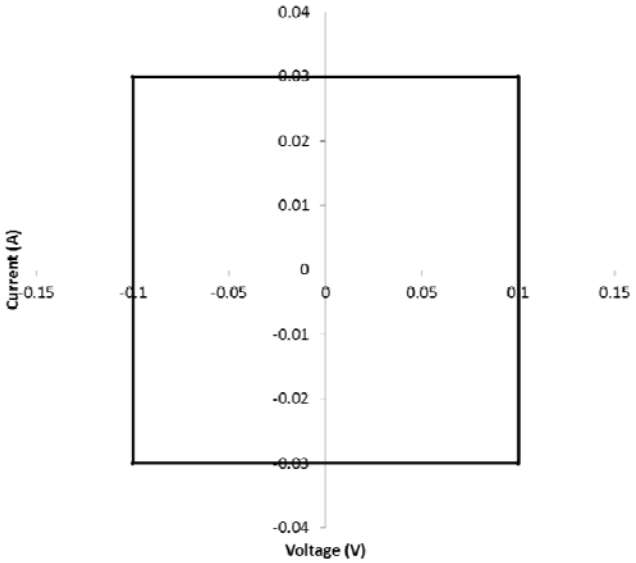

Figure 56: Modeled response of an ideal capacitor with 0.3 F capacitance and 100 mV s^{-1} scan rate.

The detection of electrical shorts between anode and cathode electrodes would be valuable for process control related to lamination pressure and quality control. While an ideal case of electrochemical capacitance would result in a box-like I-V relationship, an electrical short distorts the box inversely proportional the electrical resistance (Figure 57). The degree of electrical shorting can be calculated from the slope of the top and bottom of the box ($R = \frac{dV}{dI}$). With an electrical short approaching infinity (zero short), the slope approaches zero and the response approaches that of Figure 56.

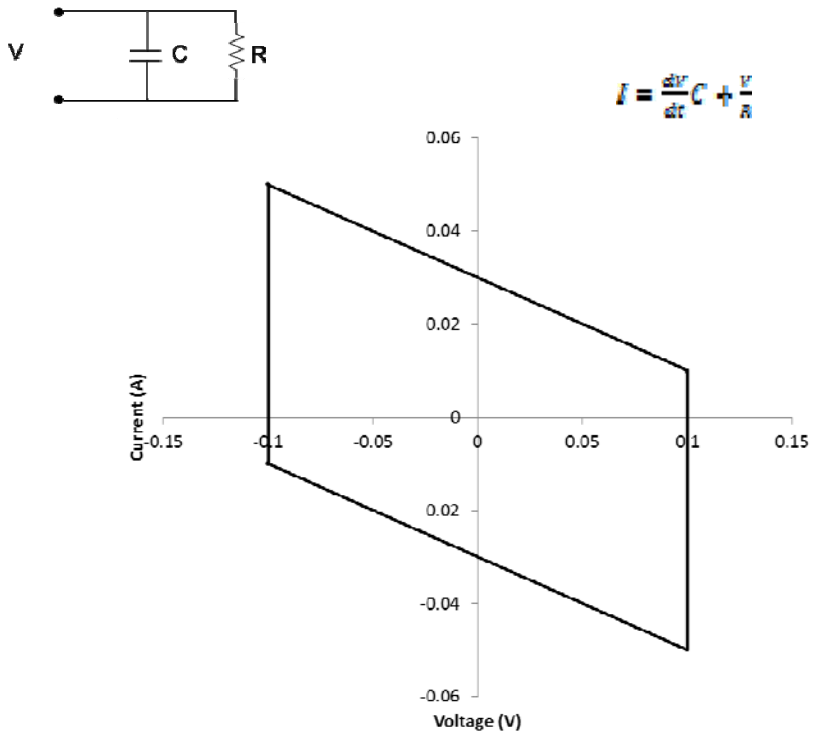

Figure 57: Modeled response of an ideal capacitor with partial electrical shorting of electrodes (0.3 F, 100 mV s^{-1}, 5 Ohm electrical short).

As in any device, there are imperfections which manifest themselves as inefficiencies in the form of electrical shorting and resistances within the electrode structure. Such internal resistances retard the overall temporal response, leading to rounded corners after switching between positive and negative scan cycles, as shown in Figure 58.

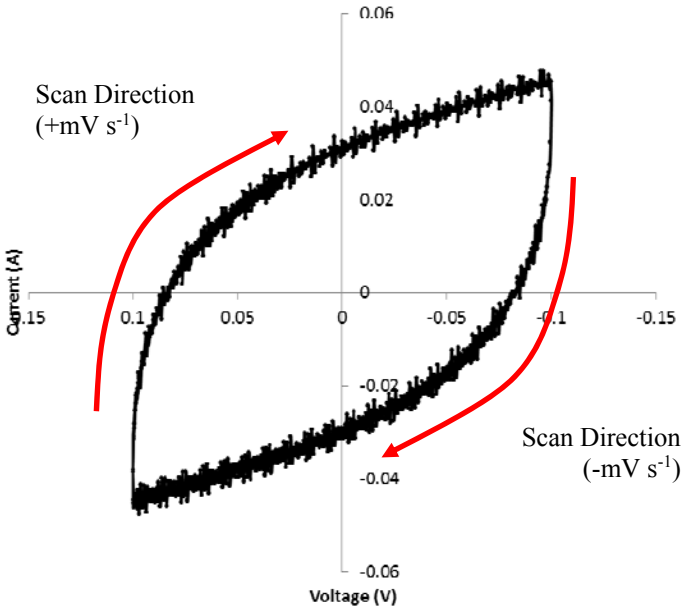

Figure 58: 100 mV s^{-1} scan rate CV of 45 cm^2 MEA with approximate 0.3 F capacitance, 5 Ohm electrical short, and internal resistance.

As previously discussed, MEA capacitance measurement in ambient symmetric conditions is sensitive to the capacitance, degree of electrical shorting and internal resistances of the electrode structures. These characteristics will have sensitivities to test conditions such as temperature, humidity and compressive load. Temperature and humidity will impact internal resistances as local ionic conduction within the electrode is sensitive to these environmental variables. Compression of the test rig will influence interfacial resistance as well as conduction within the gas diffusion layer. The degree of sensitivity to, and control of, test variables will dictate measurement system resolution.

Speed and Cost: As with any process control, implementation cost is a critical parameter. The rate at which measurement can be performed will dictate the magnitude by which the approach would be deployed (slower systems requiring more parallel installations). In the simple model of a parallel capacitor-resistor network, sensitivity to capacitance is driven by the rate at which the voltage is scanned. Faster scan rates increase the current response for a given capacitance. Measurement of electrical shorting is a function of voltage. Scans to larger voltages (negative and positive) will heighten sensitivity to shorting. Internal resistances dampen the cell response to changes in scan direction (switching between positive and negative voltage scan rates). The ability to rapidly switch scan direction and stabilize the scan rate will minimize the chance of misinterpreting capacitive effects on the temporal response to scan direction changes, thus maximizing sensitivity to internal resistances.

It was found that the slowest scan rates produced high variability in measurements. An underlying cyclic characteristic was observed in all scans, but more so during slower scan rates (shown later in Figure 59). More rapid scan rates produced consistent results; however the fastest scan rates resulted in capacitive effects overshadowing sensitivity to electrical shorting. This aligns with expectations, given that capacitance couples well with scan rate and shorting has more sensitivity to elevated voltages. Armed with expectations of capacitance and shorting magnitudes, one can design an inspection routine which maximizes sensitivity to each element of interest.

Instrumentation: While implementation of CV for measurement of fuel cell MEA electrochemical surface area is typically limited by the maximum current of the potentiostat, the absence of fuel and

subsequent net transport (hydrogen pumping in the case of acid cells) minimizes the maximum current draw. Tests performed in this study involved a 45 cm^2 active area, producing maximum currents of roughly 0.06 A (1.33 $mA \cdot cm^{-2}$) when scanning at 150 $mV \cdot s^{-1}$. A standard 2 A capacity potentiostat would have the capability of measuring MEAs up to 1500 cm^2 in area. The addition of a booster would provide additional capacity.

Experimental: Phosphoric acid imbibed polybenzimidazole (PBI) membranes and proprietary catalyzed gas diffusion media (GDM) were supplied by BASF Fuel Cell (Somerset, NJ). Anode and cathode electrodes were side specific. Electrodes and membrane were cut to size by hand. Preparation of PBI MEAs included the use of FEP coated Kapton sub-gaskets. Sub-gaskets were mounted in metal frames to aid with alignment and handling during various lamination steps. Internal features (active area opening) were cut on a laser cutting station. Framed sub-gaskets were then laminated to anode or cathode catalyzed GDM using ultrasonic bonding. Pairs of anode and cathode gasket-electrode-assemblies were then assembled to sandwich a PBI membrane. Layers of Kapton were placed on either side of the MEA to protect ultrasonic lamination tooling from acid. The active area of each MEA was then laminated using ultrasonic motion at 15 kHz, 30 μm peak-to-peak amplitude, 0.65 MPa, and reaching 5000 J of energy applied. The membrane of cell #2 was intentionally misaligned to simulate electrical shorting and reduced active area. Porting (internally manifolded stack hardware), alignment features and outside dimensions were then laser cut, releasing the MEAs from the alignment frames used during fabrication. Each cell was numbered 1-10.

Measurement: Each cell was then run through CV scans at rates of 30, 50, 75, 100 and 150 $mV \cdot s^{-1}$ before and after heat treating. Measurement consisted of placement within a symmetric stack of gold plated current collectors, POCO graphite flow field plates and the MEA. A 4.54 kg mass was placed on top of the stack to maintain consistent interfacial resistances (0.89 $N \cdot cm^{-1}$). A Princeton Applied Research Parstat 2273 was used for CV scanning with a four probe configuration. Voltages were scanned between -0.1 and 0.1 V. MEAs were then heat treated at 160°C in air for 30 minutes. Cells 9 and 10 were not heat treated to investigate measurement sensitivity to treatment. After heat treating, a second set of identical CV scans were performed on the MEAs.

Stack Assembly: A 10-cell stack consisting of stainless steel end plates, Teflon film insulators (0.020”), gold plated copper current collectors, polar POCO flow plates (end cells and cooling plate cells), bi-polar POCO flow plates, perfluroalkoxy (PFA) flat gaskets (target 20% compression / 80% of MEA thickness), a single stainless steel cooling plate, and tie rods, belleville washers and nuts. O-rings were used to seal internal manifolds at the interface of stainless steel end hardware, insulators, current collectors, end flow plates and cooling plates. PFA flat gaskets were used for sealing at individual MEA – plate interfaces. Anode plates utilized a double parallel-serpentine flow pattern, whereas cathode plates utilized a triple parallel-serpentine pattern. Temperature and voltage were monitored for each individual cell (see Figure 49b).

Stack assembly started at cell #10, with the anode facing down (. Alignment rods used during assembly to maintain component registration were removed after assembly and tie rod compression.

After the stack is assembled, eight tie bolts were inserted with two Belleville washers at each end. Heat shrink tubing was used to minimize the chance of electrical shorting between tie rods and active hardware. Once all the tie bolts were inserted, a nut was installed following by finger tightening of the bolts. Each bolt is finally torqued to 45 in-lb in a star pattern to prevent uneven loading of the stack. Each bolt supplies an estimated 900 lb of compressive load for a total of approximately 2700 lb force to the stack. The final stack is shown in Figure 49a. The stack was placed in an insulating box (see Figure 49c) to aid in warm up and thermal management. Two silicon pad heaters clamped to the stainless steel end plates were used for warm up.

The stack was pressure tested for overboard and cross-over leakage (anode – cathode cross leaks) at 3 psi with nitrogen. Substantial cross-leaks were observed (> 100 ccm), likely due to membrane misalignment on cell #2. The stack was not disassembled to address the leak since cell #2 data was desired for comparison to CV testing.

Test Station: A fuel cell test station capable of handling the voltage and current output was used to operate the 10-cell stack. The station was configured to control and monitor anode and cathode gas sources (H_2 / reformate, Air / O_2) and flow rates (< 20 slm), end plate heaters, cooling, individual cell voltages and temperatures, and load. The station was coupled with a LabView interface for control and data management. Cooling was provided by compressed air, ported to the stainless steel cooling plate at the center of the stack and controlled manually. The station does not have humidification capabilities and all gas flows were dry. N_2, O_2 and H_2 were all supplied from standard compressed gas cylinders at purities of better than 4.5 9's. Air was supplied by a compressor outfitted with a moisture trap.

Startup consisted of heating to greater than 100°C with nitrogen gas on the anodes and cathodes flowing at 200 ccm. Above 100°C, H_2 and O_2 were introduced at 200 ccm to the anode and cathode chambers, respectively. After fully purged of N_2, a small load was drawn on the stack to aid in warm up. Current was gradually increased while maintaining at least 0.6 V per cell and stoichiometries of greater than 2 for the anode and cathode. Such operation continued until the stack reached a nominal operating temperature of 160°C.

A test protocol including cathode air or O_2 and anode H_2 was then started. Preliminary operation of the 10-cell stack on O_2 was successful. However, subsequent operation on air proved challenging for cell #2 (i.e. the defective one). Cell #2 voltages quickly degraded to 0 V and below. The stack was then cooled under N_2 flow at 200 ccm on the anode and cathode with no load. The stack was disassembled and cell #2 was removed. The reassembled 9-cell stack was then prepared for testing with similar procedures to the 10 cell stack. Operation of the 9-cell stack was successful up to 1 A cm^{-1} on O_2 and air.

Analysis:

Cyclic Voltammetry: CV data consisted of voltage, current and time for each cell and scan rate. A total of 100 scans were reviewed (10 cells, 5 scan rates, pre- and post-heat treatment), and one sample scan is shown in Figure 59. The inclusion of internal resistance and preliminary charge up response dictated that specific portions the scans were analyzed.

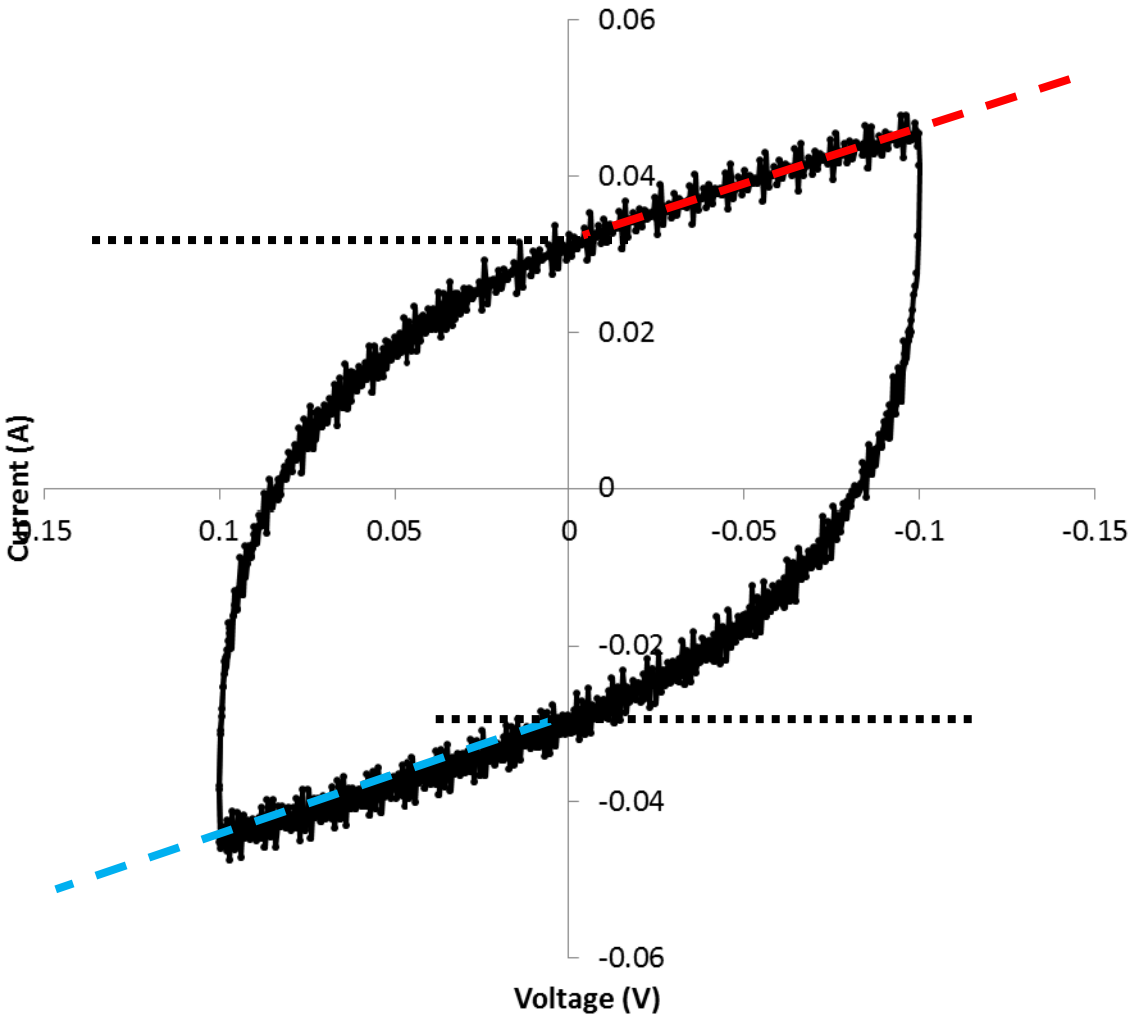

Figure 59: Sample CV scan (100 mV s^{-1}). The degree to which the current vs. voltage is misaligned from the x-axis (slope $dIdV^{-1}$) is related to electrical shorting between the electrodes. Non-linear regions are an artifact of internal resistances within the electrode. Limiting analysis to the linear sections (red and blue dashed lines) allows for the isolation of the effects of electrical shorts. The y-axis intercepts relate to the electrochemical capacitance of the cell (black dotted lines). Data is shown as the negative of the actual current drawn (due to data processing characteristics).

Curved regions in the current-voltage relationship occur immediately after changes in voltage scan direction and are related to internal resistances within the electrode. This series resistance effectively delays charging of the capacitance (Figure 60). The linear region and y-axis intercept correspond to electrical shorting and cell capacitance (see Figure 59). Isolating these regions and filtering the higher frequency cyclic noise was done in Matlab.

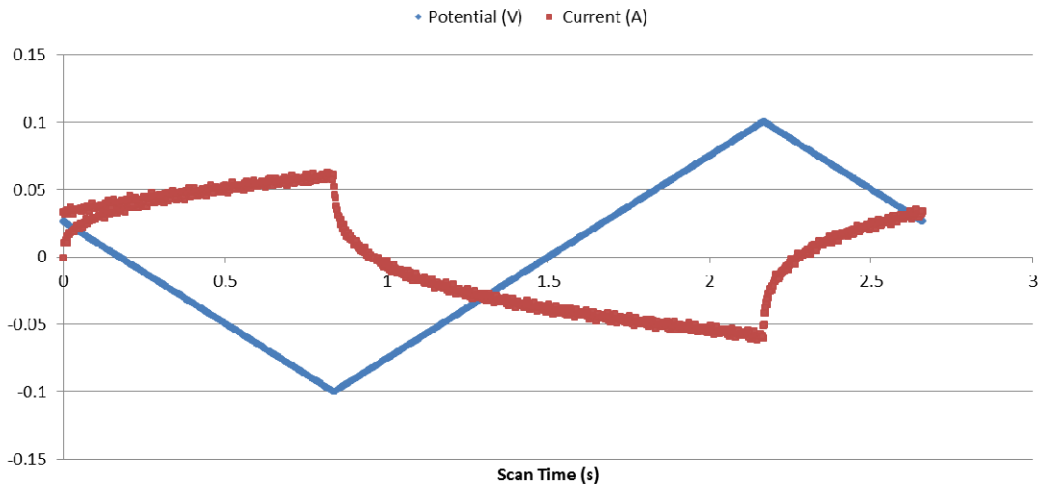

Figure 60: Sample time series data of the CV. Two scans are shown as an overlay. Immediately after time 0 s of the 1st scan, one can see the trend of initial capacitive charge up (originating at 0,0).

A script was written in Matlab to perform unbiased and rapid analysis of the data sets. The script consists of the following high level steps.

1. Set upfront parameters to avoid charge up transients and varying array sizes
2. Collect file list information from directory
3. Load data
4. Iterate to collect and process data from each scan before heat treatment
5. Repeat for post-heat treatment
6. Process and plot resistance and capacitive measurements for pre-heat treatment, post-heat treatment and comparison.
7. Save plots to files.

Results: Individual CV scans (similar to basic data in Figure 59) is somewhat overwhelming for 100 tests. Hence, measures of electrical shorting and electrochemical capacitance were computed for each cell before and after heat treatment. Resistances to electrical shorting are shown in Figure 61. It is observed that very slow scan rates result in excessive noise, likely due to the cyclic signal observed in the raw data. Scan rates of greater than 50 mV s^{-1} did not produce as great a signal. However, a filter was added to the analysis routine to minimize effects.

Cell #2 shows a noticeable electrical short in excess of the other 9 cells for scan rates below 150 mV s^{-1}. It is believed that the elevated scan rate (150 mV s^{-1}) results in increased capacitive current, masking electrical shorting. Detection of shorting is amplified in the post-heat treatment scans (middle plot), even for the maximum scan rate. A comparison of two sets of scans was performed by calculating the ratio of resistances after and before heat treatment (bottom plot). This has the effect of normalizing for scan rate.

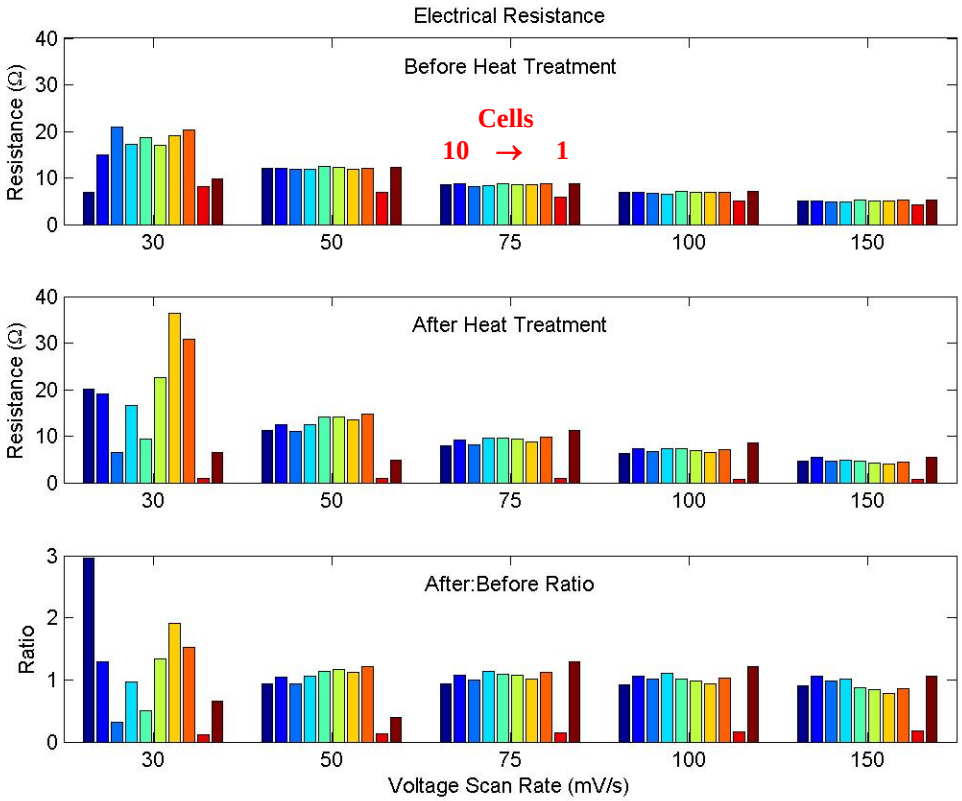

Figure 61: Electrical short measurements derived from ambient environment CV tests. Results are shown for 10 MEAs (left to right) for each voltage scan rate. Measurements taken before and after heat treating at 160°C for 15 minutes (top and middle plots) were compared as a ratio (after-heat treatment / before-heat treatment) to investigate options for conditional pass-fail testing.

Capacitances were reviewed in a similar fashion to the electrical shorting (Figure 62). Alternatively to resistance, there is essentially no indication of the misplaced membrane in cell #2; leading to the conclusion that there is little to no impact of the misplaced membrane on overall capacitance. However, the effect of heat treating is quite noticeable. Capacitances increased by a factor of 3 to 4 after heat treatment. Cells 9 and 10 were not heat treated and show little change in capacitance (as expected).

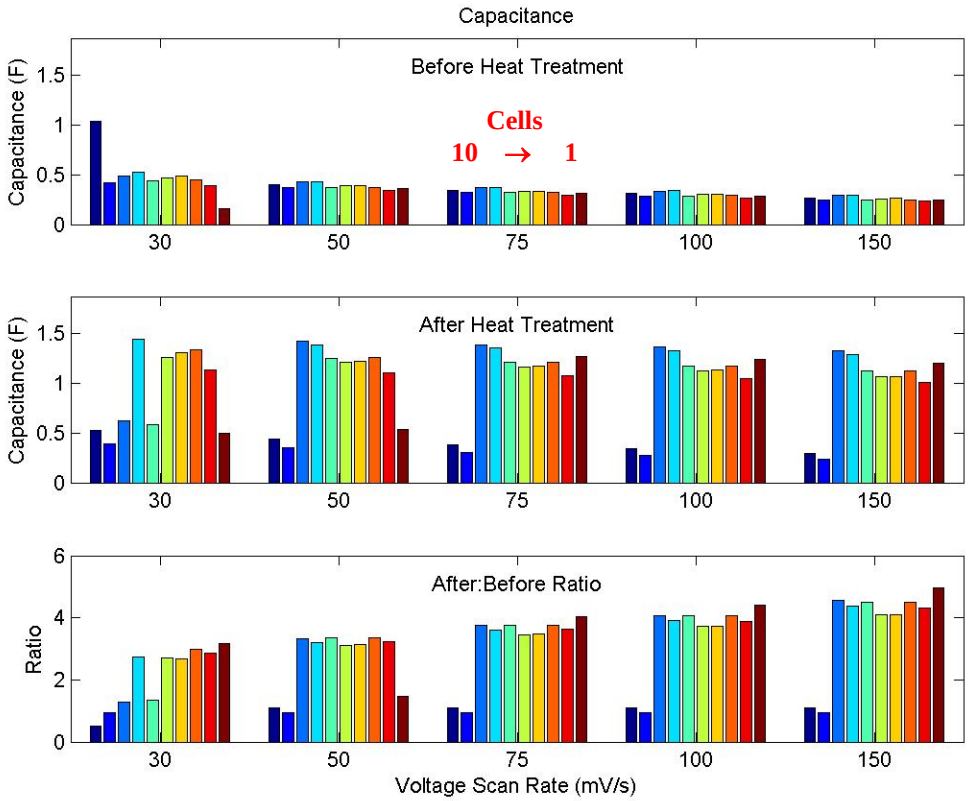

Figure 62: Capacitance measurements derived from ambient environment CV tests. Results are shown for 10 MEAs (left to right) for each voltage scan rate. Measurements taken before and after heat treating at 160°C for 15 minutes (top and middle plots) were compared as a ratio (after-heat treatment / before-heat treatment) to investigate options for conditional pass-fail testing.

Performance Testing: Preliminary testing was limited, due to large cross-over and over-board leaks in cell #2. The membrane misalignment observed during assembly and testing allowed large flow rates of reactants to exchange between the anode and cathode chambers. It also caused a poor seal in the gasket area, leading to over-board leakage. Shorting of the electrodes also contributed to poor performance on cell #2. Unfortunately, it is believed that the combined cross-over and over-board leaks also contributed to poor performance at end cells within the stack via reactant loss and effective fuel starvation.

Figures 63 and 64 show the stack performance on O_2 and H_2. Figure 64 summarizes individual cell performance at select current densities. It is observed that cell #2 performs very poorly. Cell #10 also has poor performance at 0.1 A cm^{-1} and above.

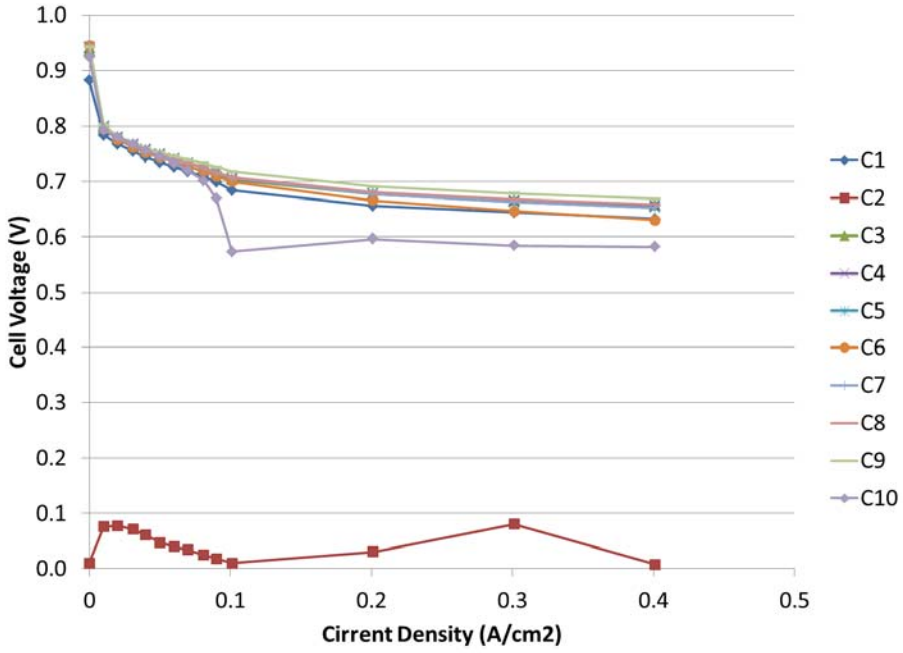

Figure 63: Polarization data for the 10-cell stack operating on H_2 and O_2 with stoichiometries of 1.2 and 2.0 respectively. Cell #2 shows very poor performance due to massive reactant crossover leakage, overboard leakage and electrical shorting.

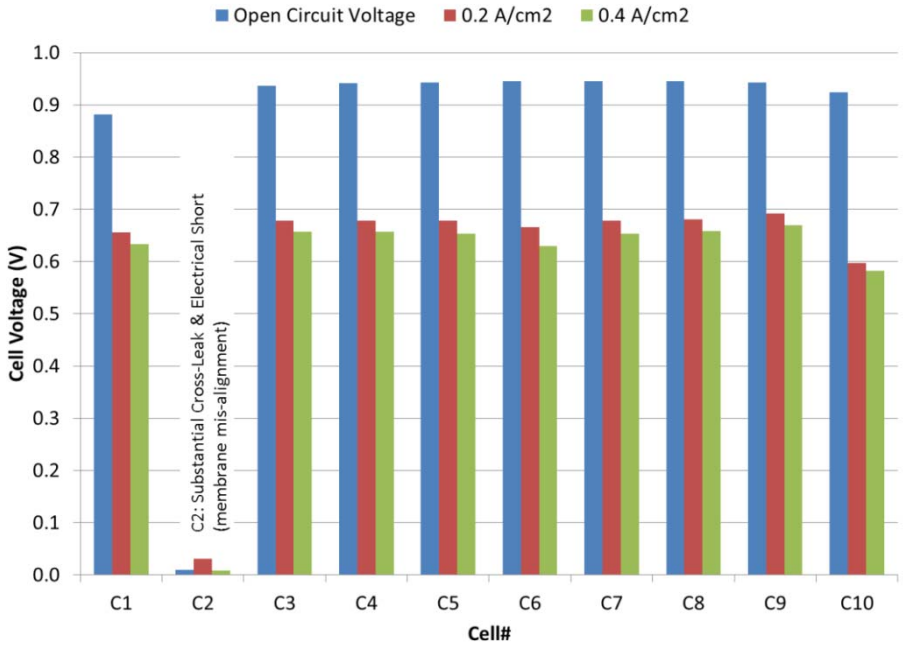

Figure 64: Individual cell performance of the 10 cell stack at select current densities, on O_2 and H_2, at 2 and 1.2 stoichiometries respectively.

Performance limitations were amplified when the stack was switched to air on the cathode at a stoichiometric ratio of 2 (Figure 65). The stack was not capable of operating above 0.5 A cm^{-2}. Above this current density, cells 2 and 10 were consuming the vast majority of the power generated by the remaining healthy cells and the test station could not support negative voltage operation on the stack (Figure 66).

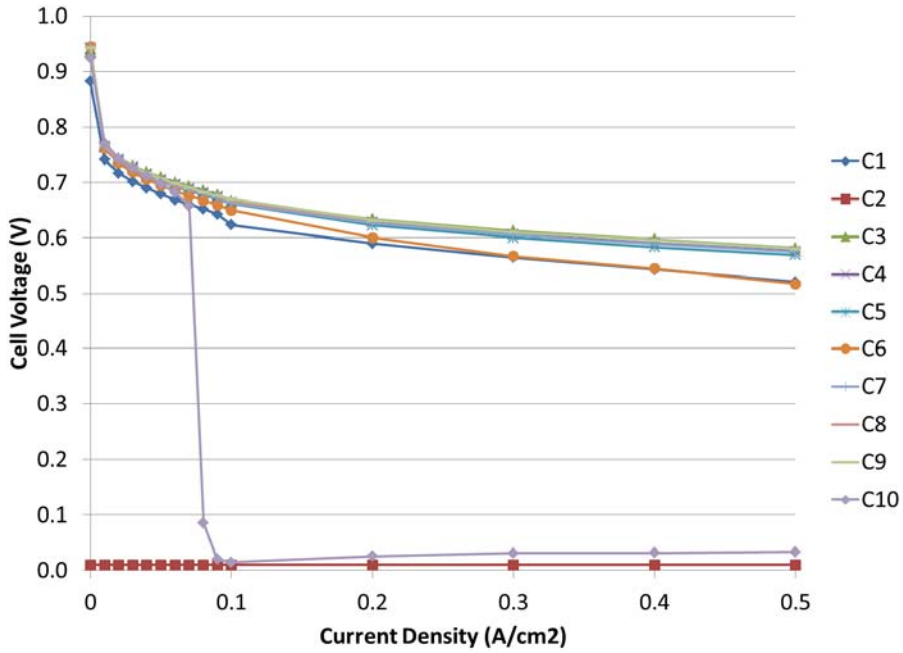

Figure 65: 10-cell stack operation on air and H_2 at stoichiometric ratios of 2 and 1.2. Operation above 0.5 A·cm^{-2} was not possible, due to extreme negative voltages on cell #2 and cell #10.

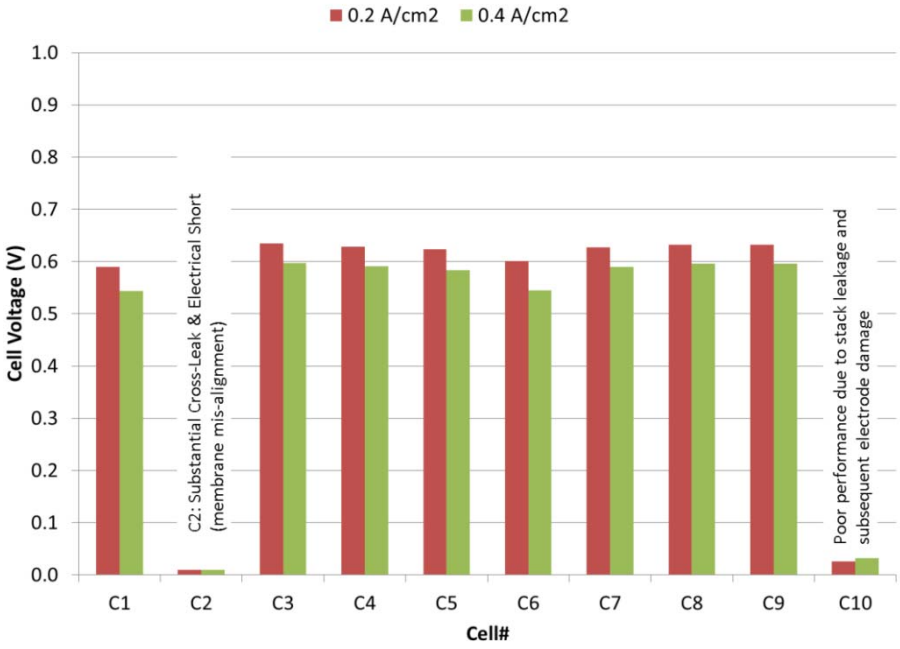

Figure 66: Individual cell performance for the 10-cell stack at select current densities, operating on air and H_2 at stoichiometric ratios of 2.0 and 1.2 respectively.

The 10-cell stack was then shut down and rebuilt as a 9-cell stack with cell #2 removed. This was done to allow more extensive testing without the negative impact of cell #2 on the remaining cells. Overall stack performance was greatly improved and polarization data was obtained for operation to 1 A cm^{-2} on both O_2 and air (Figure 67). With the exception of cells #1 and #10, individual cell performance was similar to that of the 9 cell stack (Figure 68). Cells #1 and #10 showed degraded performance which was likely caused by limited reactant supply during operation as a 10 cell stack. Overboard leakage at cell #2 may have led to limited reactant supply at stack end cells (during 9 cell testing) and irreversible electrode degradation. In addition, cell #1 measurements may have been effected by the reconfigured measurement system after the stack was rebuilt with 9 cells. Measurements are taken at each individual cell with reference starting at the first (polar) plate, but then referencing the neighboring cell (i.e. $V_{cell\_n} = V_n - V_{n-1}$). When the stack was rebuilt with 9 cells, the first voltage tap (reference) was not connected to cell #1, leaving the potential for the reference voltage to drift and potentially impacting cell #1 readings. The stack was then switched to air and run through current densities up to 1 A cm^{-2}. Results of this test are shown in Figures 69 and 70. As observed during operation on O_2, cells #1 and #10 performed poorly.

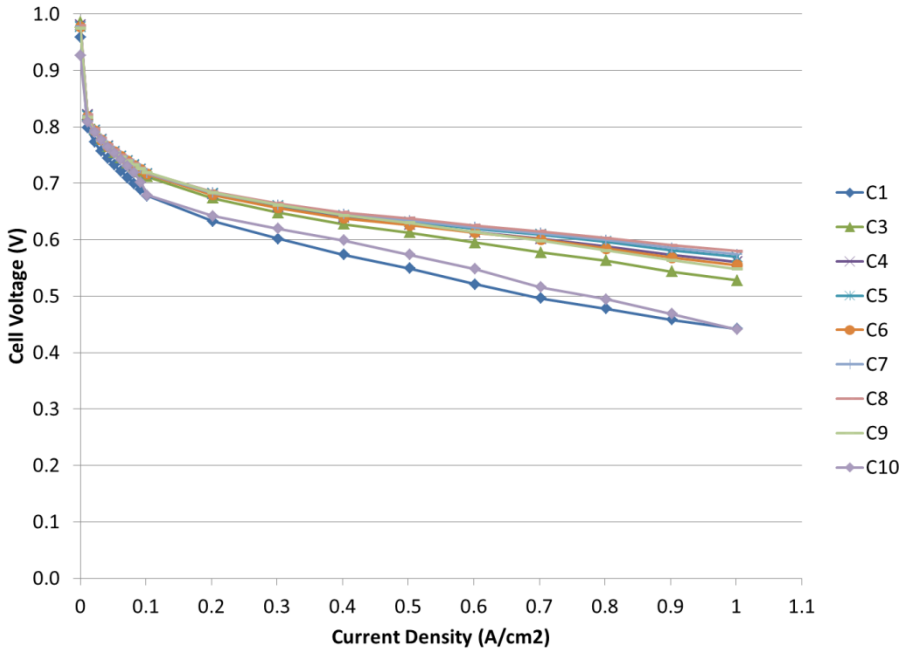

Figure 67: Nine-cell stack performance (cell #2 removed) on O_2 and H_2 at stoichiometric ratios of 2 and 1.2 respectively.

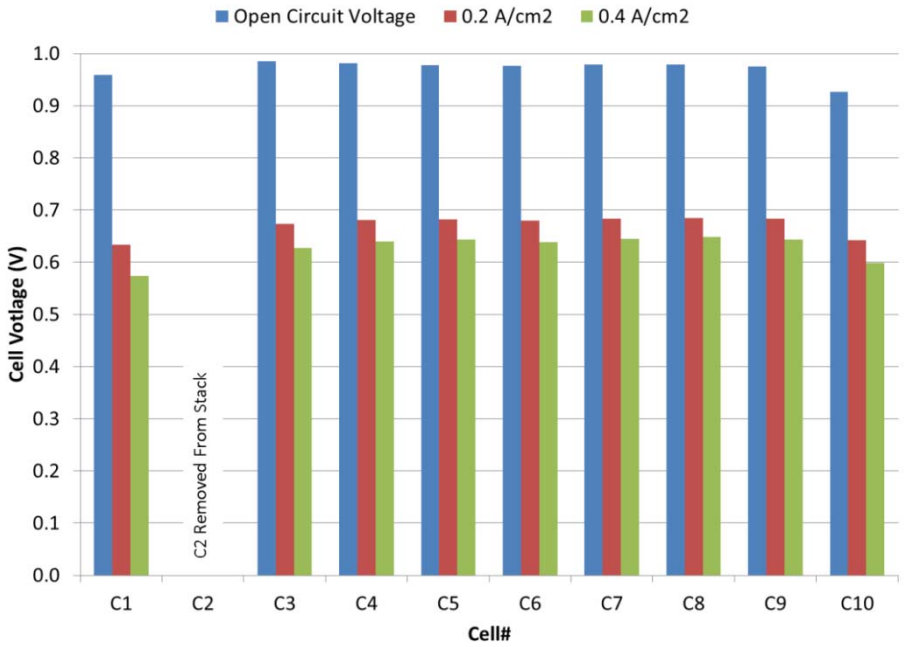

Figure 68: Individual cell performance of the 9 cell stack on O_2 and H_2 at stoichiometric ratios of 2 and 1.2 respectively.

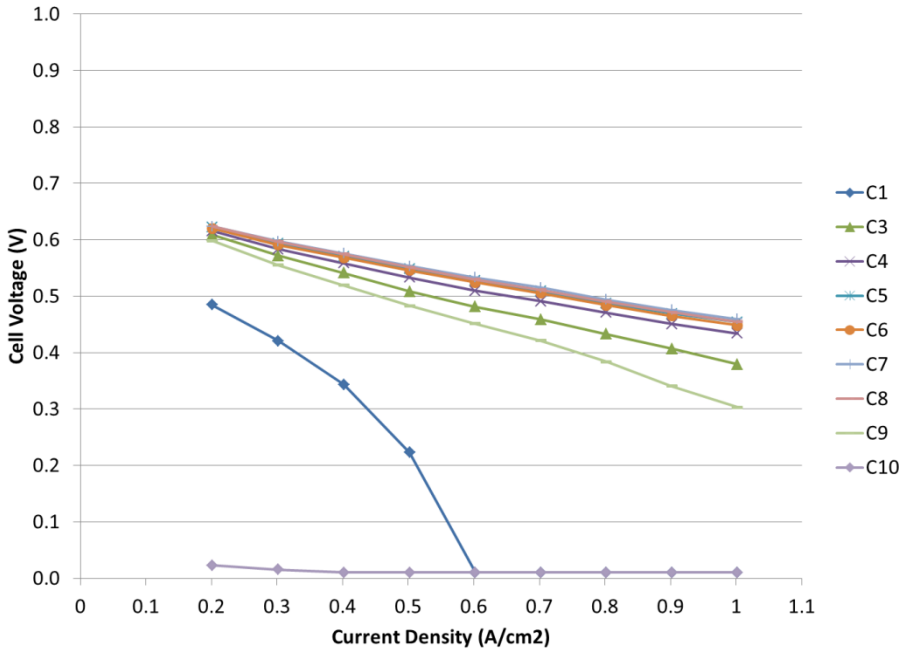

Figure 69: Polarization data of the 9 cell stack running on air and H_2 at stoichiometric ratios of 2 and 1.2 respectively.

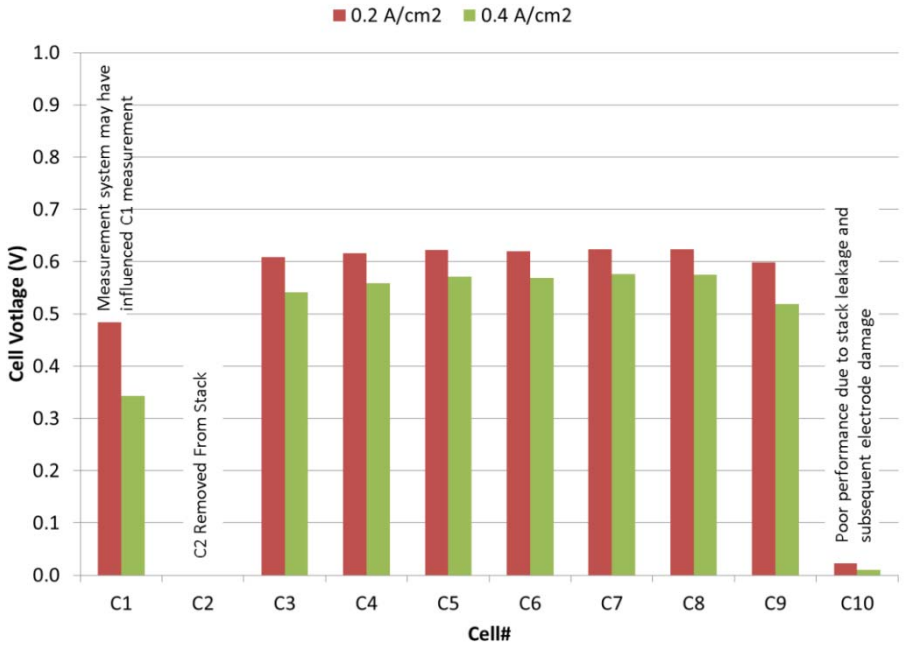

Figure 70: Individual cell performance for the 9 cell stack operating on air and H_2, at stoichiometric ratios of 2 and 1.2 respectively.

Conclusions – *Relation of Polarization Data and CV*: Cell #2 was shown to have substantial electrical shorting in CV testing. Detection of the cell #2 short was amplified after heat treatment, while all other cells showed similar electrical shorting measurements before and after heat treating (Figure 61). These results indicate that performing CV, with the intent of electrical short detection, may be more sensitive after heat treatment. However, pre-heat treatment seems to also be viable. Cell #2 performance during fuel cell testing reflected this substantial shorting and membrane displacement. The cell was able to support only minimal voltages, and likely influenced degradation of end cells (#1 and #10) with reduced

reactant availability through cross leakage and overboard leakage. Any impact of membrane misalignment and shorting on CV-derived capacitance was undetectable.

Cells #9 and #10 were not heat treated. As one would expect, there is no difference in the pre- and post-heat treatment measurements for these cells. Cells # 1-8 do show substantial increases in capacitance after heat treatment (up to 4X, Figure 62). Low capacitances of cells #9 and #10 would be expected to result in some form of reduced performance during fuel cell testing; perhaps characterized by enhanced activation polarization or mass transport losses. However, these effects are difficult to isolate in the polarization data. In addition, massive leakage and test station issues resulted in repeated attempts to operate the stack during initial testing. The stack was exposed to multiple startup cycles and 4-5 hours of operating temperature prior to successful testing, potentially contributing to effective in-situ heat treatment.

The application of ambient condition CV before and after heat treatment of PBI MEAs was compared to 10-cell stack performance. Measurement of electrical shorting was derived from the CV data and correlated to membrane misalignment in cell #2. Electrical short detection was enhanced in post-heat treatment CV data. Corresponding poor performance was observed during stack testing on both O_2 and air.

CV-derived capacitance measurement was demonstrated to be sensitive to heat treatment of MEAs. An increase in capacitance of 3-4X was observed in cells exposed to 30 min at 160°C in air. Corresponding performance enhancement was not observed in stack testing. However, the cells may have been effectively heat treated in-situ through multiple start up, idle and shut down cycles.

CV scan rates as low as 30 mV s^{-1} and up to 150 mV s^{-1} were run. Very low scan rates (30 mV s^{-1}) appeared to be susceptible to low signal-to-noise ratios. They are also relatively long, requiring more than 13 s to complete two full cycles of -0.1 to 0.1 V. The nature of the measurement method enhances capacitance sensitivity at higher scan rates. However, electrical shorting measurement should be insensitive to scan rate. Selection of a high scan rate may cause some masking of electrical short sensitivity. It was found that scan rates of 50 mV s^{-1} to 100 mV s^{-1} provided a good balance of sensitivity to both electrical shorting and capacitance for pre- and post-heat treatment sampling, and reasonable measurement time (100 mV s^{-1} requires 4 s for complete 2 full cycles). Post heat treatment measurement, or comparison of pre- and post-heat treatment measurements, seems to provide for sensitivity to electrical shorting and capacitance.

Ambient CV measurement of electrical shorting and capacitance provides a viable method for detection of electrical shorts and reduced capacitance as part of either process or quality control. Further development of the process would provide for cycle time reduction, quantification of sensitivity, quantification of internal resistance, and overall process refinement and implementation (part handling, process variability due to environmental factors, etc.).

Task 15.0– Expanded Cost Analysis.

CATS researchers were tasked with performing a cost analysis that compares roll-to-roll manufacturing and discrete manufacturing (current) approaches for high temperature MEAs. The first question that must be answered is: ‘Can a continuously moving or periodically moving roll-to-roll system be implemented?’ Based on discussions with the ultrasonic equipment manufacturer (Branson Ultrasonics) and the researchers own experience with MEA manufacturing, a rolling sonotrode ultrasonic system concept could work for low-temperature PEM due to membrane rigidity, but not for the sol-gel PBI/PA membrane used in high-temperature MEAs. Due to the visco-elastic mature of the membrane, some of the material would simply dam up ahead of the sonotrode (rolling ultrasonic horn) with some squeezing out the end of the MEA. Hence, the sealing operation must be done as a discrete step.

The second and more important question for this task is: ‘What cost and/or cycle time reductions may then be possible using a roll-to-roll system for discrete manufacturing steps?’ BASF’s production lines in Frankfurt, Germany and Somerset, New Jersey employed a walking beam transfer system. The time to lift, transfer and place a pallet from one station to the next was approximately ten seconds, but this could be adjusted.

To answer the second question, the RPI researchers took advantage of work performed by RPI mechanical engineering graduate student, Mr. Jake Pyzza, involving the design, fabrication, and testing of a roll-to-roll system for ultrasonically sealing high temperature MEAs. Features of the system include:

- Pneumatic, sliding H-frame supporting an ultrasonic stack and horn

- Provisions for both robotic and manual placement of MEA components
- H-frame support structure is adaptable to any size or style of bonding system
- Pin-on-belt drive system (i.e. roll-to-roll) eliminates discrete component transport methods while still maintaining accurate registration.
- Machine vision used for measuring placement accuracy
- Test bed is capable of operating with a wide range of MEA sizes and process parameters with minimal downtime for changeover.

A CAD image of the entire concept is shown in Figure 71, and pictures of the actual proof-of-concept testbed are shown in Figure 72.

Time Comparison: The fastest overall cycle time for the production of an MEA on the test bed was 12.8 seconds, as shown in Figure 73, plus the cycle time of the welding or sealing operation (~3 sec) for a total cycle time of 16 seconds. This could have been significantly reduced by increasing shuttling speed of the ultrasonic stack H-frame, although the same is possible for BASF's walking beam transfer system, as previously mentioned.

Cost Comparison: A frame-based discrete MEA sealing/welding system has higher capital costs (e.g., frames) but lower web consumable costs; whereas a roll-to-roll system has lower capital costs (e.g., no frames) but higher web consumable costs. Hence, no clear cost advantages are seen with either approach when considered in isolation. This may change when the entire MEA component manufacturing and assembly system is considered.

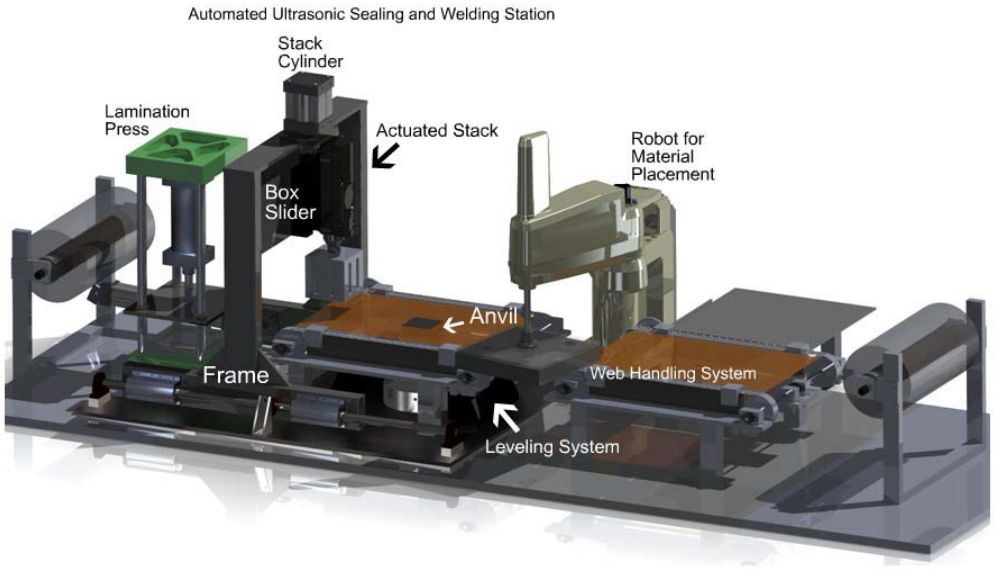

Figure 71: CAD model of automated roll-to-roll ultrasonic sealing and welding station concept

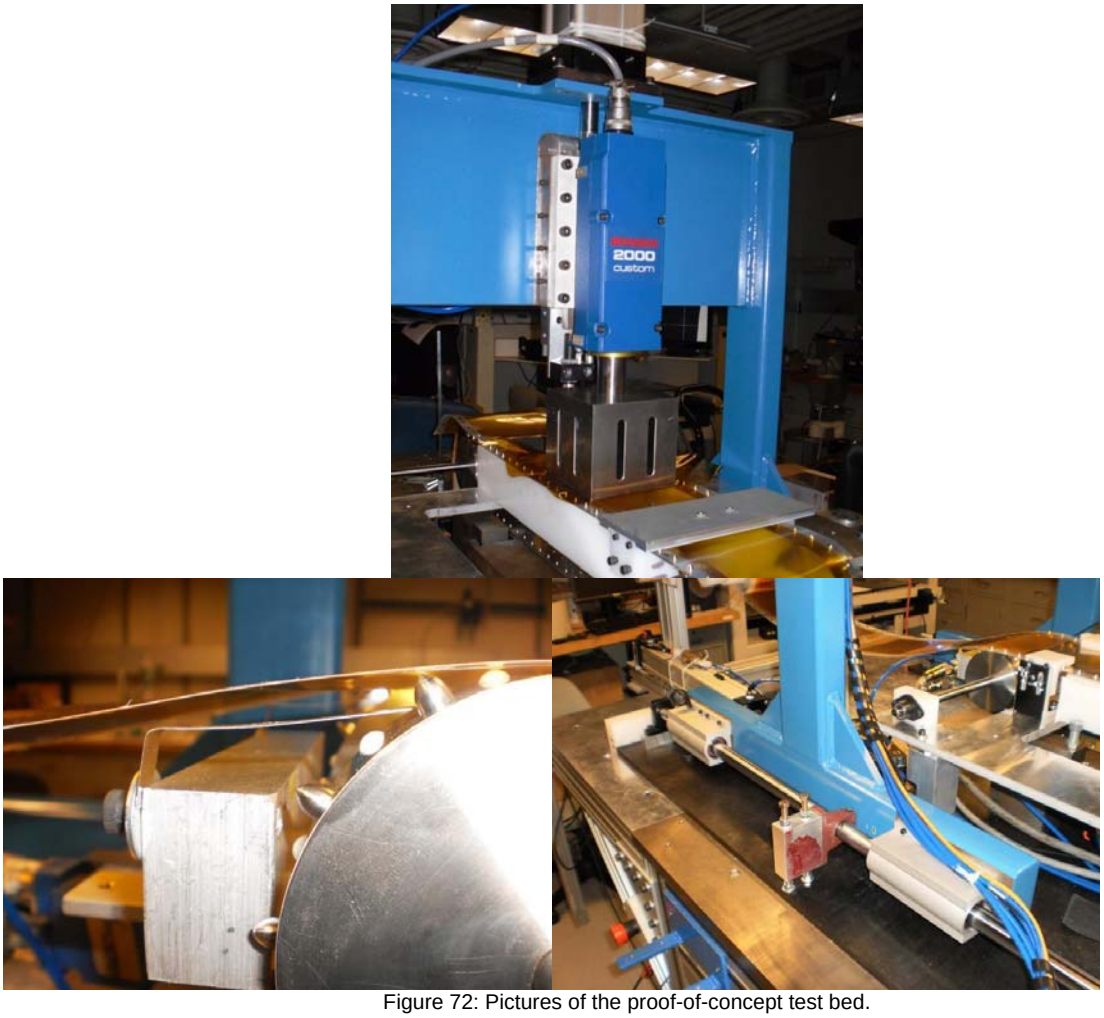

Figure 72: Pictures of the proof-of-concept test bed.

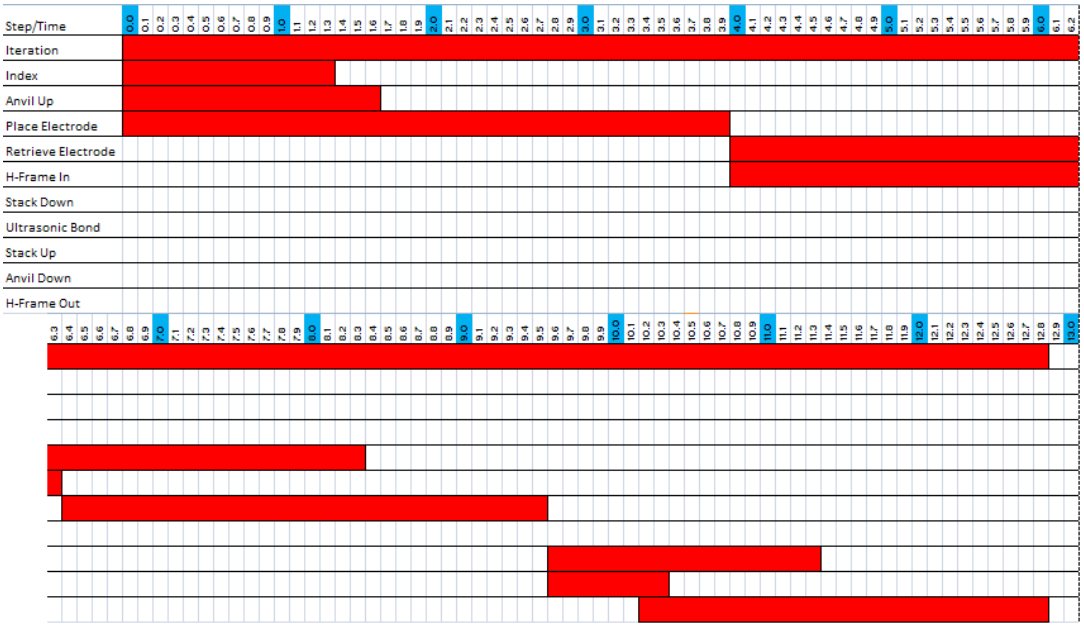

Figure 73: Timing Diagram for MEA Sealing Operation

Accordingly, cycle times did not need to be updated since the previous cost analysis in Task 10.0, so Table 4 is still valid.

Task 16.0– Ultrasonic Bonding Implementation Design Guidelines.

An ultrasonic MEA lamination design guide was co-authored by Dr. Daryl Ludlow, Senior Research Scientist at RPI, and Dr. Daniel Walczyk, Project PI, for use by BASF and other fuel cell companies interested in implementing ultrasonic welding or sealing for MEA manufacturing. This design guide is included in Appendix A for reference.

Task 17.0- Phase III program review.

The program review was conducted on December 17, 2013 with Nancy Garland and Jesse Adams in attendance via teleconference, and RPI was notified of this requirement was satisfied at the conclusion of this meeting.

Products Developed under the Award and Technology Transfer Activities

Publications:

1. Buelte, S., Walczyk, D., and Sweeney, I., "Effect of MEA Bonding Technique on Fuel Cell Performance and Platinum Crystallite Size," *Journal of Fuel Cell Science and Technology,* 11(3), Jan. 2014, 031002 (10 pages).
2. Beck, J., Walczyk, D., Buelte, S, Hoffman, C., "Comparison of Performance Losses between Ultrasonic and Thermal Bonding of Membrane Electrode Assemblies in PEM Fuel Cells," *Journal of Fuel Cell Science and Technology,* 10(4), June 2013, 041004 (10 pages).
3. Walczyk, D., Rock, S., Ludlow, D., Buelte, S., Hoffman, C., Guglielmo, D., Ziomek, W. and Beck, J., "Process Development for Fuel Cell Manufacturing," Proceedings of the Fuel Cell Seminar & Energy Exposition 2012 November 5-8, 2012, Uncasville, CT, USA.
4. Beck, J., Walczyk, D., Hoffman, C., Buelte, S., "Ultrasonic Bonding of Membrane Electrode Assemblies for Low Temperature PEM Fuel Cells," *Journal of Fuel Cell Science and Technology*, 9(5), Oct. 2012, 051005 (8 pages).
5. Beck, J., Walczyk, D., Hoffman, C. and Buelte, S., "Ultrasonic Bonding of Membrane Electrode Assemblies for Low Temperature PEM Fuel Cells," *Proceedings of the ASME 2012 10th Fuel Cell Science, Engineering and Technology Conference* (FuelCell2012), Paper # FuelCell2012-91308, July 23-26, 2012, San Diego, CA, USA.
6. Beck, J., "Ultrasonic Bonding of Membrane Electrode Assemblies for Low Temperature Proton Exchange Membrane Fuel Cells," *M.S. Thesis*, Dept. of Mechanical, Aerospace and Nuclear Engineering, Rensselaer Polytechnic Institute, Troy, NY, 2012.
7. Guglielmo, D., "Modeling the Ultrasonic Sealing Process for PEM Fuel Cell MEAs Using a Numeric Solver and Scale-Up to 140 cm^2," *M.S. Thesis*, Dept. of Mechanical, Aerospace and Nuclear Engineering, Rensselaer Polytechnic Institute, Troy, NY, 2012.
8. Ziomek, W., "Design and Testing of an Experimental Ten-Cell High Temperature PEM Fuel Cell Stack," *M.S. Thesis*, Dept. of Mechanical, Aerospace and Nuclear Engineering, Rensselaer Polytechnic Institute, Troy, NY, 2012
9. Guglielmo, D., Snelson, T. and Walczyk, D., "Modeling Ultrasonic Sealing of Membrane Electrode Assemblies for High-Temperature PEM Fuel Cells," *Proceedings of the ASME 9th Fuel Cell Science, Engineering and Technology Conference*, Washington, DC, Aug. 7-10, 2011, Paper # ESFuelCell2011-54427.

10. Pyzza, J., W. Sisson, W. and Puffer, R., “Manufacturing Implementation of Ultrasonic Sealing of Membrane electrode assemblies for high temperature PEM fuel cells” *Proceedings of the ASME 9th Fuel Cell Science, Engineering and Technology Conference*, Washington, DC, Aug. 7-10, 2011, Paper # ESFuelCell2011-54441.
11. Hoffman, C., Walczyk, D. and Cichetti C. “Ultrasonic Spraying of PEM-FC Electrodes,” *European Fuel Cell Forum 2011*, Lucerne, Switzerland. June 28-July 1, 2011.
12. Puffer, R. and Walczyk, D., “Adaptive Process Controls and Ultrasonics for High Temperature PEM MEA Manufacture,” *Fuel Cell Tech Team Meeting (USCAR)*, Southfield, MI, March 16, 2011.
13. Pyzza, J., “Implementation of Ultrasonic Welders in Automated High Temperature PEM Fuel Cell Membrane Electrode Assembly Manufacturing,” *M.S. Thesis*, Department of Mechanical, Aerospace & Nuclear Engineering, Rensselaer Polytechnic Institute, Troy, NY, 2011.
14. Snelson, T., “Ultrasonic Sealing of PEM Fuel Cell Membrane Electrode Assemblies,” Ph.D. Thesis, Department of Mechanical, Aerospace & Nuclear Engineering, Rensselaer Polytechnic Institute, Troy, NY, 2011.
15. Krishnan, L., Snelson, T., Puffer, R. and Walczyk, D., "Durability Studies of PBI-Based Membrane Electrode Assemblies for High Temperature PEMFCs," Proceedings of the 6th Annual IEEE Conference on Automation Science and Engineering (CASE) 2010, Paper #222. (Best Application Paper Award Finalist)
16. Gullotta, J., Share, D., Krishnan, L., Puffer, R. and Walczyk, D. “Adaptive Process Control and In-situ Diagnostics for High Temperature PEM MEA Manufacturing,” *Proceedings of the ASME 8th International Fuel Cell Science, Engineering & Technology Conference*, Brooklyn, NY, June 14-16, 2010, Paper # FuelCell2010-33231
17. Share, D. Krishnan, L., Walczyk, D., Lesperence, D. and Puffer, R., “Thermal Sealing of Membrane Electrode Assemblies for High-Temperature PEM Fuel Cells,” *Proceedings of the ASME 8th International Fuel Cell Science, Engineering & Technology Conference*, Brooklyn, NY, June 14-16, 2010, Paper # FuelCell2010-33227.
18. Share, D., Lesperence, D., Walczyk, D., and Puffer, R., “Cold Pressing of Membrane Electrode Assemblies for High-Temperature PEM Fuel Cells,” *Proceedings of the ASME 8th International Fuel Cell Science, Engineering & Technology Conference*, Brooklyn, NY, June 14-16, 2010, Paper # FuelCell2010-33230.
19. Snelson, T., Pyzza, J.,Krishnan, L., Walczyk, D. and Puffer, R. “Ultrasonic Sealing of Membrane Electrode Assemblies for High-Temperature PEM Fuel Cells,” *Proceedings of the ASME 8th International Fuel Cell Science, Engineering & Technology Conference*, Brooklyn, NY, June 14-16, 2010, Paper # FuelCell2010-33229.
20. Lesperence, D., “Performance Testing of High-Temperature Membrane Electrode Assemblies for PEM Fuel Cells,” *M.S. Thesis*, Dept. of Mechanical, Aerospace and Nuclear Engineering, Rensselaer Polytechnic Institute, Troy, NY, 2010.
21. Dylan Share, “Sealing of High Temperature PBI Membrane Electrode Assemblies Used in Fuel Cells,” *M.S. Thesis*, Dept. of Mechanical, Aerospace and Nuclear Engineering, Rensselaer Polytechnic Institute, Troy, NY, 2010.
22. Snelson, T. and Pyzza, J., “Ultrasonic Bonding of PEM Fuel Cell Membrane Electrode Assemblies,” *Advanced Energy 2009 Conference*, Hyatt Regency Long Island, Hauppauge, NY, Nov. 18-19, 2009.
23. R. Puffer, S. Rock, “Recent Advances in High Temperature PEM Fuel Cell Manufacturing,” *ASME Journal of Fuel Cell Science and Technology*, 6(4), August 2009.

Networks or Collaborations Fostered:

- BASF Fuel Cell, Somerset, NJ

- WL Gore & Associates, Inc., Fuel Cell & EDC Technologies, Elkton, MD
- Nuvera Fuel Cells, LLC, Billerica, MA
- Ballard Power Systems, Burnaby, BC, Canada.

New Technologies/Techniques:

- New ultrasonic bonding method for high- and low-temperature PEM Membrane Electrode Assemblies (MEAs) and demonstration of process scale-up
- Using the derivative of the complex AC impedance (1 kHz) for in-situ quality measurement and process control of thermal pressing of high-temperature PEM MEAs
- Using CV scans for process and quality control of thermally and ultrasonically pressed high-temperature PEM MEAs.

Inventions and Licensing Agreements:

- Snelson, T., Puffer, R., Pyzza, J., Walczyk, D. and Krishnan, L., “Method for the production of an electrochemical cell,” U.S. and International Patents Pending, 2011. (Licensed to BASF Fuel Cell, Somerset, NJ)

Appendix A – Ultrasonic MEA Lamination Design Guide – by Dr. Daryl Ludlow and Dr. Daniel Walczyk

Introduction

Polymer electrolyte membrane (PEM) fuel cells have been on the energy system horizon for decades. The state of today's technology is in many ways a by-product of the space race and periodic efforts resulting from threats to energy security and climate change. This combination of high performance mission critical applications and an inconsistent commercial market have produced a reliable yet expensive technology. While the technology has matured substantially from a materials durability, degradation and systems perspective, not much has changed since the early developments of PEM. With the minor exception of carbon supported platinum catalysts, the general architecture is largely the same as that used decades ago. This trend extends into manufacturing processes. In the case of the membrane electrode assembly (MEA), electrodes are typically thermo-mechanically bonded to the membrane. Lamination bonding conditions consist of thermal pressing up to 5 minutes at 120-130°C and 2-3 MPa. Alternatively, nip-rollers may be used in web-processing (rather than discrete using heated platens). Nip-rollers enable a continuous production scenario, but heating of the materials can require substantial pre-warming zones. Many 10's of feet may be required to support high web speeds.

An alternative to traditional external heating is to heat the material interfaces using dynamic processes. Ultrasonic welding employs such an approach in which high frequency - low amplitude motion generates heat primarily at the bonding interface, rather than using heated platens, rollers, or other external heaters to generate bonding conditions. The resulting process can be rapid and produce high quality interfaces.

This design guide is intended to provide guidelines to those interested in utilizing ultrasonic welding processes to laminate a PEM MEA. These guidelines are based on research and development work at Rensselaer Polytechnic Institute supported by the U.S. Department of Energy (DOE) Hydrogen and Fuel Cells Program through Award #DE-FG36-08GO18053/A000.

Background

Fuel cells leverage separate, yet coupled, oxidation and reduction reactions. These two reactions are couple by the exchange of electrons and positive or negative ions. Acid electrolyte fuel cells permit the transport of protons through the electrolyte from anode to cathode. In support of these oxidation and reduction reactions, the electrode structures must have sufficient reactant and product transport capabilities. Reactants must migrate to the catalyst sites within the electrode, usually diffusing through complex gas diffusion layers (GDL). Products from the oxidation and reduction reactions must be allowed to move away from the catalyst sites as well. This means that electrons, protons (for acid fuel cells) and water (for hydrogen fuel cells) must be able to pass readily though the electrode structure. Protons released from the anode oxidation reaction must readily pass to the electrolyte layer and then to the cathode oxygen reduction reaction. Electrons are conducted from the anode electrode, through the anode GDL, anode bipolar plates, current collectors, electrical load, and return to the cathode electrode in a similar fashion. This requirement of electrical current, ion transport, and reactants and products is typically termed the three-phase interface. The lamination process generates the intimate contact which supports ion transport, while also avoiding mass transport limitations. The laminated MEA must also be durable, to

withstand handling associated with inspection, packaging, shipping, stack assembly, and the hydration and thermal cycles typical of PEM fuel cells.

Overview of MEA Manufacturing

In support of the above requirements, the MEA bond is generated through a thermo-mechanical process in which the MEA components are joined together with heat and pressure. Discrete lamination (hot platen pressing) of low-temperature PEM materials usually requires 120-130°C and 2-3MPa for 3 to 5 minutes. PBI materials may require slightly less time, in the range of XX-TT minutes at 160°C. Alternately, web-based processing with nip rollers and pre-heat zones are common for continuous lamination of catalyst coated membrane (CCM). While nip rollers only generate a brief period of pressure, the process is equally intensive. Of particular interest is that the CCM is only exposed to high compression for a small time as it proceeds through nip rollers. However, a substantial pre-heat zone may be required in order to obtain the required lamination material temperature prior to entering the nip rollers. This implies that the bonding process only requires a brief period of combined high pressure and high temperature. The use of heated platens to laminate MEAs relies of external heating of the package and is limited by conductive heat transfer through the materials, thus leading to the excessive lamination times and thermal energy usage.. The use of ultrasonic lamination rapidly heats the material interfaces, with small levels of thermal energy conducted outward to the tooling. This low-level energy loss indicates the relative efficiency of the ultrasonic lamination process. After MEA lamination, the parts can then be further processed or used directly in stack assembly.

Organization of Report

This design guide is organized into sections intended to give an understanding of how to develop and optimize thermal and ultrasonic MEA lamination processes. By including thermal processes in the guide, one can make educated decisions as to the best lamination approach for a given set of materials and desired end product. Specific materials may respond to lamination conditions differently. Thermal bonding is covered first, then ultrasonic processes, post-processes and testing, cost modeling, energy consumption and manufacturing methodology.

Fuel Cell Operation and Manufacturing Implications

Perflurosulfonic acid membrane (PFSA) consisting of a Telfon-like backbone with side chains terminating with SO_3H sites. Protons associated with SO_3^- are solvated by water molecules, generating a network of proton conduction paths through a combination of anionic sites and tightly and loosely bound water and hydronium ions. The affinity of water molecules and protons results in electro-osmotic drag which effectively pumps 1-5 water molecules per proton across the membrane. Maintaining elevated membrane hydration results in high proton conductivity, but also creates challenges related to water management and proper transport of reactant gases to the anode and cathode electrodes. PFSA MEAs are different than aqueous electrolytes, in that the generation of a 3-Phase interface throughout the electrode structure is more limited without the use of ionomer throughout the electrode depth. As such, in many PEM architectures, ionomer is added to the electrode-membrane interface and/or the electrode structure.

Polybenzimidazole (PBI) phosphoric acid membrane fuel cells are commonly referred to as high temperature PEM fuel cells. These cells are essentially phosphoric acid fuel cells that utilize a polymer matrix to retain the electrolyte. Traditional PBI fuel cells involved the use of PBI films soaked in phosphoric acid[1]. Alternatively, a sol-gel process can be used to imbibe the phosphoric acid within the

[1] D. Weng, J. Wainright, U. Landau, R. Savinell, "Electro-osmotic drag coefficient of water and methanol in polymer electrolytes at elevated temperatures," Journal of the Electrochemical Society, Vol. 143, No. 4, 1260, 1996.

PBI structure during membrane synthesis[2]. The net result is a PEM-like membrane which is processed very similarly to traditional PEM MEAs. However, the phosphoric acid electrolyte–electrode interface is an aqueous–solid interface, rather than solid–solid interface. An acid film is normally present on the membrane surface, and compressive strain of the membrane (during lamination) results in acid squeezed from the membrane and forced into the electrode structure. Thus, the electrochemical interface is less dependent on a mechanical bond, and more related to the controlled permeation of liquid electrolyte into the electrode structure. However, mechanical stability is required for reasonable durability during manufacturing, shipping, storage, and stack assembly. Insufficient electrolyte permeation can result in limited ion transport throughout the electrode structure, manifested as low cell voltages. Excessive flooding of the electrode structure with electrolyte can limit reactant transport to catalyst sites, resulting in mass transport limitation and low cell voltages. These two conditions could be detected via cell performance testing in the form of polarization data, impedance spectroscopy and cyclic voltammetry. Excessive electrolyte in the electrode structure would be indicated by elevated diffusion losses at high current densities (poor polarization, elevated low frequency impedance), yet the cell would demonstrate normal high frequency impedance. Insufficient electrolyte in the electrode could be indicated by elevated high frequency impedance (impacting cell polarization throughout the performance range), reduced electrochemical active area measured by cyclic voltammetry, and enhanced mass transport losses at high current densities.

Thermal Lamination

The electrode-electrolyte interface is usually obtained by a thermo-mechanical process. Thermal lamination is typically performed using heated (nip) rollers or a hot platen press, as shown in Figure 1. The PEM is brought above its glass transition temperature during the bonding process to conform to the electrode topography. Many laboratory guidelines utilize a sealed package with layers of fiber reinforced silicone (outside) and Teflon coated fiberglass (inside, in contact with GDL or transfer film) placed within a hot platen press. The Teflon coated fiberglass (Armalon™) extends beyond the MEA materials. The silicone extends beyond the Teflon coated fiberglass, created a sealed package when the layers meet under load. This approach allows for the retention of membrane water when bonding hydrated membrane. The package is placed in the pre-heated press, the temperature is brought to the target bonding temperature, held for the target time period, turned off, cooled well below 100°C, and then removed. Maintaining the sealed package while at elevated temperature allows for the retention of membrane water, maximizing proton conductivity. While this approach produces high performance via maximum proton conductivity, it is slow and handling of hydrated membrane during manufacturing is difficult. Sealed lamination of hydrated membrane is commonly used in laboratory experiments, but is not common in commercial manufacturing. Thermal lamination with dry membrane is more typical.

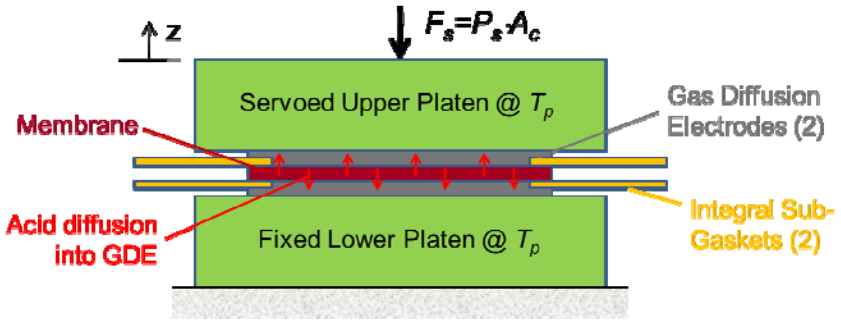

[2] L. Xiao, H. Zhang, E. Scanlon, L. Ramanathan, E.W. Choe, D. Rogers, T. Apple, and B. Benicewicz, "High-Temperature Polybenzimidazole Fuel Cell Membranes via a Sol-Gel Process," Chem. Mater., 2005, 17, 5328-5333.

Figure 1. Schematic of components comprising a high temperature PEM MEA being thermally laminated into a unitized structure.

Dry thermal lamination can be performed on discrete components or as a continuous web-based process. Without the need to retain membrane hydration, a sealed lamination package is not required. Components can be placed directly in contact with press platens if contamination or tooling wear is not a concern. PFSA-based MEAs do not rely on a liquid electrolyte and, thus, do not pose contamination risks to tooling. High-temperature PBI MEAs rely on liquid phosphoric acid electrolyte which commonly seeps from the MEA during lamination. As such, PBI MEAs generally require corrosion resistant metals (stainless steel) and a barrier film to protect tooling. Material degradation (from hot phosphoric acid) dictates that high performance corrosion resistant polymers be employed as barrier films. Fluorinated polymers or polyimides work well.

Ultrasonic Lamination

Ultrasonic lamination utilizes high frequency, low amplitude motion to generate heat via friction at material interfaces. Heat is rapidly generated at the interface to be bonded, thus minimizing bonding time. A potential negative effect of this high frequency motion is the damage to and/or destruction of critical gas diffusion and electrical conduction paths in the gas diffusion media (GDM). As such, the period and severity of exposure should be minimized to only that which is required to generate an adequate interface. Ultrasonic amplitude, load (pressure) and power level can all be controlled. In general, the power level is rather dependent on the load applied (higher load results in higher power for a fixed amplitude).

Ultrasonic motion is generated by a piezoelectric stack (transducer/converter) driven by a high-frequency high-voltage controller. This motion is applied to the materials of interest via a specifically tuned (welding) horn. Details of the ultrasonic head are shown in Figure 1. Ultrasonic stroke (amplitude) may be modified with the use of a booster placed between the piezoelectric stack and horn. The booster can be oriented for amplification or reduction of the horn stroke. For instance, a 1.5× booster would increase the motion of a 30μm stack to 45μm. Changing the booster orientation (flipping it over) would result in a 1.5× reduction in amplitude, reducing the 30μm motion to 20μm. Amplitude can be further tuned through the ultrasonic driver power controls.

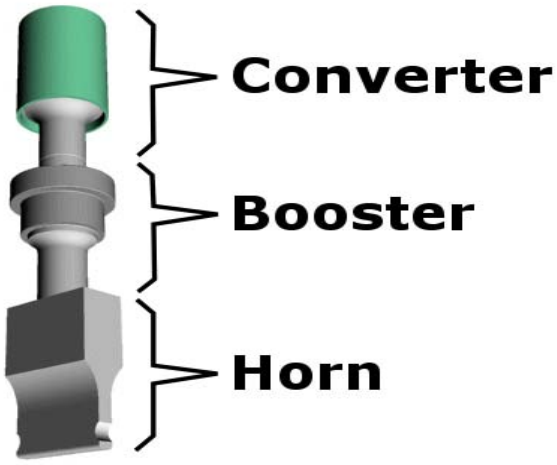

Figure 1. Motion generated by the converter (piezo stack) can be increased or reduced in amplitude with the aid of a booster. The booster then drives motion at the horn.

The lamination materials are clamped between the ultrasonic horn and an anvil. The clamping force may be applied by any usual method (e.g., air cylinder, hydraulic), with either the anvil or ultrasonic assembly actuated. A schematic of a top-mounted and actuated ultrasonic tool with rigid bottom anvil is shown in Figure 2. However, clamping actuation of the anvil can also be configured in order to avoid overly complex mounting schemes for the ultrasonic converter.

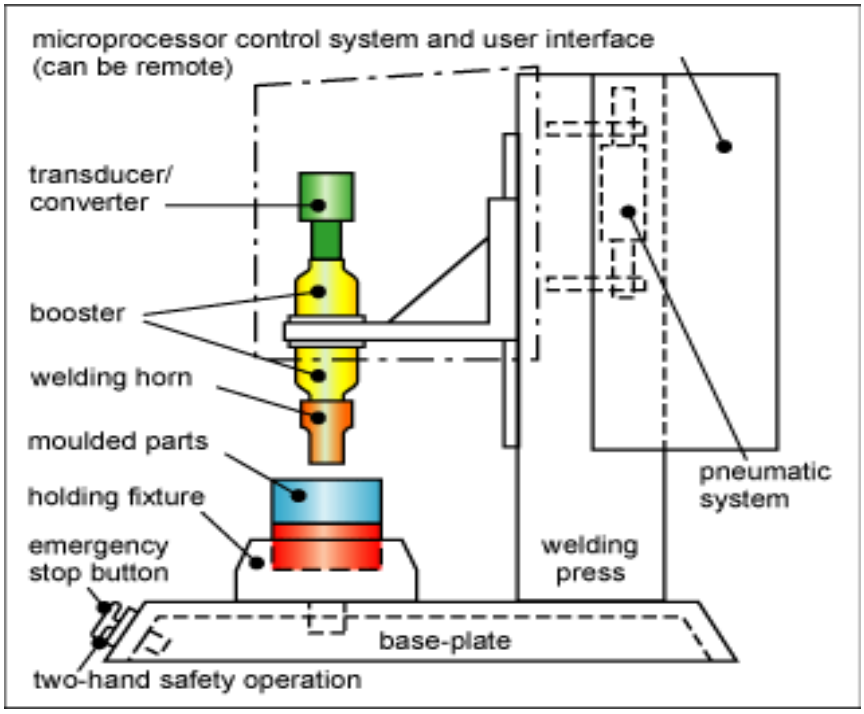

Figure 2. Example of ultrasonic welding rig. A pneumatic actuation is depicted at the back of the unit, used to move the ultrasonic assembly into contact with materials to be laminated. Due to the complexity of the ultrasonic tooling, this actuator can be placed under the lower "anvil" tooling for simplicity.

Attached to the ultrasonic "stack" (Figure 1) is the ultrasonic horn (welding tool, lamination tool, Figure 3). Lamination of the active area of the MEA generally requires a flat tool which applies a uniform load to the lamination surface. However, the use of sub-gasket assemblies (with electrodes, or other components) may require a tool which targets a specific geometry (Figure 4). Rather than adding geometry specific features to the ultrasonic horn, these features are more easily incorporated into the anvil which provides the counter force to the ultrasonic horn.

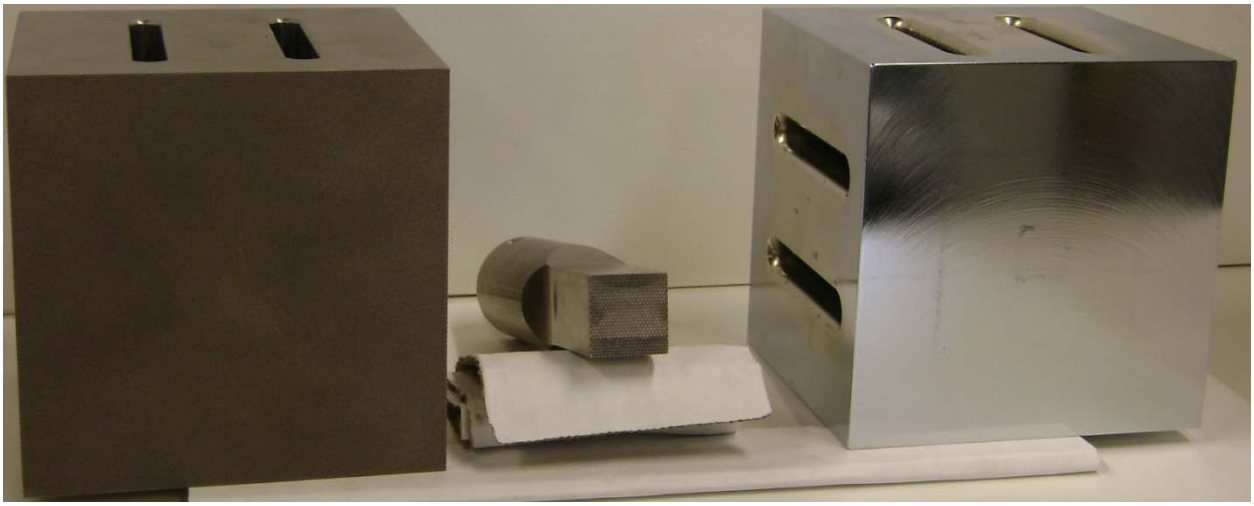

Figure 3. Horns can range in size and shape. However, they are designed specifically for the frequency applied with the aim of maintaining uniform amplitude across the entire face.

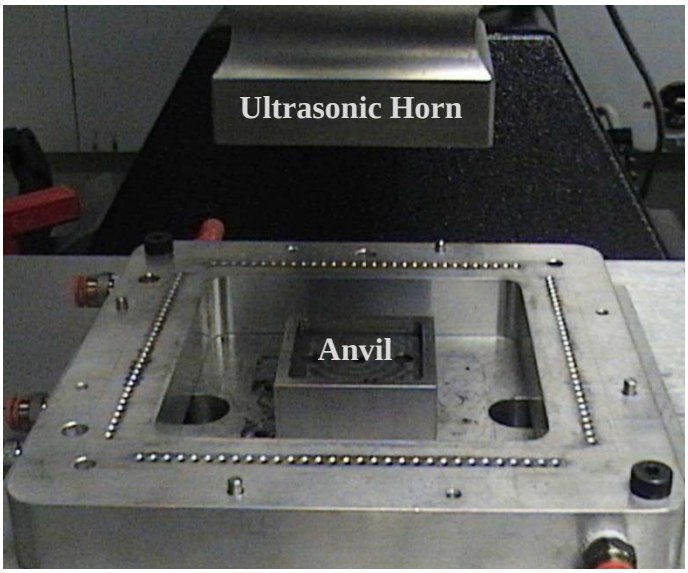

Figure 4. Geometry specific tooling may be employed at the anvil (lower tool) for the lamination of gasket electrode assemblies, or other parts which do not require a uniform lamination surface. The ultrasonic horn (upper tool) can remain generic, thus avoiding the need for complex modeling (to obtain a well-tuned horn) and extensive tooling libraries.

Ultrasonic horns are usually fabricated from lightweight high-strength metals. Rapid displacement of the horn means that increased mass requires higher power levels. The high loads required to generate strain in the materials being laminated requires that the tool be strong. The desire for uniform bond quality across the entire lamination area dictates that the tooling be stiff enough to uniformly displace the MEA during lamination. Aluminum and titanium are materials of choice. The selection between aluminum and titanium is largely driven by cost (titanium is more expensive) and suitability of available converters/booster combinations. The higher mass of aluminum, combined with a large tool, may exceed the capabilities of a given converter and booster for the desired process conditions. Anvil material selection is less critical, only requiring that the tool is sufficiently rigid to avoid deformation under the dynamic loads of the ultrasonic process.

Tooling surfaces can be smooth, or contain features. Snelson found that a knurled surface worked well at focusing energy for the lamination of PBI MEAs. The focused pressure applied by knurl features resulted in quality lamination with less total force (and resulting energy) than required for a flat tool. In the case of the relatively thick and compliant PBI MEA, knurled features were appropriate. Alternately, the thin and less compliant Nafion MEA is not as suitable. This is especially true when attempting to laminate Nafion MEAs without GDL or other largely compliant layers.

Tool/Process Design Methodology

Thermal Pressing – Time, Temperature, and Pressure

Thermal lamination achieves bonding of the electrochemical interface through thermo-mechanical bonding. The electrochemical interface in a PFSA MEA is established through contact between the membrane and ionomer in the electrode structure and/or direct contact between catalyst sites and the membrane. Lamination temperature is determined by the material set, and the rate and degree of control employed. Thermal degradation of the materials provides an upper lamination temperature limit. PFSA membranes will degrade above 170°; PBI is stable up to ~ 350°C and phosphoric acid can readily withstand 200°C without excessive vaporization. Thus lamination is performed such that the materials do not exceed these temperatures. Lower limits are traditionally influenced by glass transition temperatures for PFSA MEAs. Nafion exhibits multiple varying glass transition temperatures depending on hydration. The lower T_g is believed to the associated with Teflon-like backbone, ranges up to ~ 130°C (dry), and is referenced for lamination purposes[3]. PFSA MEAs are typically laminated with materials held at 130-145°C[4,5]. High temperature relaxation of the membrane and electrode ionomer and/or PTFE allows for conformation of the materials and mechanical bonding to neighboring surfaces. PBI seems to be an entirely different story. The glass transition temperature for PBI is much higher (413°C) and "other plastics in melt do not stick to PBI."[6] Bond development in the PBI phosphoric acid system appears to be somewhat dependent on the development of the aqueous acid-electrode interface, via acid permeation into the electrode structure.

Gross thermal uniformity during PFSA lamination must (at a minimum) fall within the range defined by the glass transition and thermal degradation temperatures. Further refinement of temperature uniformity is likely to result in enhanced mechanical adhesion, improved cell performance and longevity. However, such refinement requires in-depth analysis and experimentation for the specific material set, processing scenario and application of interest. For example, Mehta and Cooper include a very broad review of various MEA configurations and manufacturing steps in their PEM fuel cell design and manufacturing review[7]. While the materials sets are likely to be similar for most PFSA or PBI architectures, the processing approach will demand that electrode-electrolyte bonding conditions are adjusted accordingly to optimize performance. Share reported that BASF Fuel Cell specifies temperature uniformity of +/- 5°C during thermal pressing in their manufacturing process [8]. Further refinement in the thermal lamination process was had by monitoring lamination temperatures within the MEA material stack versus the tooling

---

[3] H.Y. Young and J.W. Kim, "Role of the glass transition temperature of Nagion 117 membrane in the preparation of the membrane electrode assembly in a direct methanol fuel cell (DMFC)," *International Journal of Hydrogen Energy*, 37 (2012), 12580-12585.

[4] S. Srinivasan, "Fuel Cells, From Fundamentals to Applications," Springer, 2006.

[5] J. Larminie and A. Dicks, "Fuel Cell Systems Explained," 2nd Ed., Wiley, 2003.

[6] Boedeker Plastics, Inc., Celazole Polybenzimidazole Specifications, www.boedeker.com/celazole.htm, 2013.

[7] V. Mehta and J.S. Cooper, "Review and analysis of PEM fuel cell design and manufacturing," *Journal of Power Sources*, 114 (2003) 32-53.

measurement point. A consistent deviation was found and temperature controller set points were offset accordingly to obtain the desired lamination temperature.

Bonding is achieved when target temperatures are obtained and materials are held under pressure for some minimal time period. The externally applied heat of thermal lamination requires that heat flux move from the heated platens inward toward the MEA interfaces. By its nature, this heat flux process will require time to achieve the desired lamination temperature at material interfaces. Typical PFSA lamination times are 1.5-5 minutes[4]. However, these time frames were developed utilizing traditional thermal lamination.

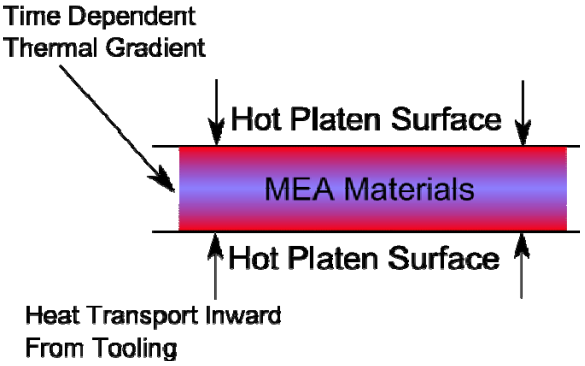

One approach to determining the precise time and temperature behavior is to embed fine gage temperature sensors into the lamination package. If thermal lamination process settings are already known for the materials of interest, embedded temperature sensors can provide detailed information regarding preliminary temperature and time targets in the ultrasonic process.

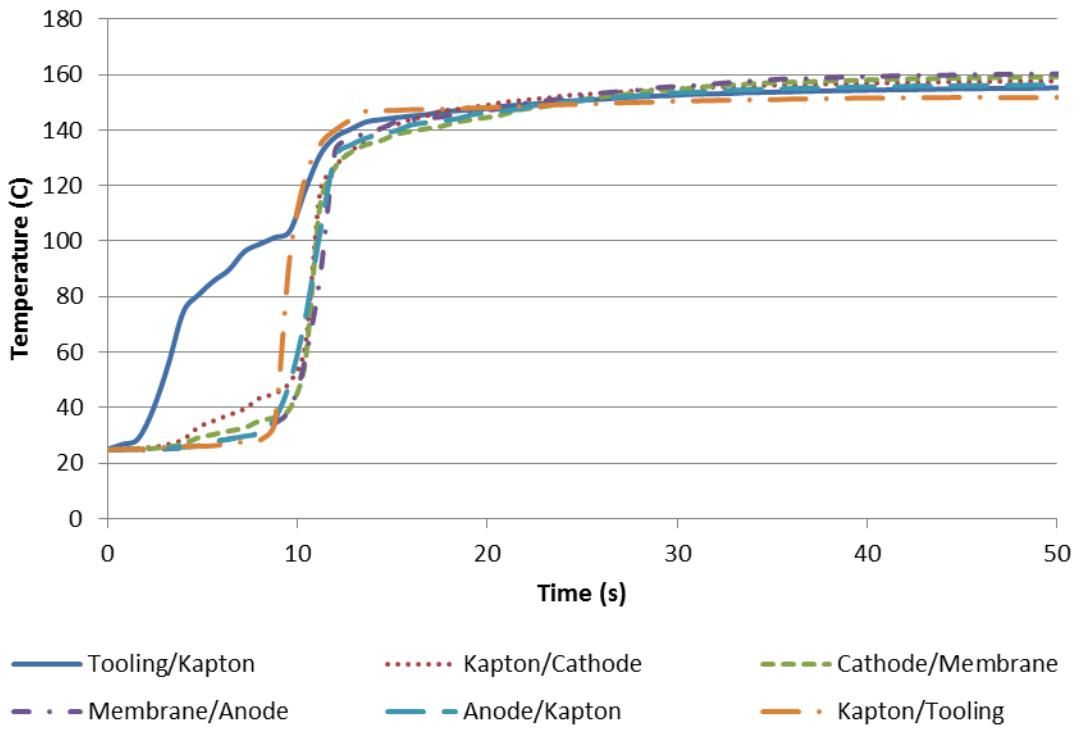

Figure 5. Thermal lamination transient temperature measurements. Parts were inserted into a pre-heated press at time 0s; press closed at time 8s; parts reach 140°C at ~ 12s.[8]

Heating of the press tooling can be performed using imbedded electric heaters or fluidic channels in which hot liquid is circulated. The use of electric membrane heaters is not common, as the heater package adds significantly to the tolerance stack up in the press platens and proves difficult in the obtaining platen flatness specifications necessary for a consistent and high quality bond. Temperature set points are easily controlled using off-the-shelf controllers, and tooling flatness and stiffness requirements lead to large thermal masses which provide a large degree of thermal stability. The use of multiple heater elements, sensors and independently operating controllers is dictated by the bonding temperature specification for the specific material set and application of interest.

The transient behavior of thermal lamination is a function of the heater power, thermal masses, initial temperatures, thermal conductivities, insulation and target temperature of the tooling and MEA components. A 2D dynamic model of the thermal system can be created considering these properties and operating conditions. Share and Snelson present examples of transient thermal and ultrasonic thermal behavior and modeling for PFSA and PBI materials [8,9]. These models are easily verified utilizing an array of temperature probes within the MEA assembly and tooling. Alternatively, thermal behavior of the composite thermal system (tooling with and without MEA) can be characterized and fit to a non-dimensional transient model. Such a model can be generated by solving a simple energy balance accounting for heater power (top and bottom tooling), convective losses (likely from uninsulated sides of the tooling, and the thermal masses and transient temperatures of the tooling and MEA.

[8] D. Share, "Sealing of High Temperature PBI Membrane Electrode Assemblies Used in Fuel Cells," Masters Thesis, Rensselaer Polytechnic Institute, 2010.
[9] T. Snelson, "Ultrasonic Sealing of PEM Fuel Cell Membrane Electrode Assemblies," Doctoral Thesis, Rensselaer Polytechnic Institute, 2011.

$$Q_{heaters} = Q_{conv} + m_{tt}c_{p_{tt}}\frac{dT_{tt}}{dt} + m_{bt}c_{p_{bt}}\frac{dT_{bt}}{dt} + m_{mea}c_{p_{mea}}\frac{dT_{mea}}{dt}$$

Convective losses can be determined experimentally by leaving the pre-heated tooling closed and monitoring the average heater power consumption over time. This simplifies the energy balance to a steady state condition.

$$Q_{heaters} = Q_{conv}$$

Convective losses can be modeled using the temperature difference between the tooling surface, surround temperature and a lumped convective heat transfer coefficient. This coefficient can be accurately determined by running the steady state experiment described above at multiple temperature set points.

$$Q_{conv} = (T_{tooling} - T_{\infty})h_{conv}A_{tooling}$$

Top and bottom tooling thermal masses ($m_{tt}c_{ptt}$, $m_{bt}c_{pbt}$) can be determined through a simple tooling heat-up experiment in which the transient tooling temperature is monitored in conjunction with heater power consumption for individual top and bottom tooling.

$$Q_{heaters} = Q_{conv} + m_{tt}c_{p_{tt}}\frac{dT_{tt}}{dt}$$

MEA thermal behavior can also be determined using similar transient experiments by placing the MEA within the heated press and monitoring the thermal response. This incremental construction of a non-dimensional model only requires heater power consumption measurement capability in addition to the thermal measurement capabilities previously described (tooling and embedded MEA measurements).

Press tonnage (maximum applied force) is dictated by the required lamination pressure and total active area of the MEA being laminated. For instance, a 250cm^2 MEA lamination at 300psi requires 75,000lbs of force. While the optimal lamination pressure is specific to the type of MEA, materials and application of interest, tonnage will scale with active area for both thermal and ultrasonic approaches.

Ultrasonic Lamination

Alternatively, ultrasonic lamination generates the bonding temperature internally, within the materials and material interfaces. Materials can heat more rapidly, with minimal thermal sinking to the tooling. Tool warming is generally slight (warm to the touch), even with rapid minimal off-time lamination cycles. This is in stark contrast to the necessary, always heated, hot tooling used in thermal pressing.

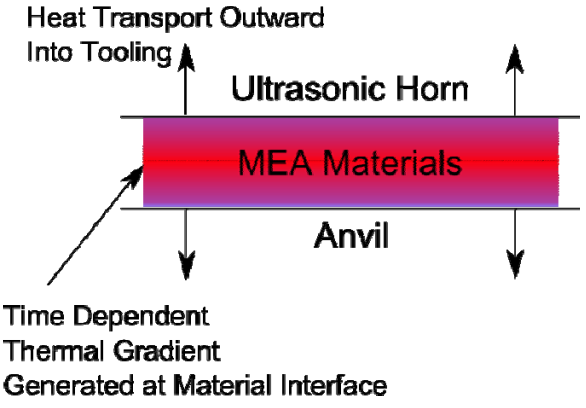

Heat Generation

Materials are heated via the ultrasonic motion of the horn. Pressure, frequency, displacement (amplitude) and material properties will dictate the thermal response of the materials. Heating (Q_{MEA}) is generally rapid once effective settings are determined. Complex loss modules (E''), frequency (ω), and applied strain (ε) will dictate heat generation for each material[10]. The substitution of ultrasonically induced material heating for heater power, in the energy balance developed for the thermal pressing process, should provide a starting point for a similar transient model.

$$Q_{MEA} = \frac{\omega \varepsilon_0^2 E''}{2} \qquad \textit{Eq. 1}$$

The generally low tooling temperature results in insignificant convective heat transfer and model simplification. Tooling thermal mass is large compared to the MEA, especially considering the relatively short process duration. This allows for a simple model incorporating the tooling as an infinite heat sink (constant temperature), with heat transfer limited by thermal conductivity.

$$Q_{MEA} = Q_{cond} + m_{mea} c_{p_{mea}} \frac{dT_{mea}}{dt} \qquad \textit{Eq 1}$$

Once again, experiments may be executed to complete the model. Specifically, the MEA can be pre-heated or heated ultrasonically, then allowed to cool within the closed tooling to determine the conductive heat transfer into the tooling.

$$0 = Q_{cond} + m_{mea} c_{p_{mea}} \frac{dT_{mea}}{dt} \qquad \textit{Eq 2}$$

Conductive heat transfer can be described as a function of thermal gradient (*dT/dx)* and thermal conductivity of the materials (*k*). In a very simplistic sense, the thermal gradient can be described as the difference between the MEA and tooling temperatures (likely ambient). MEA heat capacity can be found as described earlier.

$$Q_{cond} = \frac{dT}{dx} k \qquad \textit{Eq 3}$$

While process power (*P*), energy, and time monitoring is provided by the converter controller, the efficiency by which the controller power output is converted to motion (via the converter) and then transferred through the amplifier and horn is unknown and likely to be variable with process conditions. As such, experimentation to determine this process efficiency is required in order to rely on the controller instrumentation for the energy balance model. Completing the model and monitoring the variation in this energy transfer efficiency (η) may be an appropriate process control parameter during manufacturing. In fact, the temperature dependent nature of MEA material properties leads to a time variant behavior which is characteristic of the process. Unfortunately, this would require a means for process temperature feedback in addition to the real time process monitoring provided by the ultrasonic controller.

$$\eta(t) = \frac{Q_{mea}}{P} \qquad \textit{Eq 4}$$

Replication of the sensing approach for MEA temperature (described above) can be used to determine the length of time and process settings required to obtain similar temperatures and dwell times to that of thermal lamination for the ultrasonic process. However, it is noted that this approach only gives a starting point from which to perform further process optimization. The ultrasonic process is dynamic in nature, introducing the many rapid compression/relaxation cycles to the MEA. While the process does emulate a

[10] T.R. Kirkland, "The implications of the fundamental formulas for frequency selection in ultrasonic plastics welding," *Ultrasonics Industry Association 31st Annual Symposium,* 2001.

thermal lamination process in some respects, it is by no means identical. Further refinement via a design of experiments will likely enhance the lamination and cell performance, and avoid detrimental side effects.

Ultrasonic Process Parameters

As shown in equation 1, response to the ultrasonic process is a function of the dynamic material behavior, strain rate and frequency. The ultrasonic horn must be large enough to cover the entire lamination area, and robust enough to support the desired bonding pressure without distorting during oscillation for a specific frequency and amplitude. Thus, tooling design and material response are coupled with respect to operating frequency.

Material Response

Material characteristics can be determined experimentally via dynamic mechanical analysis (DMA) or instrumented indentation[11]. DMA (or simple compression testing) can also provide the modulus of elasticity, and an understanding of the pressure required to obtain a desired strain. Given that one is interested in laminating multiple materials, a complete understanding of each material property (and limitation) may help set boundaries for preliminary ultrasonic lamination process settings (ω, ε) to obtain a desired heating rate (ignoring thermal losses to the tooling). It is noted that the strain rate (ε) has a substantial impact on heat generation. Also relevant, *Kirkland*[10] stresses that frequency and amplitude are generally not independent, but inversely proportional to each other for a given tooling set (20μm @ 20kHz translates to 10μm at 40kHz). However, the ability to drive a material to higher strain rates requires that sufficient force (and tooling robustness) be available, and that neighboring materials can handle such strain rates. This is especially important for MEA lamination, considering the nature of Nafion (thin, dense, stiff) versus gas diffusion media (porous, thick, relatively limited compressive strength).

Frequency

Frequency selection for ultrasonic lamination is dictated by the desired MEA geometry. The ultrasonic horn must be capable of uniformly applying pressure and displacement across the entire bonding surface. Horns are generally designed for uniformity across their entire working surface (lamination surface). Thus the horn must be at least as large as the MEA. Ultrasonic frequency is inversely proportional to the horn size (smaller horn can be driven at higher frequency). When scaling the ultrasonic lamination process to larger format MEAs, higher loads and larger horns were required. For instance, a newly developed system at the Center for Automation and Technologies Systems was designed for 15 kHz rather than 20 kHz to accommodate large active areas (up to ~ 600 cm^2).

Pressure and Displacement Amplitude

The pressure applied during ultrasonic lamination influences the rate at which the ultrasonic motion can compress the material and generate heat. Higher pressure results in larger displacement and a higher strain rate. As shown in equation 1, a higher strain rate leads to higher heat generation rate. Thus, pressure and amplitude are coupled with respect to material deformation. The non-linear influence of strain (squared) is observed by heightened sensitivity, in which lamination does not proceed at all below a minimal pressure. Excess pressure can result in high strain rates and very high temperatures leading to rapid material damage. Additionally, excess pressure (and strain rate) can damage more delicate materials such as gas diffusion media.

---

[11] J. Hay, "Measuring the Complex Modulus of Polyethylene Using Instrumented Indentation," Agilent Technologies Application Note, 2001.

In a static sense, tooling clamping pressures below that required to sufficiently support the desired material strain rate (to achieve heat generation) can result in displacement of the tooling, rather than material strain. However, given the high frequency nature of the process, tooling response to ultrasonic actuation is more complex than a simple static force balance. Stiff materials require high compressive loads to achieve desired strain rates. In a steady state force balance, hydraulic or pneumatic actuation must supply the full load to achieve strain. The dynamic nature of the ultrasonic process results in rapid acceleration; the material will compress to some strain rate, or the tooling and any other “sprung mass” must be accelerated to match the horn motion. The tooling effectively acts as an impedance to horn and MEA motion. The incorporation of high mass anvil tooling can be leveraged to achieve material strain rates in excess of that which are obtained in a static system with similar static compression. For the same reason, the ultrasonic horn and anvil must be rigid enough to avoid deformation under the potentially high loads generated with rapid acceleration.

The amplitude of the motion applied to the lamination package will influence the ability to transfer motion to the lamination interface. Thicker and more compliant materials will require higher amplitudes in order to achieve the desired strain rate and subsequent heat generation. Excessive amplitudes can lead to damage to GDL structures. As such, preliminary amplitude selection should be made with knowledge of bonding material thicknesses and compliances. For example, it has been found that gel-like membranes in combination with ~ 200μm GDL layers may require +/- 30μm amplitudes. The use of thinner and less compliant layers (Nafion) may require +/- 10μm of motion for adequate bonding.

Amplitude can be selected through hardware and/or software (controls). The booster can amplify or attenuate the displacement generated by the converter. The ultrasonic controller can also be used to adjust the displacement amplitude. These two approaches to amplitude control are slightly different. The ultrasonic controller adjusts amplitude by limiting the maximum power level available to achieve the desired displacement. A negative side effect of utilizing the controller for amplitude control is the potential for reaching the (reduced maximum power limit) and stalling the converter. Alternately, the booster limits maximum displacement via the dynamic mechanical system. Full power can still be leveraged, yet at reduced displacements. For this reason, it is advisable to achieve gross amplitude via the proper booster/reducer selection, and then fine tuning with the controller. This way, full power is available for use with dense materials.

Energy/Power/Time

Power consumption will generally be dictated by the materials set, applied pressure and amplitude. Increased pressure or amplitude will result in higher power levels and more rapid bonding. However, excessive pressure can lead to GDL pore damage, ultimately revealed as poor cell performance with elevated mass transport losses and modified water transport characteristics. Generally, a user can target a specific total energy or power and time. Selection of a threshold bonding energy will result in a lamination process in which the system will run until the total target energy has been achieved (power × time). Power consumption is dictated by the process conditions (amplitude, pressure) and material properties (stiffness, thickness, damping). The system will deliver the necessary power to achieve the target

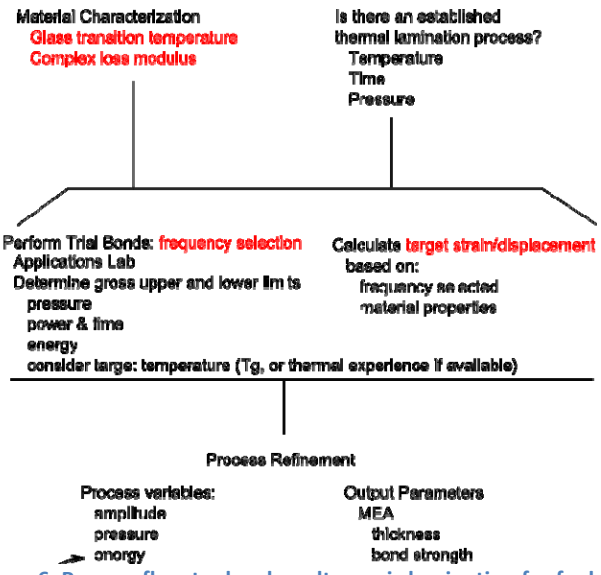

Figure 6. Process flow to develop ultrasonic lamination for fuel cell MEAs. Ideally should incorporate materials characterization to aid in rapid down-selection of process variable set points.

process conditions for the period of time required to reach the target energy level. Alternately, one may program a specific power level and time period.

The above factors (time, temperature, pressure, amplitude, energy and power) all must be chosen based on the materials set of interest, MEA size, and desired qualities. An approach which incorporates material analysis, expertise from an ultrasonic applications lab (for preliminary assessment and frequency selection), and a design of experiments is ideal (Figure 6).

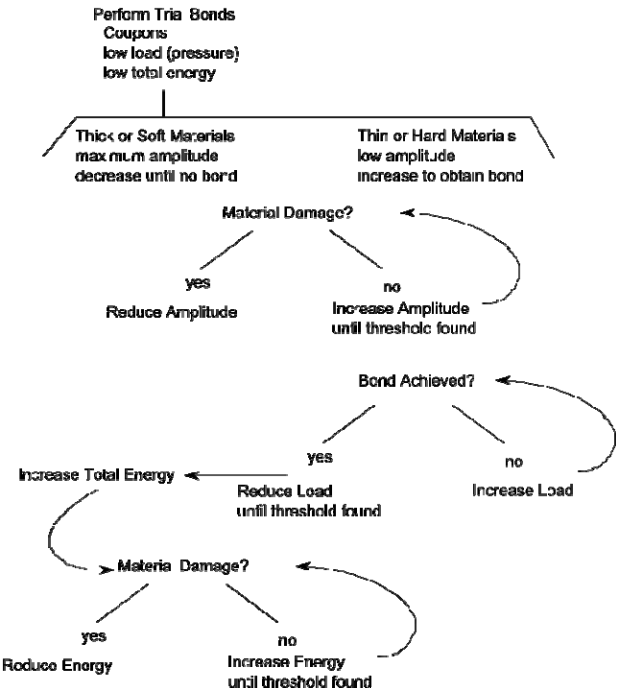

Figure 7. An iterative approach to ultrasonic lamination process parameters which focuses on achieving a basic weld, while monitoring for materials damage.

Since tooling frequency is not adjustable, an ideal approach to process development would include would follow a path of material characterization, testing in an applications lab (where multiple frequencies and tooling are available), tooling selection, target strain rate, and refinement (design of experiments, analysis of variance). A series of broad experiments with a range in frequencies and amplitudes while monitoring thermal response can quickly achieve lamination. More focused optimization is then attempted once successful lamination has been demonstrated. Follow on experiments focused on fuel cell performance, GDL permeability, GDL thickness, and bond strength will further strengthen process refinement.

An iterative approach (not as ideal) can also be utilized if materials characterization and ultrasonic application expertise are not available (Figure 7).

The use of barrier films to protect the MEA from contamination is advisable for ultrasonic lamination, just as used in thermal press processes. In the case of PBI MEAs, where phosphoric acid is freely available on the MEA surface, barrier films are also desired to avoid contamination and corrosion of the tooling. Thin and dense barrier films are advisable with the ultrasonic process, to avoid energy consumption and disruption of the process. For this reason, barrier films should be incorporated in process development.

Testing

Determine sensitivity of GDL characteristics to ultrasonic and thermal (and other) bonding process conditions. Thermal bonding at elevated pressures or ultrasonic motion under excessive compressive load may collapse and densify the GDL structure. Additionally, the application of extended ultrasonic power (high lamination energy) can degrade the GDL structure. Achieving rapid temperature increase and subsequent excess temperatures is also possible, such that membrane degradation can occur.

Permeability and GDL Thickness

Just as one would approach optimization of the thermal lamination process, a range of lamination conditions while monitoring the GDL thickness and permeability before and after lamination may provide an indication of minimal lamination energy and pressure to achieve a sufficient bond, yet avoid excessive GDL damage.

GDL permeability influences the mass transport losses associated with reactant and product transport to and from the electrode. As reactant rates (per unit area) increase, bulk transport to and from the electrode is more challenging, resulting in partial pressure induced over-voltages. While pressure-related lamination process will result in some degree of irreversible GDL collapse (compression), the ultrasonic process has the potential to severely damage GDL fibers and fiber-fiber junctions. The measurement of GDL permeability and/or porosity is helpful in refining the ultrasonic lamination process for optimal fuel cell performance.

Since GDL permeability is impacted by the initial static load applied by closing the ultrasonic tooling (similar to thermal lamination) and the dynamic motion of the process, it can be helpful to characterize both of these factors. Characterization of GDL permeability is commonly performed via permeability measurement (pressure differential induced flow) and/or mercury porosimetry (pore size).

1. Characterize virgin GDL samples (thickness, permeability/porosity)
2. Repeat after static loading
3. Repeat after simulated ultrasonic lamination

Characterization before and after simulated (static and dynamic) lamination will provide an indication of process influence on material permeability and/or pore sizes. The lamination process can be simulated by inserting a barrier film between the GDL and membrane prior to lamination. Uncoated Kapton works well to avoid bonding of the electrode-membrane interface. The use of the same MEA package is required during simulated lamination, to maintain an accurate simulation of the dynamic process (all components, plus any surrounding materials used during lamination).

Coupling these measurements with complete MEA characterization in the fuel cell (polarization and impedance spectroscopy) should reveal threshold process conditions from which unacceptable GDL damage occurs. In these cases, decreased permeability is observed in concert with low fuel cell voltages and increased low-frequency impedance (high mass transport losses).

The Gurley densometer is widely employed for measuring fuel cell GDL permeability. It is noted that while permeability is a material characteristic, and simply described by the relationship between pressure differential and flow, there appears to be some level of measurement system influence on final results. So much so, that the Gurley densometer is a de facto standard for comparison with 3rd parties. Model 4118N (5oz cylinder, measurement of uncoated GDL), with a digital timer and 20oz cylinder (measurement of catalyzed GDL) provides repeatable results and use for a range in GDL permeabilities. Alternately, mercury porosimetry aids in the characterization of pore size. This process seems to be used in tandem with the Gurley densometer to elucidate multiple aspects of reactant permeability in the GDL.

Thickness should be measured using a sprung web-thickness gauge (micrometer) with large surface contact. The compressive nature of GDL will result in GDL compression during thickness measurement, even with a proper gauge. However, use of the same gauge for all testing will still reveal relative results (before, after, varying process conditions). Resolution should be in the 10s of μm. The Mitutoyo thickness gauges are a good example (547-520).

Process Temperature

High power levels can also lead to high generation rates and rapid temperature increases. Thus, extended lamination periods at high power levels can easily result in elevated temperatures and material degradation. The efficient and rapid nature of the ultrasonic process (lamination in seconds) means that process development is best performed with the incorporation temperature measurement. The use of very fine thermocouples imbedded within the MEA package is necessary to avoid the generation of hot spots. In cases where the MEA materials are very thin and rigid (Nafion catalyst coated membrane

lamination) it may be necessary to place measurement probes within pockets in the package. Response rate of temperature measurement should be sufficient to resolve process dynamics (seconds). Fine gage thermocouples or optical probes work well.

	Test	Notes
1	Thickness	Spring loaded web-gage w/ large head, > 3x places, before and after bonding. Measurement resolution of 0.01 mm is adequate for MEAs with GDL. CCM may require finer resolution depending on total thickness. A sprung micrometer is appropriate for thickness measurement of soft textiles (to avoid compression variability).
2	Permeability	Gurley densometer outfitted with 5oz and 20oz cylinders. (additional/alternate - mercury porosimetry)
3	Visual inspection	Inspection of the GDL under a microscope may reveal GDL fiber damage (depending on GDL structure). Breakage can occur in the fiber itself, or at fiber junctions resulting in reduced GDL compression or bending stiffness). Damage may be visible with before/after visual inspection under > 50x microscope.
4	Instron bending	Bending strength is relevant to GDL strength across flow field channels, especially when the application includes operation with pressure differentials (between anode and cathode).
6	Cell testing	Impedance spectroscopy (low frequency associated with mass transport) Polarization (Air and O_2, analysis of interface and mass transport)

Testing of samples before and after simulated and real MEA bonding conditions will be performed on individual components and at the cell level. In some cases the testing will alter the material structure of the GDL. As such, multiple samples will be used to allow parallel testing.

Bending testing

The gas diffusion layer contributes heavily to the overall strength of the MEA and is responsible for maintaining the MEA structure while spanning flow field geometry. The specific structural requirements of the composite MEA and individual GDLs is unique to the cell design and cannot be generalized. Demands on the MEA composition and structural strength will be a function of flow field geometry, reactant composition, fuel utilization, operating temperature, pressure differential, and many other factors. However, it is sufficient to state that knowledge of the manufacturing process impact on GDL strength is important in obtaining the desired fuel cell performance characteristics.

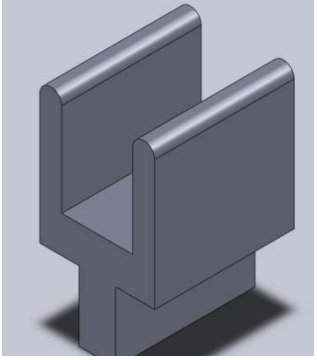

Figure 8. 3-Point bending fixture can be mounted in an Instron machine outfitted with clamping jaws.

The use of a bending strength test can reveal structural damage to the GDL layer. Just as in permeability measurement, samples should undergo a simulated lamination process. An Instron test machine capable of compression testing and a simple 3-point bending fixture (Figure 8) are required. A relative comparison of GDL bending strength before and after static compression and simulated ultrasonic lamination may reveal severe structural damage. GDL orientation in the bending fixture must be monitored. GDL is commonly manufactured as a web and exhibits directional strength characteristics. Machine and transverse directions will have different strengths.

Cell Performance Testing

The overall goal of a quality MEA lamination is cell functionality. Any design of experiments for optimization of an MEA lamination process should include a consistent cell testing program. The Department of Energy has published a fuel cell testing protocol which is appropriate for thorough and consistent testing.[12] Whether utilizing an established protocol or in-house testing protocol, consistency is required for resolution of manufacturing process variable and parameter impact on cell performance. The MEA lamination process can influence cell performance via multiple effects such as electrical shorting, ionic conductivity, mass transport impedance, startup incubation requirements, lifetime degradation, sensitivity to condensate formation (low-temperature cells), and other characteristics. Some of these impacts are outlined in Table 1. However, thorough refinement of the lamination process requires in-depth expertise in electrochemical cell performance beyond that explained here.

[12] Florida Solar Energy Center, “Procedure for Performing PEM Single Cell Testing,” DOE Contract # DE-FC36-06G016028, 2009.

Table 1. Examples of cell performance characteristics, potential lamination process causes, and tests to isolate significance. Absolute values for test results will be a function of the MEA and application at hand.

Characteristic	MEA Lamination Influence	Test / Indicator
Electrical shorting	Excessive pressure or ultrasonic amplitude	Capacitive CV measurement Steady state DC resistance Low fuel cell operating voltage Low open circuit voltage Low fuel utilization (for given stoichiometric ratio and measured current) Low high frequency impedance (1000 Hz) / high frequency intercept
Ionic conductivity	Insufficient bond Poor tooling alignment	Elevated high frequency impedance (1000 Hz) / high frequency intercept Low fuel cell operating voltage Check tooling alignment Check electrode transfer
Mass transport impedance	Excessive pressure Excessive ultrasonic amplitude or energy	Elevated low frequency impedance Reduced cell potential at high current density Reduced GDL permeability Reduced GDL thickness Reduced GDL hydrophobicity Electrode flooding by electrolyte (aqueous electrolyte system, PBI)

Analysis

Design of experiments and analysis of variance techniques are highly efficient when optimizing multi-parameter and complex cause-effect processes. These techniques are commonly employed for process optimization and are appropriate for MEA lamination processes. The use of Excel or Minitab can aid in the design of experimental matrices and analysis of results. Snelson employed these techniques extensively in his dissertation, providing an explanation of the statistical theory and demonstrating sensitivities (or lack of) to process conditions.[9] An example of sensitivity analyses for lamination pressure and ultrasonic energy flux are shown in Figure 9. The results indicate that lamination pressure has a substantial impact on cell current density at 0.4V, while lamination energy does not. These results for are the specific MEA type (PBI) and operating conditions used in the study.

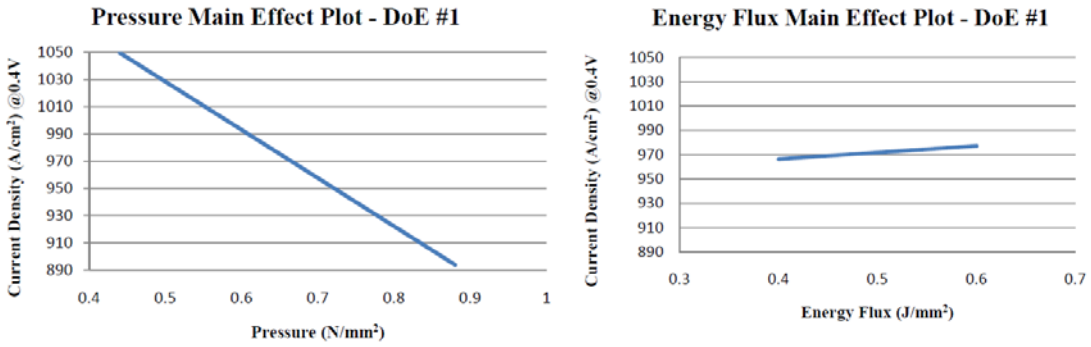

Figure 9. Samples of sensitivity analyses performed on ultrasonic MEA lamination. Lamination pressure is shown to have a significant impact on cell current density at 0.4V, while lamination energy does not.

Any process variable or material parameter (factors) for which the investigator has influence can be studied in this method. However, the total number of factors studied should be limited to those with the most probability of causing an effect. Small increases in the number of factors studied have a large impact on the total number of experiments required. An example ANOVA matrix from Snelson's thesis is shown in Table 2. In this example four variables result in sixteen different test conditions. With duplicates this requires 32 tests. The total number of tests can be reduced through various partial factorial matrices, but statistical significance is reduced for smaller matrices.

Table 2. Example of ANOVA (analysis of variance) matrix from Snelson's dissertation.

A	B	C	D	Treatment Combination
High	High	High	High	abcd
High	High	High	High	
High	High	High	Low	abc
High	High	High	Low	
High	High	Low	High	abd
High	High	Low	High	
High	High	Low	Low	ab
High	High	Low	Low	
High	Low	High	High	acd
High	Low	High	High	
High	Low	High	Low	ac
High	Low	High	Low	
High	Low	Low	High	ad
High	Low	Low	High	
High	Low	Low	Low	a
High	Low	Low	Low	
Low	High	High	High	bcd
Low	High	High	High	
Low	High	High	Low	bc
Low	High	High	Low	
Low	High	Low	High	bd
Low	High	Low	High	
Low	High	Low	Low	b
Low	High	Low	Low	
Low	Low	High	High	cd
Low	Low	High	High	
Low	Low	High	Low	c
Low	Low	High	Low	
Low	Low	Low	High	d
Low	Low	Low	High	
Low	Low	Low	Low	(1)
Low	Low	Low	Low	

15 kHz Ultrasonic Design Case Study

The standard ultrasonic welding systems available through Branson Ultrasonic utilize a "C" frame. This type of clamping configuration is appropriate for small loads, similar to those encountered on 50cm^2 cells or smaller (~2,300 lbs at 300 psi). Under load, the "C" frame flexes resulting in a loss of planarity between the anvil and ultrasonic horn. Tooling misalignment is heightened when dealing with large areas and thin materials (smaller displacements of the ultrasonic horn during lamination). The use of an H-Frame configuration benefits from the balanced load support, and uniform deflection of the tooling support structure. Scaling of the ultrasonic lamination process to greater than 140cm^2 formats demanded that the

support frame be strengthened, and a higher load ultrasonic converter (stack) be utilized. The larger format ultrasonic horn required for large MEAs lead to the selection of a 15kHz converter as well.

Introduction

As in any design process, understanding the ultrasonic welding process is paramount to achieving a successful system. The basic concept of ultrasonic welding is that electricity is fed into a piezoelectric converter, which converts electrical energy into linear motion in the form of vibration. This motion in turn is fed to the booster which maintains the frequency of those oscillations, but can alter the amplitude. The final component to the ultrasonic stack is the horn, which applies those vibrations to a given workpiece. The combination of the converter, booster, and horn are referred to as a sonotrode or ultrasonic stack. An important part of an ultrasonic welder is the frame that allows the sonotrode to apply pressure to a workpiece in addition to ultrasonic energy. The general formula for an ultrasonic welding machine is a sonotrode mounted to a linear carriage actuated by a pneumatic cylinder, which brings the horn into contact with the workpiece.

Figure 10: Branson Ultrasonics 2000X welder

When discussing ultrasonic welding there are several key components to achieving a satisfactory weld and not mastering these components will yield a myriad of problems. The problems can range from unsatisfactory welds all the way through failure of the major components. The first major component is to ensure that the ultrasonic horn is uniformly loaded. Uneven loading of the horn causes premature failure of the stud that joins the ultrasonic booster to the horn and can potentially cause damage to the booster and converter. The loading of the horn can be separated into two parts which are the static loading and dynamic loading. The static loading of the horn is simply the force applied to the part between the tooling and the horn once the relative motion between the horn and workpiece has ceased. An even static load is achieved by ensuring parallelism between the face of the horn and the tooling. Although a more traditional definition of the dynamic load would involve the forces from firing the sonitrode for this design it

is defined as the initial collision of the tooling and the horn. An even dynamic load is achieved by ensuring that the tooling surface is raised parallel to the horn.

The Frame

A large problem with the factory direction configuration of most ultrasonic welders (Figure 10) is the cantilevered c-frame design. The problem with the cantilevered design is that the static load is inherently uneven, though at very low loadings as is common in plastics welding the difference is minimal. Although this may seem like a glaring problem with the original design, the system was never meant to experience loads above 500 lbf and the system allows for easy adjustment of the height of the sonotrode. In our experiments we found the original 500 pounds of force was inadequate and so the system was modified to accept a pneumatic cylinder that could apply 1,200 pounds of force (Figure 11).

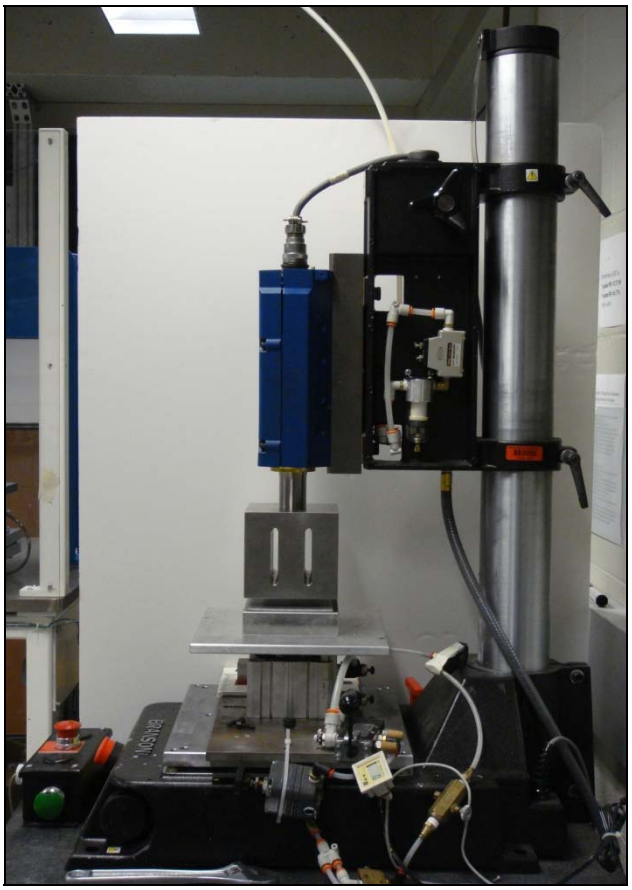

Figure 11: Side view of the modified Branson 2000X

At this higher loading we began to experience unsatisfactory welds where the rear (closest to the frame) portion of the workpiece was extremely thin and the front of the work piece was virtually untouched and exhibited no bonding. Further, sometime after the modification the ½”-20 stud that joins the booster to the horn failed, which we together with the manufacturer attributed to the uneven static load. We concluded that it was the static load instead of the dynamic loading because the system used guided cylinder to raise the tool. After the failure of the horn stud we decided to measure the deflection of the horn under loading using a dial indicator mounted to the base of the machine. When the deflection of the system was measured at the full 1200 lbf, it was found the front of the horn rose approximately 0.20”, while the rear of the horn moved 0.014” (Figure 12). When these values were measured they seemed

extremely high and it was only after the measurement that it was discovered that the rear mounting post for the sonotrode head was hollow and would also flex at its attachment point to the machine base.

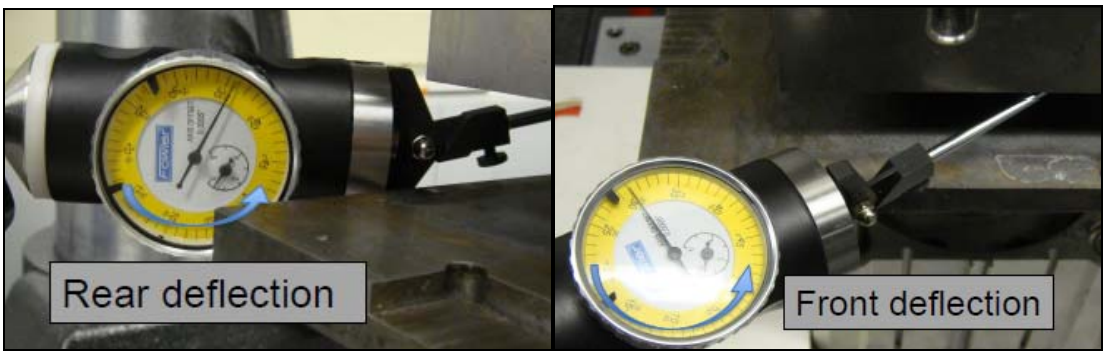

Figure 12: Front and Rear deflection of C-Frame design

As the new system was required to achieve at least 6,500 lbf, it was clear that the cantilevered designed would be scrapped in favor of an axially loaded h-frame. The new h-frame design ensures that regardless of the loading, any deflection in the system would occur along the axis of the sonitrode, thus isolating it from any moments. Further the axially loaded frame would be much simpler to secure to the machine base as there are no moments involved. The biggest downside to moving to the axially loaded frame is the lack of adjustability in the overall height of sonotrode and in combination with the limited 1" range of the pneumatic cylinders, there is a very narrow window for tool thicknesses. The limited adjustability could cause problems for machines that are not but for a single purpose. For our application the limited adjustability was perfectly acceptable and the 1" gap was enough room for placing our materials for welding.

The overall dimensions of the frame were determined by the length between sonitrode clamping points, the height of the leveling system, and motion generation. Careful attention should be paid to the distance between clamping points the converter and the booster and how they change with the selection of different boosters. Related to the dimensions are the placement and usage of pins and threaded holes to secure the clamps to the frame. The top clamp has precision pins that maintain its position on top of the frame, while the lower clamp is only secured by bolts with clearance holes and once it is set half of the clamp is tightened for good. This allows both of the clamps to be aligned axially without worry of manufacturing errors.

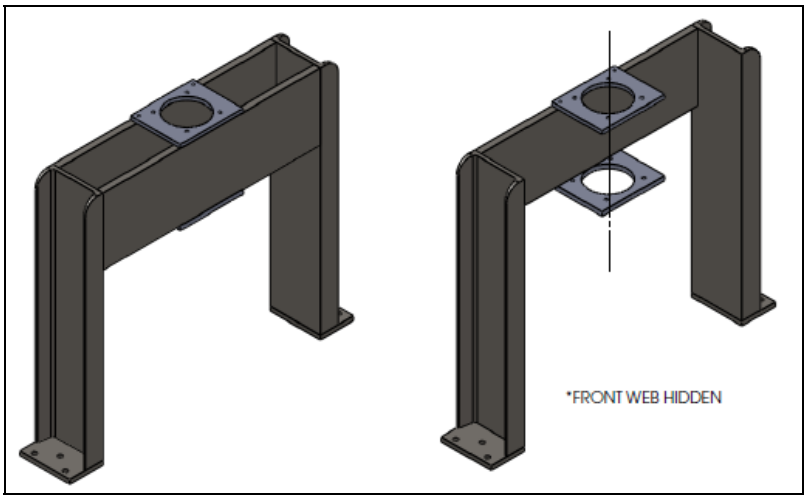

Figure 13: Solid model of h-frame design with cut away

Another important aspect of the design after ensuring axial loading was the overall deflect. Despite already minimizing its effect on the parallelism between the tooling and the horn we still wanted to minimize the deflection of the frame. For this design there was also no cost to over building and so the frame was tested using a simple finite element analysis up to roughly three times its intended loading. Then the components of the frame, structural C-channel and plate steel were chose to ensure deflection of less than 0.005" at that loading (Figure 14).

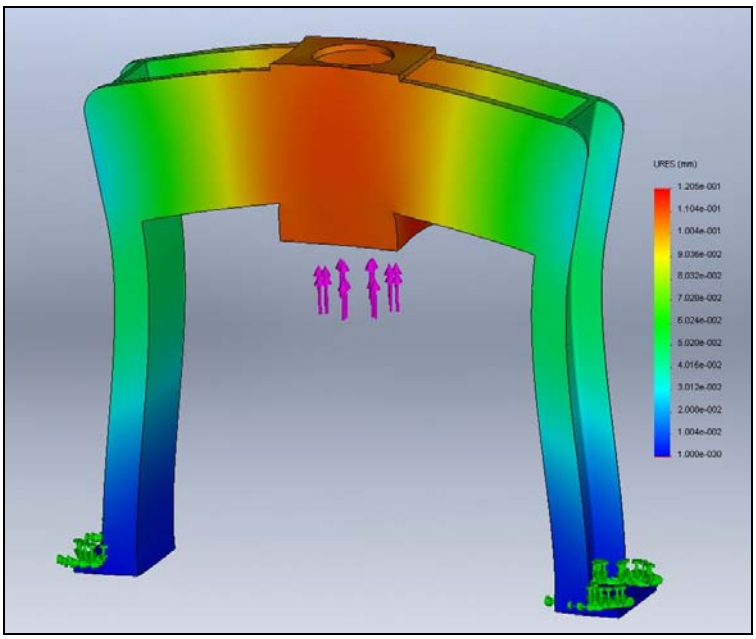

Figure 14: H-Frame FEA Analysis at 15,000 lbf, maximum deflection of 0.0047"

Leveling System

In a perfect world the tooling and the sonotrode would be attached to the same base, which combined with careful manufacturing would ensure they are perfectly parallel, but in reality there are tolerances and errors which stack up to ensure that this is almost never the case. Errors and variations in manufacturing make it necessary to have some amount of adjustment in the orientation of the tooling plane relative to the face of the horn. Just as in the flexing of the mounting frame, a lack of parallelism between the horn face and the tool face would result in uneven loading.

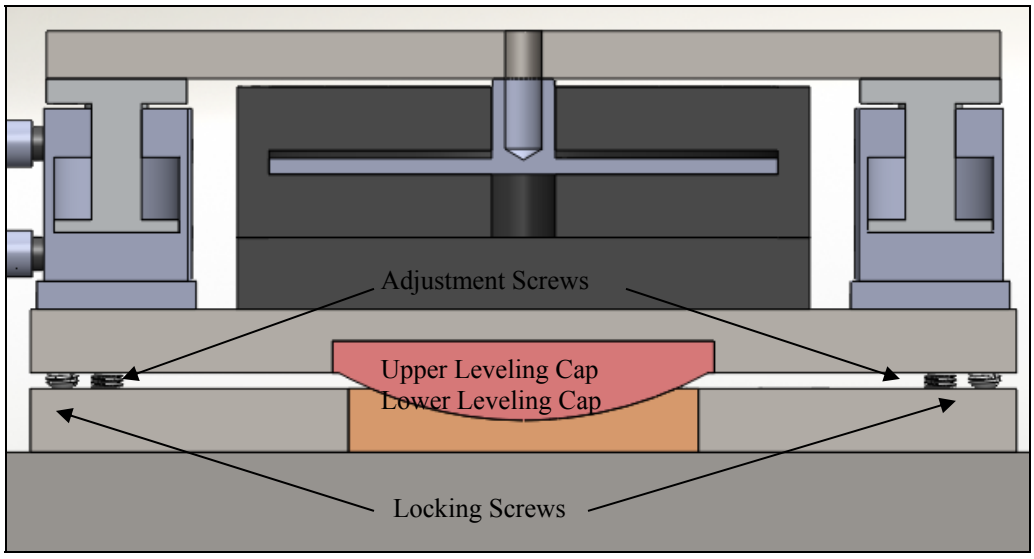

Figure 15: Cut away of level assembly

On the original Branson system planar adjustment was achieved with a swiveling leveling foot mounted to the underside of the tooling. This solution was designed around the original 500 lbf maximum loading and worked well for this design but when the new system was designed the maximum loading specification was 6,500 lbf. Attempting to use a single leveling foot that could support this load would have required a massive base plate and would have elevated that base plate well off of the machine base, unlike the original design which was effectively flush. Instead a new design was proposed that consisted of mating spherical caps, which would allow for smooth adjustments and a more even distribution of the load (Figure 15). Adjustment of the level system would happen through the use of pressure sensitive paper, a dial indicator, and the adjust screws located on the four corners of the leveling plate.

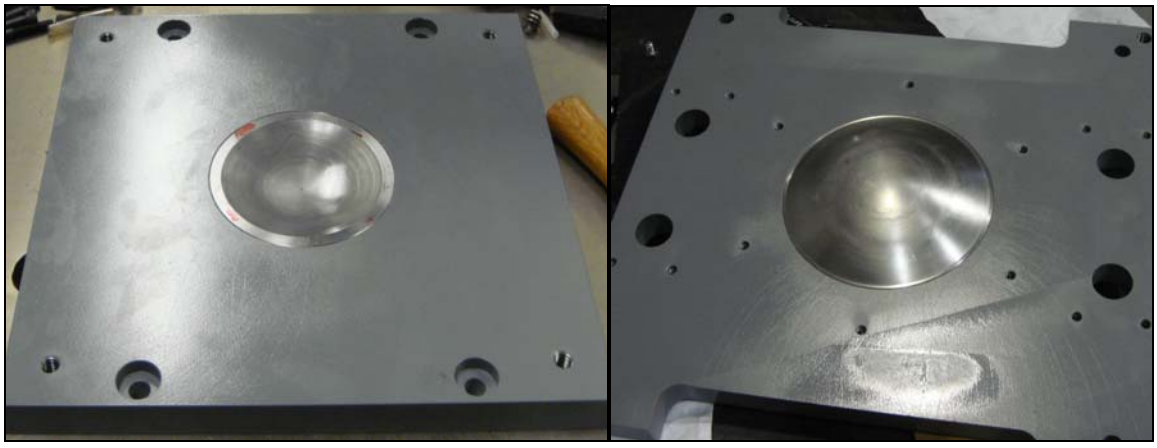

Figure 16: Lower and Upper leveling caps

With this new system adjustment to the tooling plane is as simple as the old design. To level a new combination of tooling and ultrasonic horn the adjustment and locking screws would first be loosened. The system would then be pressurized so that the tooling contacts the horn and the set screws and locking screws would be hand tightened. The system would then be lowered, pressure sensitive paper inserted on top of the tooling and then clamped between the horn and tooling. Adjustments would

then be made using the dial indicator until the pressure sensitive paper shows an even distribution across the entire surface. In practice this method worked extremely well for tools with a small surface area and on large area tools secondary adjustments were not necessary.

Motion Generation

When moving the tooling to contact the horn there were several key design specifications. The first and most obvious was that the system was required to output at least 6,500 lbf. The second specification was that it utilized pneumatics, which would help maintain the cleanliness of the lab. The final specification was for precision motion, ensuring that the tooling rose with its surface parallel to the horn. In previous work it was found that when the tooling did not rise parallel to the horn it would cause motion of the layers to be laminated. In addition to decreasing the accuracy of layer placement we found that this movement would also damage the individual layers.

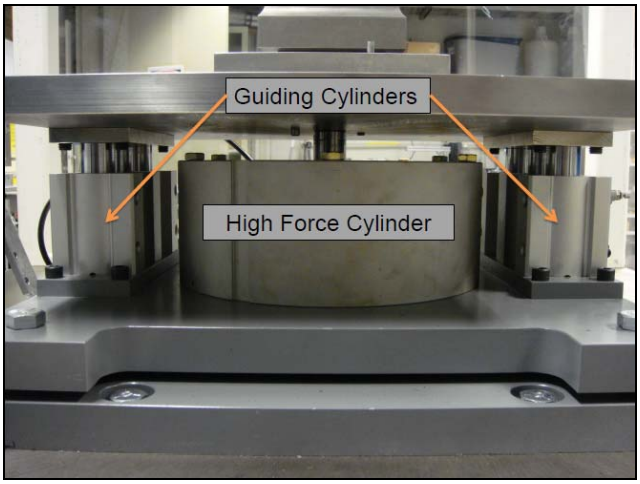

Figure 17: Pneumatic System

The need for pneumatics meant that a very large cylinder would have to be used to be able to generate such a high load on standard compressor pressures (110 psig). Large bore cylinders are not typically guided and so the decision was made to separate the lifting of tooling from the application of the force (Figure 17). Since the two actions had to be separated, the application called for the use of two precision guided cylinders. The guided cylinders chosen for this system were from the MGQM line of SMC Pneumatics and they were chose because of their extremely high off axis loading capabilities. High off axis loading capabilities means that the guided cylinders are extremely resistant to racking. One problem with attempting to raise two separate cylinders in unison is that every cylinder moves at a slightly different speed at a constant pressure due to manufacturing limitations. We were able to mitigate this problem by using a pressure manifold and equal length tubing in combination with precision speed controls on each individual cylinder. In addition to the speed controllers on the individual cylinders the supply manifold also uses speed controllers to control the overall speed once the two cylinders were tuned to rise in unison.

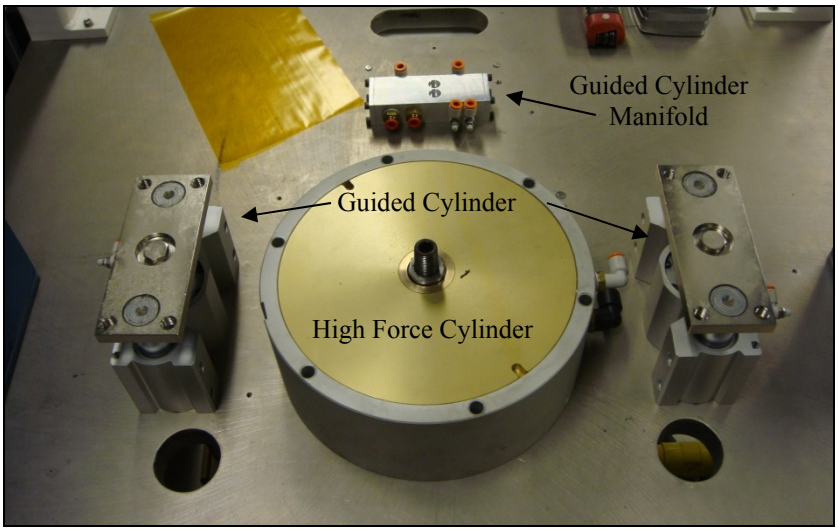

Figure 18: Mock layout of cylinders and guided cylinder manifold

Tuning the speed controllers on the guided cylinders greatly improves their performance and lowers the minimum pressure required to raise the tooling. Without tuning the cylinders one cylinder would inevitable rise faster and would cause the system to stick and not continue. The only way to solve this problem without tuning is to increase the pressure in the guided cylinders. The cylinders were tuned by simply place a steel plate on top and observing the motion of the cylinders. At the start the speed controls were wide open and slowly the faster cylinder was increased until the two rose evenly. The result of the tuning operation was a decrease in minimum operating pressure by 10 psig. The overall rising speed of the tooling could then be adjusted by use of the speed control on the manifold.

Sonitrode Clamping

The clamping of the sonitrode components was derived directly from the original manufacturer's methods. Clamping of the sonitrode is not trivial but is very simple and must be factored into the design of the frame. The converter can only be clamped above a particular point on the canister and so the distance between that point and the top surface of the booster ring should be factored into the design of the frame. The dimensions of the clamps each of the clamps are determined by the dimensions of the converter and the booster, but they differ slightly. The converter clamp should be a tight interference fit to prevent it from moving, while the booster should have a very light interference fit. The booster is held into the clamp more by the mounting screws that contact the underside of the booster ring than the clamp itself. On the booster clamp there should be enough screws of sufficient size to support the full weight of the ultrasonic horn if it is sufficiently large.

Manufacturing

The manufacturing of all of the components of the ultrasonic welder is equally important as the design itself. Although the system was designed to give adjustability in the planar alignment between the horn and the tooling it is extremely important that each component of the system is manufactured to a high degree of parallelism. In the new design there are several mating surfaces that stand to affect the final parallelism between the horn face and the tooling, and so any error in manufacturing each of the individual components has the potential to stack up to cause a large error in the final system. Although the system was design to account for errors in parallelism, use of the leveling system was view as a last resort and so Blanchard grinding was chosen for the final machining operation for each of the plates to ensure parallelism. Blanchard grinding utilizes two surfaces that are trued to be perfectly parallel on the machine before parts are placed for grinding, which provides almost perfect parallelism between sides.

For smaller plates a surface grinder was used in conjunction with an inspection table to ensure parallelism.

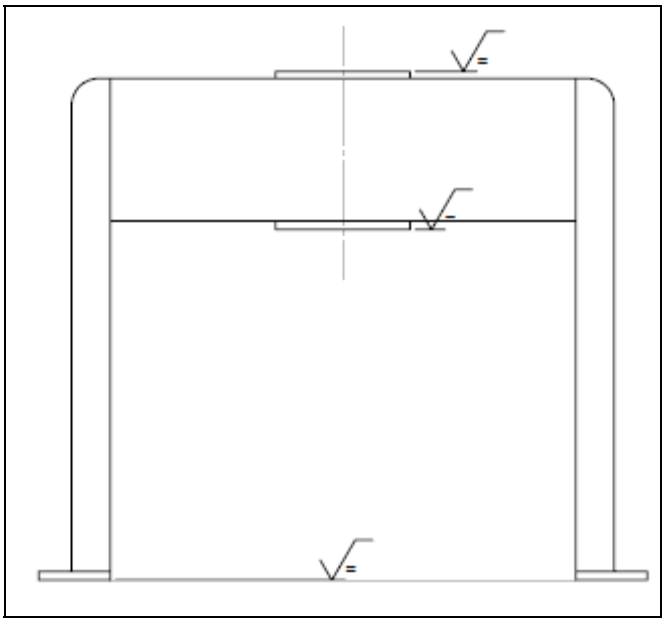

Figure 19: Front two dimensional technical drawing of h-frame, showing the machined surfaces

Parallelism is not only important between tooling components but also between the frame and sonotrode clamping components. For this reason it was specified that the frame components be welded together and then the three mating surfaces be machined flat and parallel (Figure 19). Any skewness between the components of the sonotrode has the potential to cause catastrophic damage to the converter. In addition to machining of the frame each of the clamps was ground to ensure orthogonality between the clamp mount and the frame surface.

Natural Frequency

One area of the design that was not fully explored until construction was complete was the natural frequency of the entire system. It was observed during several tests that the ultrasonics excited a resonance within the system and caused violent shaking of the entire machine. Tuning of the pneumatics could potentially reduce this as it would change the spring constant and thus the natural frequency of the cylinders. Another alternative would be to alter the weight of the tooling to prevent such violent coupling.

15 kHz Design Example Conclusion

The most important aspect of designing and manufacturing an ultrasonic welder is parallelism throughout all horizontal surfaces at rest and while in motion. Parallelism takes different forms throughout the design such as ensuring axial loading on the support frame or controlling the motion of the tooling so that it is always parallel with the horn. The manufacturing of the design is equally important as orthogonality between the sonitrode axis and the tooling surface is paramount to a properly function and durable ultrasonic welder.